

**A MINI PROJECT**  
**ON**  
**“THE CASE STUDY ON SOIL EROSION IN THE SUBANSIRI RIVER**  
**BASIN USING THE R.U.S.L.E. MODEL AND GEOGRAPHIC**  
**INFORMATION SYSTEM (GIS)”**

*Submitted in Partial Fulfillment for the Requirements for the award of*

*Degree of*

**MASTERS OF TECHNOLOGY (CIVIL ENGINEERING)**

**UNDER**

**ASSAM SCIENCE AND TECHNOLOGY UNIVERSITY**



**ANNAJYOTI SAIKIA**  
**MTECH 3<sup>RD</sup> SEMESTER**  
**Roll no-230620061004**

**Under the guidance of:**  
**Dr. BHARATI MEDHI DAS**  
**PROFESSOR**

**DEPARTMENT OF CIVIL ENGINEERING**  
**ASSAM ENGINEERING COLLEGE**  
**JALUKBARI, GUWAHATI-781013**  
**SESSION: 2023-2025**

## **ACKNOWLEDGEMENT**

I am highly honored to express our sincere and heartfelt gratitude to **Dr. JAYANTA PATHAK**, Head of Department, Civil Engineering Department, for encouraging and allowing us to present the project on the topic at our department premises for the partial fulfilment of the requirements leading to the award of Bachelor of Technology in Civil Engineering.

We would like to express our heartfelt gratitude to our Project Supervisors, **Dr. BHARATI MEDHI DAS**, Professor, Department of Civil Engineering for their guidance, encouragement and for providing us necessary facilities, valuable suggestions and constructive criticism in carrying out the project work.

Last but not the least, we are thankful to the Faculty and Staff of the Civil Engineering Department of our college and other technical and non-technical staff who helped us to learn a lot of new things and we are extremely grateful to them.

**Date:**

**Place: Kamrup(M)**

**ANNAJYOTI SAIKIA**

**M.Tech 3<sup>RD</sup> SEMESTER**

**Roll no-230620061004**

## **CANDIDATE DECLARATION**

I hereby certify that the work presented in the project entitled **“THE CASE STUDY ON SOIL EROSION IN THE SUBANSIRI RIVER BASIN USING THE R.U.S.L.E. MODEL AND GEOGRAPHIC INFORMATION SYSYTEM (GIS)”** is the authentic record of our own work carried out under the guidance of **Dr. BHARATI MEDHI DAS**, Professor, Department of Civil Engineering, Assam Engineering College, Jalukbari. The project is submitted in partial fulfillment of requirements for the award of the degree of **“Master of Technology in Civil Engineering”** under specialization on Water Resources Engineering to the Department of Civil Engineering, Assam Engineering College, Jalukbari, Guwahati-781013, Assam.

The matter embodied in this dissertation has not been submitted to any other institute for the award of any other degree. We have followed the guidelines provided by the Department of Civil Engineering, Assam Engineering College, Jalukbari, Guwahati-781013, Assam. Whenever materials from other sources are used, due acknowledgement is given to them by citing them in the text of this project and giving their details in the references.

This is to certify that the above statement made is correct to the best of my knowledge.

**Date:**

**Place: Assam Engineering College  
Jalukabri, Guwahti, Assam**

**NAME - ANNAJYOTI SAIKIA**

**ROLL NO - 230620061004**

**SIGNATURE**

## **CERTIFICATE FROM THE SUPERVISOR**

This is to certify that the dissertation report **entitled “THE CASE STUDY ON SOIL EROSION IN THE SUBANSIRI RIVER BASIN USING THE R.U.S.L.E. MODEL AND GEOGRAPHIC INFORMATION SYSYTEM (GIS)”** is submitted by **Annajyoti Saikia, Roll No 230620061004**, a student of 3<sup>rd</sup> semester in the Department of Civil Engineering, Assam Engineering College, Guwahati in partial fulfilment for the award of degree of **MASTERS OF TECHNOLOGY** in Civil Engineering with specialization in **Water Resources Engineering** under **ASSAM SCIENCE AND TECHNOLOGY UNIVERSITY** has been carried out under my guidance.

The content of this report has not been submitted to any other university for the award of any degree.

**Date –**

**Place – Kamrup(M)**

**Dr. Bharati Medhi Das**

Professor

Department of Civil Engineering

Assam Engineering College

Jalukbari, Guwahati, 781013

**DEPARTMENT OF CIVIL ENGINEERING  
ASSAM ENGINEERING COLLEGE  
JALUKBARI, GUWAHATI -781013**



**CERTIFICATE  
FROM THE HEAD, CIVIL ENGINEERING DEPARTMENT**

It is to certify that the project report entitled “**THE CASE STUDY ON SOIL EROSION IN THE SUBANSIRI RIVER BASIN USING THE R.U.S.L.E. MODEL AND GEOGRAPHIC INFORMATION SYSTEM (GIS)**” is hereby accorded our approval as a study carried out and presented in a manner in their 3<sup>rd</sup> semester courses for acceptance in partial fulfilment for the award of Master of Technology in Civil Engineering under specialization on Water Resources Engineering degree for approval does not necessarily endorse or accept every statement made, opinion expressed or conclusion drawn as recorded in the report. It only signifies the acceptance of the project report for the purpose for which it is submitted.

Date:

Place: Kamrup (M)

**Dr. Jayanta Pathak**

Professor & Head  
Department of Civil Engineering  
Assam Engineering College  
Jalukbari, 781013

## ABSTRACT

This study evaluates soil erosion risks within a sub-watershed of the Subansiri River basin in Lakhimpur District, Assam, using the Revised Universal Soil Loss Equation (RUSLE) model. The research integrates key factors influencing soil erosion, including rainfall erosivity (R), soil erodibility (K), slope length and steepness (LS), cover management (C), and support practices (P), to assess annual soil loss. Spatial analyses were conducted using ArcGIS, converting the core factors into raster layers for processing with a raster calculator. This approach facilitated the development of soil erosion risk maps that classify the watershed into zones of varying erosion severity, providing insights for sustainable land management and targeted conservation efforts.

The study, employing a GIS-based time-series approach, analyzed soil loss trends for the years 2014, 2022, and 2023. Two RUSLE variants were compared: one utilizing flow length and the other flow accumulation to estimate the LS factor. Inputs included USGS remotely sensed data, digital elevation models, precipitation records, and soil maps. Results indicated no significant trends in soil erosion, precipitation, or land cover changes over the past decade. Despite reports of increasing rainfall intensity in the region, this could not be corroborated through climate data analysis or modeled soil erosion trends. Findings suggest that improved agricultural practices may have offset potential erosion from land exploitation, highlighting the importance of sustainable land use management in mitigating soil degradation.

**Keywords:** Soil erosion, RUSLE model, GIS, Subansiri River basin, rainfall erosivity, soil erodibility, slope length and steepness, cover management, support practices, sustainable land management, soil degradation, time-series analysis.

# CONTENTS

<b>CHAPTERS</b>	<b>TITLE</b>	<b>PAGE NO</b>
	List of Figures	10
	List of Tables	14
	List of Abbreviations	17
<b>CHAPTER 1</b>	<b>INTRODUCTION</b>	<b>16</b>
	1.1 General Background	16
	1.2 Objectives	20
	1.3 Study Area	21
	1.3.1 Hydrological and Geological Features	22
	1.3.2 Climate and Environmental Conditions	23
	1.3.3 Topographic Features	24
	1.3.4 Seismicity	25
	1.3.5 Hydrological Network	26
<b>CHAPTER 2</b>	<b>MATERIALS</b>	<b>27</b>
	2.1 DIGITAL ELEVATION MODEL (DEM)	27
	2.2 PRECIPITATION DATA FROM NETCDF FILE	28
	2.3 LANDSAT IAMGE	30
	2.3.1 DETAILED DESIGNATION OF LANDSAT SATELLITES	31
	2.4 SOIL DATA	32
<b>CHAPTER 3</b>	<b>LITERATURE REVIEW</b>	<b>33</b>
	3.1 SOIL FORMATION AND ITS HISTORY	33
	3.2 ROLE OF SOIL BIODIVERSITY	34
	3.3 SOIL CLASSIFICATION	35
	3.4 SOIL DEGRADATION	35
	3.4.1 TYPES OF SOIL DEGRADATION	36
	3.5 SOIL EROSION	36
	3.5.1 SOIL EROSION VULNERABILITY MAP	37
	3.5.2 EROSION AND ITS TYPES	37
	3.5.2.1 WATER EROSION AND ITS TYPES	38
	3.6 EROSION MODEL	40
	3.6.1 EMPEIRICAL MODELS (STATISTICAL)	41
	3.6.2 PHYSICAL MODELS	41
	3.6.3 HYBRID MODELS	42
	3.6.4 MODEL AND ITS IMPORTANCE	42
	3.6.4.1 USLE	42
	3.6.4.2 SWAT	42
	3.6.4.3 WEPP	42
	3.6.4.4 EROSION 3D	43
	3.6.4.5 MCE	43

3.7	RUSLE MODEL	43
3.8	RUSLE FACTORS	44
3.8.1	RAINFALL EROSIVITY (R) FACTOR	44
3.8.2	SOIL ERODIBILITY (K) FACTOR	45
3.8.3	SLOPE LENGTH AND SLOPE STEEPNESS (LS) FACTOR	48
3.8.4	COVER MANAGEMENT (C) FACTOR	49
3.8.5	SUPPORT PRACTICE (P) FACTOR	51
<b>CHAPTER 4</b>	<b>METHODOLOGY</b>	<b>56</b>
4.1	THE RUSLE MODEL	56
4.2	RUSLE FACTORS	57
4.2.1	RAINFALL EROSIVITY (R) FACTOR	57
4.2.1.1	WORKING WITH PRECIPITATION IN NETCDF FILE OF CRU 2014	59
4.2.1.1.1	REPROJECT OF MONTHLY RAINFALL DATA 2014	64
4.2.1.1.2	CALCULATION OF R FACTOR USING PROJECTED RAINFALL DATA 2014	65
4.2.1.2	WORKING WITH PRECIPITATION IN NETCDF FILE OF CRU 2022	66
4.2.1.2.1	REPROJECT OF MONTHLY RAINFALL DATA 2022	69
4.2.1.2.2	CALCULATION OF R FACTOR USING PROJECTED RAINFALL DATA 2022	70
4.2.1.3	WORKING WITH PRECIPITATION IN NETCDF FILE OF CRU 2023	71
4.2.1.3.1	REPROJECT OF MONTHLY RAINFALL DATA 2023	74
4.2.1.3.2	CALCULATION OF R FACTOR USING PROJECTED RAINFALL DATA 2023	75
4.2.2	SOIL ERODIBILITY (K)	76
4.2.2.1	USE OF FAO SOIL MAP FOR SOIL STUDIES YEAR 2014, 2022 & 2023	76
4.2.2.2	K FACTOR EXTRACTED FROM FAO SOIL DATA FOR DOMINANT SOIL	78
4.2.2.3	CONVERSION OF K FACTOR MAP TO RASTER IMAGE	79
4.2.3	SLOPE LENGTH (LS) FACTOR FOR SOIL STUDIES YEAR 2014, 2022 & 2023	80
4.2.3.1	FLOW DIAGRAM FOR LS FACTOR CALCULATION	80
4.2.3.2	CREATION OF FILL AND FLOW DIRECTION	81
4.2.3.3	CREATION OF FLOW ACCUMULATION MAP	82
4.2.3.4	CALCULATION OF SLOPE IN RADIANS	84
4.2.3.5	EVALUATION OF LS MAP	85
4.2.4	C- FACTOR (LAND USE/LAND COVER)	86
4.2.4.1	WORKING WITH LANDSAT IMAGE OF 2014	87
4.2.4.1.1	EVALUATION OF COMPOSITE BAND OF YEAR 2014	87
4.2.4.1.2	EVALUATION OF NDVI MAP OF YEAR 2014	88
4.2.4.1.3	EVALUATION OF C- FACTOR MAP OF YEAR 2014	89
4.2.4.2	WORKING WITH LANDSAT IMAGE OF 2022	90

4.2.4.2.1 EVALUATION OF COMPOSITE BAND OF YEAR 2022	90
4.2.4.2.2 EVALUATION OF NDVI MAP OF YEAR 2022	91
4.2.4.2.3 EVALUATION OF C- FACTOR MAP OF YEAR 2022	92
4.2.4.3 WORKING WITH LANDSAT IMAGE OF 2023	93
4.2.4.3.1 EVALUATION OF COMPOSITE BAND OF YEAR 2023	93
4.2.4.3.2 EVALUATION OF NDVI MAP OF YEAR 2023	94
4.2.4.3.3 EVALUATION OF C- FACTOR MAP OF YEAR 2023	95
4.2.5 P - FACTOR (CONSERVATION PRACTICE FACTOR)	96
4.2.5.1 P - FACTOR WORKING FOR STUDY AREA 2014	96
4.2.5.1.1 SUPERVISED CLASSIFICATION FOR THE YEAR 2014	96
4.2.5.1.2 RECLASSIFY SLOPE AND COMBINE WITH CLASSIFICATION MAP	97
4.2.5.1.3 ASSIGNING P - FACTOR VALUES FOR CLASSES IN AN ATTRIBUTE TABLE	98
4.2.5.2 P - FACTOR WORKING FOR STUDY AREA 2022	100
4.2.5.2.1 SUPERVISED CLASSIFICATION FOR THE YEAR 2022	100
4.2.5.2.2 RECLASSIFY SLOPE AND COMBINE WITH CLASSIFICATION MAP	101
4.2.5.2.3 ASSIGNING P - FACTOR VALUES FOR CLASSES IN AN ATTRIBUTE TABLE	102
4.2.5.3 P - FACTOR WORKING FOR STUDY AREA 2023	105
4.2.5.3.1 SUPERVISED CLASSIFICATION FOR THE YEAR 2023	105
4.2.5.3.2 RECLASSIFY SLOPE AND COMBINE WITH CLASSIFICATION MAP	105
4.2.5.3.3 ASSIGNING P - FACTOR VALUES FOR CLASSES IN AN ATTRIBUTE TABLE	107
<b>CHAPTER 5 RESULTS AND DISCUSSION</b>	<b>108</b>
5.1 RAINFALL EROSIVITY (R) FACTOR	108
5.1.1 ANNUAL PRECIPITATION OF STUDY AREA FOR YEAR 2014, 2022 & 2023	108
5.1.2 RAINFALL EROSIVITY (R) OF STUDY AREA FOR YEAR 2014, 2022 & 2023	111
5.2 SOIL ERODIBILITY (K) FACTOR	113
5.3 SLOPE LENGTH (LS) FACTOR VALUE FOR YEAR 2014, 2022 & 2023	117
5.4 C- FACTOR (LAND USE AND LAND COVER)	118
5.4.1 C- FACTOR STUDY FOR PERIOD 2014, 2022 & 2023	118
5.5 P - FACTOR (CONSERVATION PRACTICE FACTOR)	120
5.5.1 P - FACTOR STUDY FOR PERIOD 2014, 2022 & 2023	120
5.6 RUSLE WORKS	121
5.6.1 RUSLE A - FACTOR STUDY FOR PERIOD 2014, 2022 & 2023	121
5.7 VALIDATION OF SOIL EROSION	124
5.7.1 RAINFALL EROSIVITY	124
5.7.2 SOIL ERODIBILITY	124

5.7.3 VEGETATION COVER & NDVI	125
5.7.4 SOIL EROSION RATES	125
5.7.5 EROSION AND DEPOSITION ANALYSIS	126
<b>CHAPTER 6 CONCLUSION</b>	<b>129</b>
<b>CHAPTER 7 REFERENCES</b>	<b>130</b>

## LIST OF FIGURES

<b>FIGURES</b>	<b>HEADINGS</b>	<b>PAGE NO</b>
1.1	Study Area	21
1.2	Study Area with labels	22
1.3	Precipitation chart of 25 years	24
1.4	Seismicity map	25
1.5	Seismicity Zone value	25
2.1	NetCDF map	29
3.1	Soil components	33
3.2	Soil Horizons	33
3.3	Soil Biodiversity map	34
3.4	Soil classification chart	35
3.5	Erosion vulnerability map	37
3.6	Water erosion sketch	38
3.7	Soil erosion at study area	39
3.8	K - FACTOR CHART	47
3.9	C- FACTOR CHART	51
3.10	P – FACTOR CHART WITH SLOPE %	52
3.11	P – FACTOR OF DIFFERENT LAND SLOPE %	53
3.12	P – FACTOR OF DIFFERENT LAND USE TYPE	55
4.1	RUSLE FLOW DIAGRAM	57
4.2	NetCDF MAP 2014	59
4.3	Annual ppt calculation 2014	60
4.4	Cell statistics interface	60
4.5	Annual precipitation map of 2014	61
4.6	Annual precipitation point map of 2014	62
4.7	Kringing Interpolation dialog box	62
4.8	Kringing Interpolation interface	63
4.9	Kringing Interpolation map	63
4.10	Model building of raster projection	64
4.11	Cell statistics interface	65
4.12	Raster calculator interface	65
4.13	NetCDF MAP 2022	66
4.14	Annual ppt calculation 2022	66
4.15	Annual precipitation point map of 2022	67
4.16	Interpolation precipitation map of 2022	68
4.17	Kringing Interpolation map of 2022	68
4.18	Model building of raster projection	69
4.19	Model building of raster projection	70
4.20	NetCDF MAP 2023	71
4.21	Annual ppt calculation 2023	71
4.22	Annual precipitation point map of 2023	71
4.23	Interpolation precipitation map of 2023	73

<b>4.24</b>	Model building of raster projection - 1	<b>74</b>
<b>4.25</b>	Model building of raster projection - 2	<b>75</b>
<b>4.26</b>	FAO SOIL MAP	<b>76</b>
<b>4.27</b>	FAO SOIL WITH STUDY AREA MAP	<b>77</b>
<b>4.28</b>	K_FACTOR ATTRIBUTE CHART	<b>78</b>
<b>4.29</b>	K_FACTOR RASTER MAP	<b>79</b>
<b>4.30</b>	K_FACTOR SOIL MAP	<b>79</b>
<b>4.31</b>	CONVERSION OF POL TO RASTER	<b>79</b>
<b>4.32</b>	FLOW CHART OF LS WORKS	<b>80</b>
<b>4.33</b>	LS MODEL BUILDING INTERFACE	<b>81</b>
<b>4.34</b>	FLOW DIRECTION MOSAIC MAP	<b>82</b>
<b>4.35</b>	FLOW ACCUMULATION MODEL BUILDER	<b>83</b>
<b>4.36</b>	FLOW ACCUMULATION MAP	<b>83</b>
<b>4.37</b>	SIN_SLOPE_RADIAN MAP	<b>84</b>
<b>4.38</b>	RADIAN MAP	<b>84</b>
<b>4.39</b>	SAGA GIS GENERATED LS MAP	<b>85</b>
<b>4.40</b>	LANDSAT IMAGE OF YEAR 2014	<b>86</b>
<b>4.41</b>	COMPOSITE BAND FCC 2014	<b>87</b>
<b>4.42</b>	COMPOSITE BAND TRUE COLOR 2014	<b>87</b>
<b>4.43</b>	NDVI MAP OF 2014	<b>88</b>
<b>4.44</b>	C-FACTOR MAP BY VATANDASLAR.ET.AL 2014	<b>89</b>
<b>4.45</b>	C-FACTOR MAP BY DURGION.ET.AL 2014	<b>89</b>
<b>4.46</b>	LANDSAT IMAGE OF YEAR 2022	<b>90</b>
<b>4.47</b>	NDVI MAP OF 2022	<b>91</b>
<b>4.48</b>	C-FACTOR MAP BY VATANDASLAR.ET.AL 2022	<b>92</b>
<b>4.49</b>	C-FACTOR MAP BY DURGION.ET.AL 2022	<b>92</b>
<b>4.50</b>	LANDSAT IMAGE OF YEAR 2023	<b>93</b>
<b>4.51</b>	NDVI MAP OF 2023	<b>94</b>
<b>4.52</b>	C-FACTOR MAP BY VATANDASLAR.ET.AL 2023	<b>95</b>
<b>4.53</b>	C-FACTOR MAP BY DURGION.ET.AL 2023	<b>95</b>
<b>4.54</b>	TRAINING SAMPLES	<b>96</b>
<b>4.55</b>	LU/LC MAP OF 2014	<b>96</b>
<b>4.56</b>	SLOPE PERCENTAGE INPUT DIALOG BOX	<b>97</b>
<b>4.57</b>	RECLASSIFICATION INTERFACE	<b>97</b>
<b>4.58</b>	SLOPE PERCENTAGE MAP 2014	<b>98</b>
<b>4.59</b>	COMBINED SLOPE MAP 2014	<b>98</b>
<b>4.60</b>	P_FACTOR VALUE MAP 2014	<b>99</b>
<b>4.61</b>	P_FACTOR UTM MAP 2014	<b>99</b>
<b>4.62</b>	LU/LC MAP OF 2022	<b>100</b>
<b>4.63</b>	TRAINING SAMPLES	<b>100</b>
<b>4.64</b>	SLOPE PERCENTAGE INPUT DIALOG BOX	<b>101</b>
<b>4.65</b>	RECLASSIFICATION INTERFACE	<b>101</b>
<b>4.66</b>	P_FACTOR VALUE MAP 2022	<b>102</b>
<b>4.67</b>	P_FACTOR UTM MAP 2022	<b>102</b>

<b>4.68</b>	<b>P_FACTOR VALUE MAP 2022</b>	<b>103</b>
<b>4.69</b>	<b>P_FACTOR UTM MAP 2022</b>	<b>103</b>
<b>4.70</b>	<b>TRAINING SAMPLES</b>	<b>104</b>
<b>4.71</b>	<b>SLOPE PERCENTAGE INPUT DIALOG BOX</b>	<b>105</b>
<b>4.72</b>	<b>RECLASSIFICATION INTERFACE</b>	<b>105</b>
<b>4.73</b>	<b>P_FACTOR VALUE MAP 2023</b>	<b>106</b>
<b>4.74</b>	<b>P_FACTOR UTM MAP 2023</b>	<b>106</b>
<b>4.75</b>	<b>P_FACTOR VALUE MAP 2023</b>	<b>106</b>
<b>5.1</b>	<b>5.1 RAINFALL VARIATION CHART</b>	<b>108</b>
<b>5.2</b>	<b>ANNUAL PRECIPITATION 2014</b>	<b>109</b>
<b>5.3</b>	<b>ANNUAL PRECIPITATION 2022</b>	<b>109</b>
<b>5.4</b>	<b>ANNUAL PRECIPITATION 2023</b>	<b>109</b>
<b>5.5</b>	<b>ANNUAL PRECIPITATION AS PER LOCATIONS</b>	<b>110</b>
<b>5.6</b>	<b>COMPARISON OF MEAN R FACTOR</b>	<b>111</b>
<b>5.7</b>	<b>R FACTOR MAP 2014</b>	<b>112</b>
<b>5.8</b>	<b>R FACTOR MAP 2022</b>	<b>112</b>
<b>5.9</b>	<b>R FACTOR MAP 2023</b>	<b>112</b>
<b>5.10</b>	<b>INDIAN TEXTURE MAP</b>	<b>113</b>
<b>5.11</b>	<b>SOIL CHARACTERISTICS STUDY MAP</b>	<b>114</b>
<b>5.12</b>	<b>DOMINANT SOIL COVERAGE AREA CHART</b>	<b>115</b>
<b>5.13</b>	<b>K-VALUE MAP</b>	<b>116</b>
<b>5.14</b>	<b>STUDY AREA K-FACTOR CHART</b>	<b>116</b>
<b>5.15</b>	<b>LS (SLOPE LENGTH) MAP</b>	<b>117</b>
<b>5.16</b>	<b>LS (SLOPE LENGTH) MAP UTM</b>	<b>117</b>
<b>5.17</b>	<b>SOIL ERODIBILITY MAP 2014</b>	<b>119</b>
<b>5.18</b>	<b>SOIL ERODIBILITY MAP 2022</b>	<b>119</b>
<b>5.19</b>	<b>SOIL ERODIBILITY MAP 2023</b>	<b>119</b>
<b>5.20</b>	<b>CONSERVATION PRACTICE MAP 2014</b>	<b>120</b>
<b>5.21</b>	<b>CONSERVATION PRACTICE MAP 2022</b>	<b>120</b>
<b>5.22</b>	<b>CONSERVATION PRACTICE MAP 2023</b>	<b>120</b>
<b>5.23</b>	<b>SOIL EROSION TREND</b>	<b>122</b>
<b>5.24 (a)</b>	<b>ANNUAL EROSION MAP 2014</b>	<b>123</b>
<b>5.25 (b)</b>	<b>ANNUAL EROSION MAP 2014</b>	<b>123</b>
<b>5.26 (a)</b>	<b>ANNUAL EROSION MAP 2022</b>	<b>123</b>
<b>5.27(b)</b>	<b>ANNUAL EROSION MAP 2022</b>	<b>123</b>
<b>5.28 (a)</b>	<b>ANNUAL EROSION MAP 2023</b>	<b>123</b>
<b>5.29 (b)</b>	<b>ANNUAL EROSION MAP 2023</b>	<b>123</b>
<b>5.30</b>	<b>PERIODIC RIVERCOURSE MIGRATION</b>	<b>126</b>
<b>5.31</b>	<b>HISTORY RIVER EROSION – DEPOSITION STATISTICS CHART</b>	<b>127</b>
<b>5.32</b>	<b>RIVER BANK EROSION 2014</b>	<b>128</b>
<b>5.33</b>	<b>RIVER BANK EROSION 2022</b>	<b>128</b>
<b>5.34</b>	<b>RIVER BANK EROSION 2023</b>	<b>128</b>
<b>5.35</b>	<b>RIVER BANK EROSION 2014-23</b>	<b>128</b>

<b>5.36</b>	RIVER BANK EROSION 2014-22	<b>128</b>
<b>5.37</b>	RIVER BANK EROSION 2022-23	<b>128</b>

## LIST OF TABLES

<b>TABLE</b>	<b>HEADING</b>	<b>PAGENO</b>
1.1	Rainfall data	23
2.1	DEM specifications data	28
2.2	DEM features data	28
2.3	Wavelength with band no	30
2.4	LANDSAT features data	30
2.5	LANDSAT image features as per resolution	31
3.1	GASEMAT database	41
3.2	R formula as per locations	45
3.3	K-factor data as per soil properties	47
3.4	C – factor data as per LU/LC	50
3.5	C – value as per slope, and different practice work	52
3.6	P – factor as per slope	53
3.7	P – factor as per slope & LU/LC	54
4.1	BAND as per month with different period	58
4.2	BAND as per month with period 2022, 2023	59
4.3	FAO SOIL MAP DATA FOR DOMINANT SOIL	78
4.4	Attribute table of period 2014	99
4.5	Attribute table of period 2022	105
5.1	Annual precipitation data	107
5.2	Precipitation data as per locations	110
5.3	R – factor data with different period	111
5.4	Attribute table of soil map of study area	114
5.5	Soil erodibility data	115
5.6	Coverage K – factor data	116
5.7	Soil texture data	116
5.8	C -factor and NDVI data of different years	118
5.9	Annual soil erosion data	121
5.10	Soil erosion description chart	122
5.11	Soil erosion and deposition trend	127
5.12	Unchanged river-course area chart	127

## LIST OF ABBREVIATIONS

<b>Abbreviation</b>	<b>Full Form</b>
<b>CREAMS</b>	<b>Chemical Runoff and Erosion from Agricultural Management Systems</b>
<b>DEM</b>	<b>Digital Elevation Model</b>
<b>ESD</b>	<b>European Soil Database</b>
<b>ESRI</b>	<b>Environmental Systems Research Institute</b>
<b>EUROSEM</b>	<b>European Soil Erosion Model</b>
<b>FAO</b>	<b>Food and Agricultural Organization</b>
<b>GIS</b>	<b>Geographical Information System</b>
<b>GDP</b>	<b>Gross Domestic Product</b>
<b>HWSD</b>	<b>Harmonized World Soil Database</b>
<b>IDW</b>	<b>Inverse Distance Weighted</b>
<b>ICIMOD</b>	<b>International Centre for Integrated Mountain Development</b>
<b>MODIS</b>	<b>Moderate Resolution Imaging Spectro radiometer</b>
<b>NDVI</b>	<b>Normalized Difference Vegetation Index</b>
<b>OLI</b>	<b>Operational Land Imager</b>
<b>RS</b>	<b>Remote Sensing</b>
<b>RUSLE</b>	<b>Revised Universal Soil Loss Equation</b>
<b>SOTER</b>	<b>Soil and Terrain Database</b>
<b>SRTM</b>	<b>Shuttle Radar Topographic Mission</b>
<b>TIFF</b>	<b>Tagged Image File Format</b>
<b>TRIS</b>	<b>Thermal InfraRed Sensor</b>
<b>UNESCO</b>	<b>United Nations Educational, Scientific and Cultural Organization</b>
<b>USGS</b>	<b>United States Geological Survey</b>
<b>USLE</b>	<b>Universal Soil Loss Equation</b>
<b>UTM</b>	<b>Universal Transverse Mercator (Coordinate System)</b>
<b>WEPP</b>	<b>Water Erosion Prediction Project</b>
<b>WGS</b>	<b>World Geodetic System</b>
<b>WISE</b>	<b>World Inventory of Soil Emission Potentials</b>

## CHAPTER 1

# INTRODUCTION

---

### 1.1 General Background

The excessive land degradation brought on by natural occurrences and human actions, known as soil erosion, is a genuine danger to natural reserves, agriculture and environment (**Rahman et al. 2009; Bhattacharya et al. 2020; Ganasri and Ramesh 2016; Rosas and Gutierrez 2020; Teng et al. 2019**). Both natural and artificial factors contribute to the major problems of soil erosion and degradation that affect human society worldwide. **Borrelli et al. 2020** suggested that land utilization and presumably shifts in the climate by an increasingly rapid flood cycle are the key causes of erosion. Globally, it is found that along with areas with typically scant year-round vegetation cover, sloping terrain and elevated-relief landscape also exhibit significant rates of erosion. Owing to steep slope and barren topography, soil erosion is most prevalent in hilly areas. Thus, consequences of global warming, such as different rainfall condition, crop diversity, and land use contribute to soil erosion (**Li and Fang 2016**).

Research in Maotiao River in Guizhou Province of Southwest China showed that soil erosion was most likely driven by the cover-management and supporting practises which are connected to how land is used and also reflect the surface settings (**Xu et al. 2011**). Soil erosion caused by rainfall was also found in Mantaro River basin, Peruvian Andes (**Correa et al. 2016**). Soil erosion is a major issue in majority of Indian watersheds that requires careful investigation. An investigation was done in the Ganga basin's watershed region around the Kaushambi-Prayagraj sector where it was found that erosion is brought on by a number of aspects, such as haphazard and unmanaged use, uncontrolled mining, and environmental factors including the number of rains, landscape, and how land is used (**Yadav and Vaishya 2023**). When the lower Sutlej River basin in Punjab, India, was explored, it emerged that rains bring about erosion and that human actions also play a significant influence (**Sharma et al. 2023**).

A detailed investigation revealed that soil loss at Chilika Lake, Odisha, was caused by the area's elevated position, substantial amount of human activity, and heavy rains that caused runoff (**Behera et al. 2023**). Nethravathi Basin in the midst of the Western Ghats in western India was investigated by (**Ganasri and Ramesh 2016**), and found that erosion of soil is a significant matter brought on by destruction of land, growth in agriculture, as well as human-caused events. Climate change risks and land use practises make India more susceptible to future floods (**Pal et al. 2022**). Storm rainfall during the monsoon season has a clear influence on large-scale erosion throughout an entire subtropical region (**Chakraborty et al. 2022**). The influence of hydrological parameters on a watershed can be revealed through the quantitative study of drainage features in conjunction with remote sensing and GIS (**Rawat et al. 2021**). In order to properly manage floods and control erosion, concerted efforts for soil management and water resource conservation will benefit from the data from identifying the regions of soil erosion and rates of erosion (**Pathan and Sil 2022**). Therefore, identifying areas in a basin when there is a high chance of eroding soil is essential for adopting preventative actions.

Over thirty percent of the country's water supplies are carried by the Brahmaputra, which is amongst the biggest rivers in the globe, located in Assam. During the monsoon, Subansiri which is the longest tributary of the river Brahmaputra leads to serious flooding issues in nearby districts and the river diverts its course by carrying a substantial volume of material and depositing it in the valley in the plains of Assam (**Goyal et al. 2018**). Bankline displacement and losses to banks in the Subansiri was studied using the satellite imagery of 1995 and 2010 and it demonstrates that, in both banks, displacement of the bankline from erosion is much prominent than displacement due to sedimentation (**Gogoi and Goswami 2013**). The Subansiri River's river channels were also mapped which is employed to determine the likelihood of riverbank erosion. Utilizing the Spatial Analyst Hydrology capabilities in ArcGIS software, the watershed of the Subansiri River and its drainage channels have been identified (**Bordoloi et al. 2020**). Erosion in and around Subansiri is mostly caused by tremendous braiding, enormous rainfall, and rising river bottom due to silt deposition.

Models in general can be divided as conceptual, empirical and physics based (**Merritt et al. 2003a**). Some empirical models are USLE (**Wischmeier & Smith 1965, 1978**), RUSLE, improved version of USLE (**Renard and United States. Agricultural Research Service. 1997**), IHACRES-WQ (**A.J. Jakeman et al. 1990; Anthony J. Jakeman et al. 1994**), SEDD - Sediment Delivery Distributed (**Ferro and Porto 2000**), SEDNET (**Merritt et al. 2003b**). Since they are completely dependent on the assessment of findings and make an effort to define the response to the facts, empirical models are indeed the easiest among all model kinds (**Merritt et al. 2003b**). Conceptual models such as EMSS (**Vertessy et al. 2001**), HSPF (**Merritt et al. 2003b**), LASCAM (**Viney and Sivapalan 1999**), etc. are models frequently only provide a generalised depiction of catchment processes, but comprehensive catchment knowledge is needed to include the specifics of process relationships. Conceptual models are vulnerable to aggregation errors. Also, ANSWERS (**D. B. Beasley et al. 1980**), CREAMS (**Merritt et al. 2003b**), LISEM (**Takken et al. 1999**), etc. are physics-based models, which explain streamflow, sedimentation, and the generation of related nutrients in a watershed, are founded on the answers of basic physical equations. Physics based models cause variability in parameter values as there are huge quantities of parameters which can have changes in characteristics and these properties then must be validated using observed data which can give errors.

Some of the soil erosion models are SWAT (**J. G. Arnold et al. 2012**), WaTEM/SEDEM (**van Oost et al. 2000**), LISEM (**de ROO et al. 1996**), MUSLE (**J. R. Williams and H. D. Berndt 1977**), EPIC (**Borrelli et al. 2021**), EUROSEM (**Borrelli et al. 2021**) etc. These models predict net erosion while RUSLE predicts gross erosion. Also, these models in general have larger values and greater variability than RUSLE. This is due to deposition of sediment inside the environment and the softening of absolute numbers by including terrain diversity in net erosion models (**Borrelli et al. 2021**). RUSLE model is very much used by researchers because of many reasons. The state and amount of soil erosion can be accurately assessed in upland with RUSLE (**Kumar et al. 2014a**). Long-term averages are more appropriately represented by the result of erosion from the RUSLE (**A. Desalegn et al. 2018**). RUSLE is sensitive to rainfall (**Pathan and Sil 2022**). It is comparatively quick, adaptable, and time-effective, and its geographical extent is doable over a large area with lower cost and higher precision (**Mengie et al. 2022**). For calculating the RUSLE erodibility parameter, geostatistical techniques that are present inside the GIS system are believed to be helpful (**Phinzi and Ngetar 2019**). It demonstrates how factors such as soil geography, climate, and others affect soil erosion

(**Duarte et al. 2016**). In RUSLE, many enhancements are made, including the addition of monthly variables, the inclusion of outward and inward curved shapes via division of uneven gradients, and enhanced factual statements in estimating the LS factor (**Shalini Tirkey et al. 2013**). RUSLE is used in this study due to its good statistical correlations amidst input and output variables makes it suitable to diverse environmental circumstances. It calculates soil erosion quickly, effectively, and with a reasonable level of precision RUSLE and GIS can be employed. Researchers from various countries used GIS and remote sensing in studying erosion along with the movement of sediment, and some of them combined several models to provide superior results.

The Modified USLE model was employed to obtain total upland erosion, and the HEC-HMS lumped hydrologic model was used in calculating debris from floods that occurred in Wadi Billi, Egypt, on March 9, 2014 (**Almasalmeh et al. 2022**). Laursen-Copeland is applied to predict the ability for sediment transport in streams. Using ArcMap 10.5 software, the NDVI was utilised to a Landsat 8 imagery taken on February 20, 2014 to estimate the natural vegetation based on its spectral imprint. Two models were used (**Alexakis et al. 2013**): the Analytical Hierarchical Process (AHP) which provided a risk evaluation map, and multiparametric quantitative empirical model RUSLE that is centred on both expert knowledge and is regarded as a cutting-edge method in assessing soil loss. According to the study, for large watersheds, utilising remote sensing and GIS methods using daily rainfall gave an accurate and efficient evaluation for erosion during a relatively brief amount of time at a cheap cost. In their article, two crucial steps were described (**Aziz et al. 2021**) in the processing of satellite imagery: image rectification and correlation analysis-based detection of deciding visual bands. The work shows that for predicting river deposition with machine learning without supervision, spectral bands such as Near Infrared band, Short-wavelength infrared band, and Thermal Infrared bands are the key bands. In order to record the catchment heterogeneity, another approach that includes spatially disintegrating the watershed into uniform grid segments was used (**Bhattarai and Dutta 2007**).

The Universal Soil Loss Equation (USLE), amidst its elements properly chosen, was employed to obtain the gross erosion in every segment. The sediment delivery ratio is employed to channel ground erosion from every cell towards the catchment outflow. A study was conducted to map the areas that flood when the Fetam River in Ethiopia's Upper Abbay Basin is inundated, using GIS and HEC RAS. (**H. Desalegn and Mulu 2021**). Flood inundation mapping serves

to determine the region's most vulnerable to flooding whenever the flow of a stream crosses a river at a level above the bank-full level. Average yearly erosion of soil has been determined with RUSLE and GIS from different rivers (**Ganasri and Ramesh 2016**), (**Borgohain et al 2019**), (**Kebede et al. 2021**), (**Kumar et al. 2014b**), etc. For proper management and safety procedures in Ekiti State, Southwestern Nigeria, evaluation was done for the possible erosion and flood risks areas applying the Revised Universal Soil Loss Equation (RUSLE) and Hand Above Nearest Drainage (HAND) models, respectively (**Olorunfemi et al. 2020**). RUSLE was merged with the software ArcGIS which may help decision-makers identify and prioritise key erosion hotspots for thorough and long-term watershed management (**Getu et al. 2022**). It is seen that GIS and remote sensing is applied in estimating soil erosion of different rivers by different researchers. Many models in combination with GIS has been studied to do so. But very limited study has been done in Subansiri river of Assam, India where GIS and remote sensing has been merged with different models to obtain erosion. The main objectives were to assess changes in the study area with high as well as low soil erosion and analyse changes in the river and the study region using a amalgam of GIS and RUSLE.

## **1.2 Objectives**

The first specific aim is thus to produce high accuracy soil erosion estimates for the study area. Secondly, possible climate and soil erosion intensity trends from 2014 to 2023 are discussed.

These aims are addressed through the following objectives:

- To understand the influencing factors in the RUSLE model and the basic usage of the model by reviewing literature and previous studies.
- To perform the two different model calculations for the years 2014, 2022 and 2023 in order to estimate soil erosion and create soil erosion intensity maps.
- To analyze and discuss the results of possible soil erosion intensity trend from the year 2014 to 2023, affecting by precipitation and land cover situation in the study area.



### 1.3.1 Hydrological and Geological Features

The Subansiri River exhibits diverse fluvial morphologies depending on the terrain. In the foothills, the river demonstrates a braided pattern, characterized by multiple interweaving channels, while in the plains, it transitions into a meandering course with significant channel migration. This dynamic nature forms varied depositional features, such as point bars, channel bars, natural levees, and back swamps. These features play a pivotal role in the geomorphology of the region, influencing flood patterns and sediment deposition.



Fig: - 1.2 Study Area with labels

Source: Google Earth Pro

### 1.3.2 Climate and Environmental Conditions

The dataset shows monthly and yearly rainfall (in mm) for the Subansiri region from **2000 to 2023**. The annual rainfall varies significantly, with the highest recorded in **2010 (2660.7 mm)** and the lowest in **2012 (1441.7 mm)**. Most of the rainfall occurs during the monsoon months (**June to September**), while the winter months (**November to February**) have much less. On average, the annual rainfall is about **2064.1 mm**, indicating a generally wet climate with clear seasonal patterns.

This information is important for managing water resources, planning agriculture, and preparing for floods and droughts. It highlights the area's strong reliance on monsoon rains and the need for weather monitoring and prediction systems. The data also helps understand how climate changes affect rainfall, aiding in sustainable planning and decision-making.

<b>Year</b>	<b>RAINFALL (MM)</b>
2000	1905.8
2001	1548
2002	1688.1
2003	2184.5
2004	2420
2005	1846.2
2006	1742.3
2007	2231.1
2008	1914
2009	1966.3
2010	2652.8
2011	1570.1
2012	1441.7
2013	1882.6
2014	2037.7
2015	2000.9
2016	2283.1
2017	2571.5
2018	2178.9
2019	2352.4
2020	2433.6
2021	1803.3
2022	2587.4
2023	2091.8

Mean precipitation for 24 years (nearly 2000-2023) is **2064.1 mm**

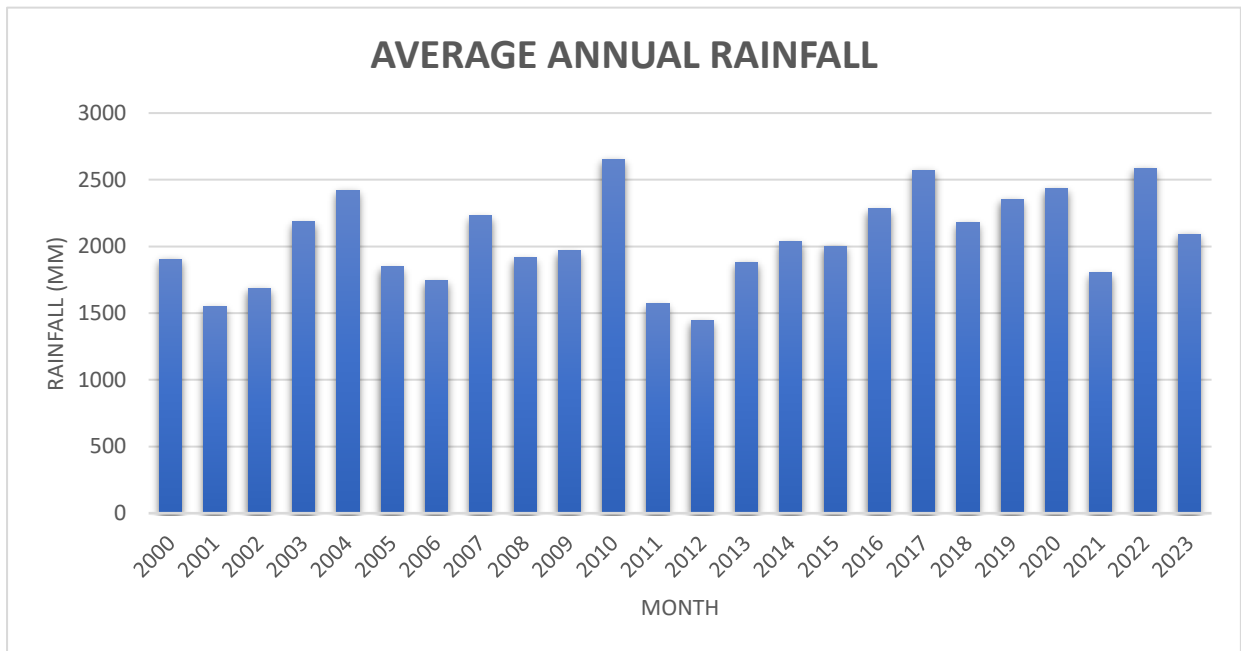


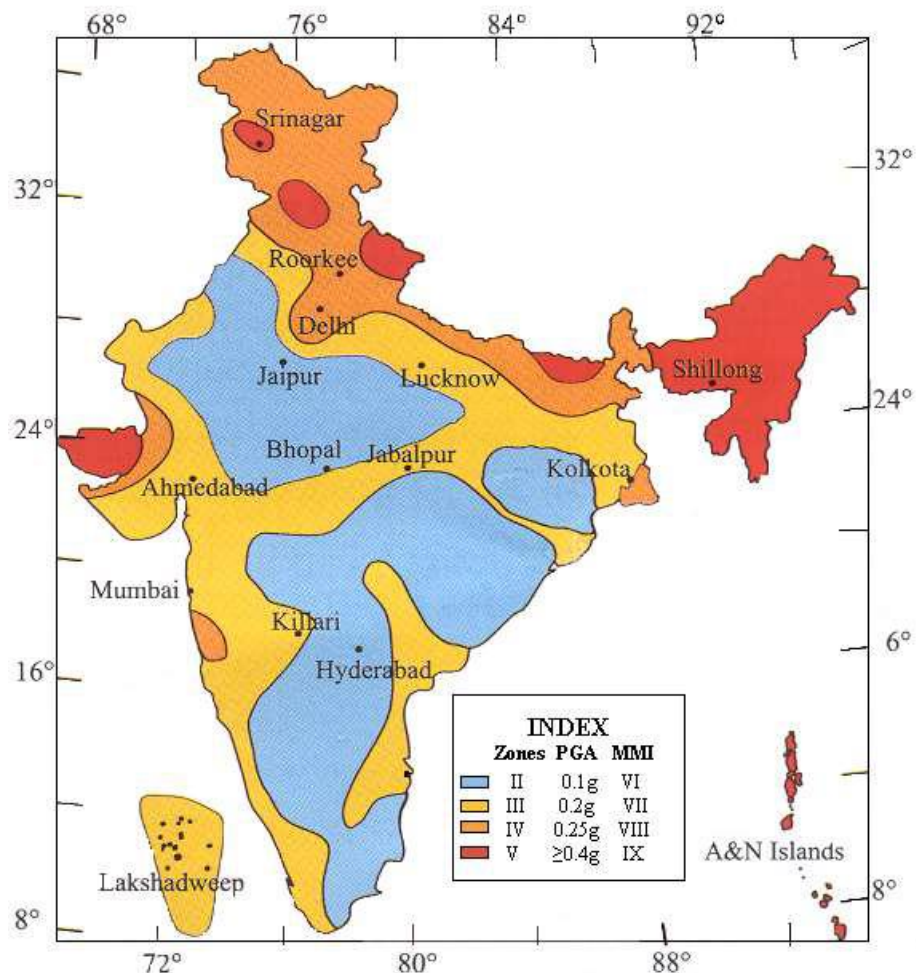
Fig: - 1.3 Precipitation chart of 25 years

### 1.3.3 Topographical Features

The study area is mostly comprised of alluvial plains with mild slopes, except for the northern hilly terrains. The average elevation of the middle and southern floodplains is about 80–85 meters above mean sea level (MSL). The slope generally declines from the northern and eastern edges toward the southern parts. The alluvial deposits in the floodplains result in fertile soils, which are suitable for agriculture but highly vulnerable to erosion during floods.

### 1.3.4 Seismicity

According to the seismic zoning map of India, the Subansiri basin falls under **Zone-V**, the highest seismic risk category. This indicates a significant vulnerability to earthquakes, which adds to the region's geomorphological and environmental fragility (**IS 1893 Part I: 2002**).



Source: Google

Fig: - 1.4 Seismicity map

ZONE	INTENSITY
ZONE - V	<b>Very High-Risk Zone</b> Area liable to shaking IX (and above)
ZONE - IV	<b>High Risk Zone</b> Intensity VIII
ZONE - III	<b>Moderate Risk Zone</b> Intensity VII
ZONE II	<b>Low Risk Zone</b> VI (and lower)

Fig: - 1.5 Seismicity Zone value

### **1.3.5 Hydrological Network**

The Subansiri River, the largest tributary of the Brahmaputra River, plays a critical role in the intricate drainage system of the region. Originating from the western part of Mount Pororu (5059 m) in the Tibetan Himalayas, it is a trans-Himalayan River with a complex network of tributaries, including the Dikrong, Ranganadi, Ghagar, Kamala, and Sampara rivers. These tributaries, which exhibit both meandering and braided patterns, contribute to the dynamic hydrology of the basin. The Subansiri–Ranganadi–Dikrong system merges into the Brahmaputra, creating an intricate drainage network that controls the region's main hydrological dynamics. The river's flow is generally perennial, with peak discharge occurring during the monsoon season. However, smaller streams in the foothills often dry up during March and April. The riverbed and banks are composed predominantly of boulders, cobbles, pebbles, and sands of varying grades, with minimal clay content. This geological composition, combined with the hydrological dynamics, amplifies challenges related to flooding and erosion, particularly during periods of heavy rainfall.

## CHAPTER 2

### MATERIALS

---

#### 2.1 DIGITAL ELEVATION MODEL (DEM)

A Digital Elevation Model (DEM) serves as a 3D representation of the Earth's surface, created using elevation data. In ArcGIS, DEMs are extensively utilized in a range of geospatial and environmental analyses, including hydrological modeling, terrain visualization, and spatial planning. They are fundamental in deriving key topographical attributes such as slope, aspect, and watershed boundaries, which are crucial for understanding the physical characteristics of an area. ArcGIS provides an array of tools to process DEMs, allowing users to create visual outputs like hillshades, contours, and 3D terrain models. These outputs enhance the interpretation of terrain features and assist in decision-making for projects related to land management, disaster mitigation, and infrastructure planning. For hydrological studies, DEMs are indispensable as they enable the modeling of water movement across the surface, helping to predict flood zones, delineate drainage networks, and identify catchment areas. High-resolution DEMs, like those derived from the Shuttle Radar Topography Mission (SRTM), are particularly valuable for detailed and precise analysis, ensuring the accuracy of results in applications such as erosion modeling and urban planning. The extracted raster DEM in this study was processed in ArcGIS 10.4 using established protocols.

It follows the **WGS 1984** spatial reference coordinate system and has been projected to the **UTM Zone 46N** projection system to ensure compatibility with other geospatial datasets and accurate spatial analysis. In the context of the Revised Universal Soil Loss Equation (RUSLE) model, DEMs play a vital role in assessing soil erosion by facilitating the calculation of the topographic factor, commonly referred to as the LS factor. This factor quantifies the combined effects of slope length and steepness on erosion rates, both of which are derived directly from DEM analysis. Using spatial analysis tools in ArcGIS, slope maps and flow accumulation maps are generated, and these layers are integrated to compute the LS factor, identifying areas at higher risk of erosion. Furthermore, DEMs aid in delineating watersheds and understanding surface runoff dynamics, which are essential for accurate soil erosion modeling. To ensure reliability in the RUSLE model, the DEM must be of high resolution and free from anomalies such as sinks or spikes, as these errors can skew the calculation of slope and flow direction. By providing a detailed representation of terrain, DEMs enhance the precision of erosion predictions, aiding in effective soil conservation and watershed management efforts.

File Name	Source	Format	Resolution	Description
n26_e093_1arc_v3.tif	USGS Earth Explorer ( <a href="https://earthexplorer.usgs.gov/">https://earthexplorer.usgs.gov/</a> )	TIF	30 meters	Covers the southern part of the study area with longitude 93°E and latitude 26°N.
n26_e094_1arc_v3.tif	USGS Earth Explorer ( <a href="https://earthexplorer.usgs.gov/">https://earthexplorer.usgs.gov/</a> )	TIF	30 meters	Represents the southern part of the study area with longitude 94°E and latitude 26°N.
n27_e093_1arc_v3.tif	USGS Earth Explorer ( <a href="https://earthexplorer.usgs.gov/">https://earthexplorer.usgs.gov/</a> )	TIF	30 meters	Covers the northern part of the study area with longitude 93°E and latitude 27°N.
n27_e094_1arc_v3.tif	USGS Earth Explorer ( <a href="https://earthexplorer.usgs.gov/">https://earthexplorer.usgs.gov/</a> )	TIF	30 meters	Represents the northern part of the study area with longitude 94°E and latitude 27°N.

Table: - 2.1 DEM specifications data

## 2.2 PRECIPITATION DATA FROM NETCDF DATA

The NetCDF files containing precipitation data from the **Climatic Research Unit (CRU) TS v4.08** dataset, specifically the files **cru\_ts4.08.2021.2023.pre.dat.nc.gz** and **cru\_ts4.08.2011.2020.pre.dat.nc.gz**, provide high-resolution global precipitation data with a spatial resolution of **0.25° x 0.25° grid cells**. These files store monthly precipitation totals over the periods **2011-2020 and 2021-2023**, offering essential data for analyzing rainfall patterns and their impact on soil erosion. The data is organized in a multidimensional format, with time as one dimension and latitude and longitude coordinates as the others, making it efficient for large datasets. The .gz compression further reduces file size for easier handling.

Feature	Description
Dataset Name	CRU TS v4.08 Precipitation Data
Files	<b>cru_ts4.08.2021.2023.pre.dat.nc.gz, cru_ts4.08.2011.2020.pre.dat.nc.gz</b>
Data Type	Monthly Precipitation Data (in mm)
Spatial Resolution	<b>0.25° x 0.25° grid cells</b>
Temporal Resolution	Monthly Precipitation Totals
Time Period	2011-2020 (for one file), 2021-2023 (for the other file)
Data Format	<b>NetCDF (Network Common Data Form)</b>
Compression Format	<b>.gz (gzip compressed)</b>
Data Structure	Multidimensional format: time (monthly totals), latitude, and longitude
Primary Use in RUSLE	Used to calculate the R-factor, which quantifies rainfall's erosive potential in the RUSLE model.

Table: - 2.2 DEM features data

In the **Revised Universal Soil Loss Equation (RUSLE)** model, the CRU precipitation data is crucial for calculating the **R-factor**, which quantifies rainfall's erosive potential. With the high spatial resolution and monthly temporal data, users can accurately model rainfall intensity and erosivity, essential components of the R-factor. ArcGIS provides built-in tools like **Multidimensional Raster** or **Rasterize (NetCDF)** to import, extract, and process this data, converting it into raster format for spatial analysis. The precipitation data can be combined with other GIS layers, such as **Digital Elevation Models (DEMs)** or land-use maps, to conduct detailed soil erosion assessments.

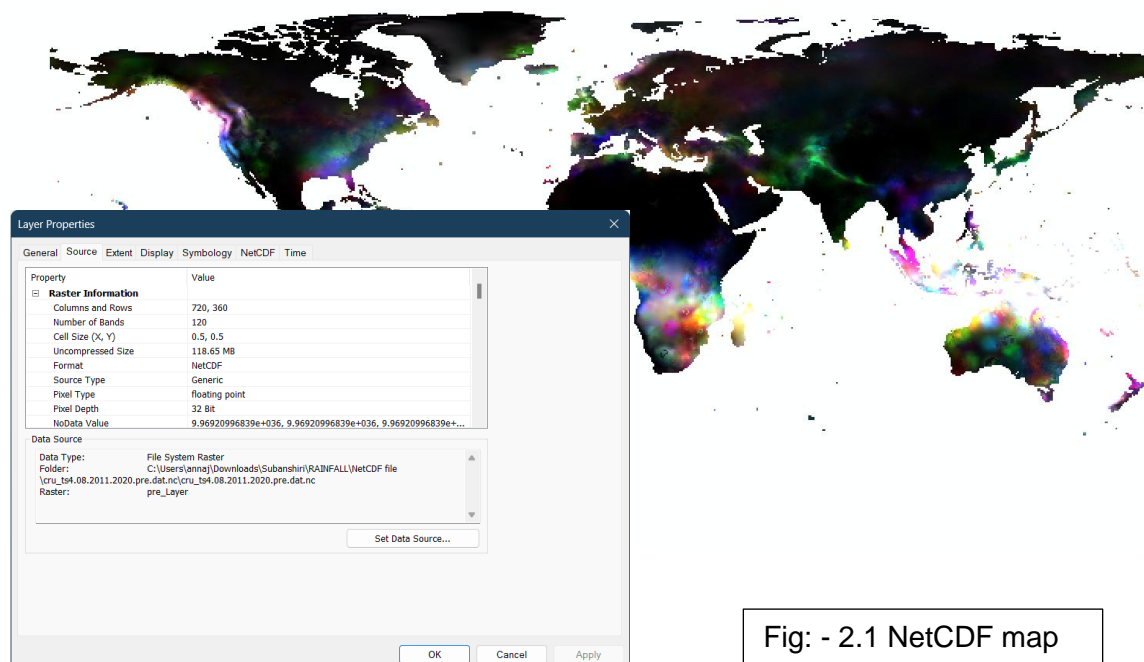


Fig: - 2.1 NetCDF map

By integrating this precipitation data with other **RUSLE factors** such as the **K-factor** (soil erodibility), **C-factor** (cover management), and **P-factor** (support practice), users can generate **R-factor maps** and estimate potential soil erosion rates across regions. The **CRU TS v4.08** dataset's consistency and reliability, along with its comprehensive metadata, ensure that the precipitation data is accurately interpreted for precise environmental modeling. Using these **NetCDF files** in ArcGIS improves the effectiveness of soil erosion risk assessments, making them a valuable tool for environmental management.

### 2.3 LANDSAT IMAGE

Landsat images, such as **LC08\_L2SP\_135041\_2014**, **LC08\_L2SP\_135041\_2022**, and **LC08\_L2SP\_135041\_2023**, play a crucial role in the **Revised Universal Soil Loss Equation (RUSLE)** model by providing high-resolution multispectral data for assessing vegetation, land use, and cover changes. These datasets, acquired from **USGS Earth Explorer**, have a **30-meter spatial resolution**, making them ideal for detailed spatial analysis. One of the primary applications of Landsat data in RUSLE is the calculation of the **C-factor** (cover management). This factor reflects the protective effects of vegetation on soil against erosion. Using Landsat’s red and near-infrared (NIR) bands, the **Normalized Difference Vegetation Index (NDVI)** is derived to estimate vegetation density and health. Higher NDVI values correspond to dense vegetation, which reduces soil erosion, while lower values indicate sparse or no vegetation, leading to higher erosion risk.

Table: - 2.3 Wavelength with band no

Band No.	Wave length (µm)	Color
2	0.45-0.495	Blue
3	0.52-0.60	Green
4	0.63-0.69	Red
5	0.78-0.86	Near-infrared

In addition to the C-factor, Landsat data is used for land-use classification to evaluate the **P-factor** (support practices), which accounts for conservation measures like terracing or contour plowing that reduce soil loss. Historical datasets such as the 2014, 2022, and 2023 images enable the study of temporal changes in land cover and management practices, improving the precision of erosion risk assessments. The workflow includes downloading the images, preprocessing steps like **atmospheric correction** and **cloud masking**, extracting indices like NDVI, and integrating the results into GIS platforms such as ArcGIS. This integration facilitates combining the calculated C-factor and P-factor with other RUSLE factors (R, K, and LS) to produce accurate soil erosion models that guide effective land management strategies.

Table: - 2.4 LANDSAT features data

Feature	Description
Datasets Used	LC08_L2SP_135041_2014, LC08_L2SP_135041_2022, LC08_L2SP_135041_2023
Source	USGS Earth Explorer
Spatial Resolution	30 meters
Bands Used	Red, Near-Infrared (NIR), Green
Primary Indices Derived	<b>Normalized Difference Vegetation Index (NDVI)</b>
Temporal Analysis	Historical land cover changes (2014, 2022, 2023) for erosion risk assessment

### 2.3.1 DETAILED DESIGNATION OF LANDSAT SATELLITES

Landsat satellite band designations define the spectral ranges captured by sensors, each optimized for specific wavelengths. These bands facilitate the analysis of environmental and surface features, supporting applications like vegetation monitoring, water mapping, urban studies, and atmospheric observations, making them essential for Earth monitoring.

**Landsat 7 Enhanced Thematic Mapper Plus (ETM+)** images consist of eight spectral bands. All of the bands can collect one of two gain settings (high or low) for increased radiometric sensitivity and dynamic range, while Band 6 collects both high and low gain for all scenes. The approximate scene size is 170 km north-south by 183 km east-west (106 mi by 114 mi).

Bands	Wavelength (micrometers)	Resolution (meters)
Band 1 - Blue	0.45-0.52	30
Band 2 - Green	0.52-0.60	30
Band 3 - Red	0.63-0.69	30
Band 4 - Near Infrared (NIR)	0.77-0.90	30
Band 5 - Shortwave Infrared (SWIR) 1	1.55-1.75	30
Band 6 - Thermal	10.40-12.50	60 (resampled to 30)*
Band 7 - Shortwave Infrared (SWIR) 2	2.09-2.35	30
Band 8 - Panchromatic	.52-.90	15

**Landsat 8 and Landsat 9 Operational Land Imager (OLI) and Thermal Infrared Sensor (TIRS)** images consist of nine spectral bands, and two thermal bands. The approximate scene size is 170 km north-south by 183 km east-west (106 mi by 114 mi).

Bands	Wavelength (micrometers)	Resolution (meters)
Band 1 - Coastal aerosol	0.43-0.45	30
Band 2 - Blue	0.45-0.51	30
Band 3 - Green	0.53-0.59	30
Band 4 - Red	0.64-0.67	30
Band 5 - Near Infrared (NIR)	0.85-0.88	30
Band 6 - Shortwave Infrared (SWIR) 1	1.57-1.65	30
Band 7 - Shortwave Infrared (SWIR) 2	2.11-2.29	30
Band 8 - Panchromatic	0.50-0.68	15
Band 9 - Cirrus	1.36-1.38	30
Band 10 - Thermal Infrared (TIRS) 1	10.6-11.19	100 (resampled to 30)*
Band 11 - Thermal Infrared (TIRS) 2	11.50-12.51	100 (resampled to 30)*

Table: - 2.5 LANDSAT image features as per resolution

## **2.4 SOIL DATA**

For calculating the Soil Erodibility Factor (K-factor) in the Revised Universal Soil Loss Equation (RUSLE) model, soil data is sourced from the FAO-UNESCO Soil Map of the World, supplemented and verified using Indian Soil Data from the Bhuvan Indian Geo-platform developed by ISRO. The FAO soil dataset provides globally consistent soil properties, such as texture, organic matter content, permeability, and structure, which are essential for estimating soil erodibility. This data forms the foundation for initial assessments, especially in areas where localized soil information is limited. To enhance accuracy, the FAO data is cross-verified and refined using detailed soil information from Bhuvan, which offers high-resolution, region-specific soil maps for India. This integration ensures that the K-factor calculations reflect local soil conditions, improving the precision of erosion risk assessments. The workflow involves preprocessing the soil datasets, extracting relevant soil parameters, and integrating them into GIS platforms to calculate the K-factor, which is then combined with other RUSLE factors for comprehensive soil erosion modeling.

## CHAPTER 3

# LITERATURE REVIEW

### 3.1 SOIL FORMATION AND ITS HISTORY

Soil is a mixture of organic matter, minerals, gases liquids and organisms that together support life. Soil is a formation of several factors: the influence of climate, relief (elevation, orientation and slope of terrain), organisms and the soil's parent materials (original minerals) interacting over time.

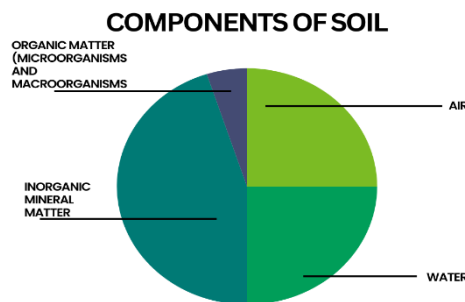


Fig: - 3.1 Soil components

Soil formation is a complex natural process driven by the weathering of parent rock material under the influence of physical, chemical, and biological factors. Weathering breaks down rocks into smaller particles through mechanical processes like temperature fluctuations, freeze-thaw cycles, and abrasion, as well as chemical processes such as oxidation, hydrolysis, and carbonation. Over time, organic matter from decomposing plants and animals integrates with the mineral particles, enhancing the soil's fertility and structure. This results in the development of distinct soil horizons, including the top organic-rich layer (O-horizon), the mineral-rich surface soil (A-horizon), and deeper layers like the subsoil (B-horizon) and parent material (C-horizon). The formation of soil is influenced by climate, organisms, topography, parent material, and time, collectively known as the soil-forming factors. This process plays a pivotal role in supporting ecosystems, agriculture, and sustainable land management, making its understanding critical for environmental and soil erosion studies.

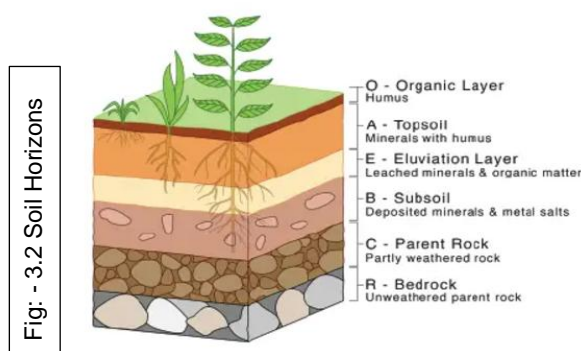


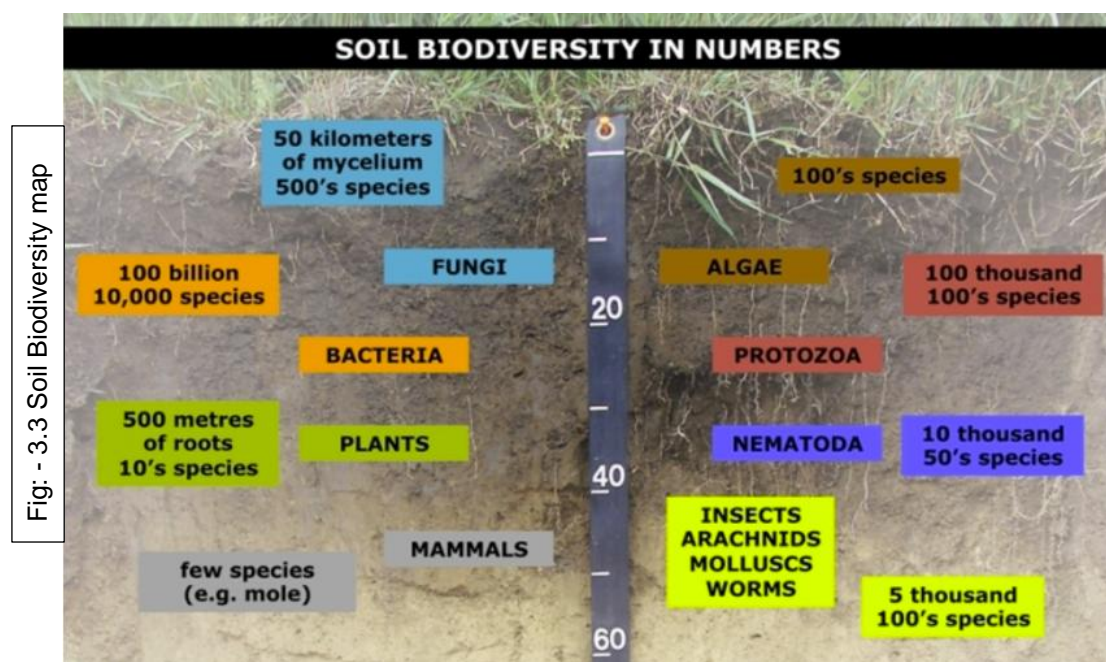
Fig: - 3.2 Soil Horizons

**O – HORIZON:** leaf litter, organic material  
**A – HORIZON:** PLOUGH ZONE, RICH IN ORGANIC MATTER  
**B-HORIZON:** ZONE OF WEATHERING  
**C-HORIZON:** WEATHERING SOIL; LITTLE ORGANIC MATERIAL OR LIFE  
**R-HORIZON:** UNWEATHERED PARENT MATERIAL

## 3.2 ROLE OF SOIL BIODIVERSITY

A healthy soil biota thrives when provided with a suitable habitat, characterized by the intricate pore network of soil that regulates the availability of gases, water, solutes, and organic substrates (Lavelle et al.). This network creates the foundation for soil life, allowing for diverse biological activity. The interactions between soil biodiversity and its functions are complex and often surpass those observed in aboveground ecosystems (Bardgett and van der Putten). These interactions can be understood through three key mechanisms: **repertoire**, which emphasizes the necessity of specific organisms for particular processes; **interactions**, illustrating how soil organisms positively or negatively influence each other; and **redundancy**, which ensures process stability even if some organisms are lost, as others step in to maintain functionality (Nielsen et al.).

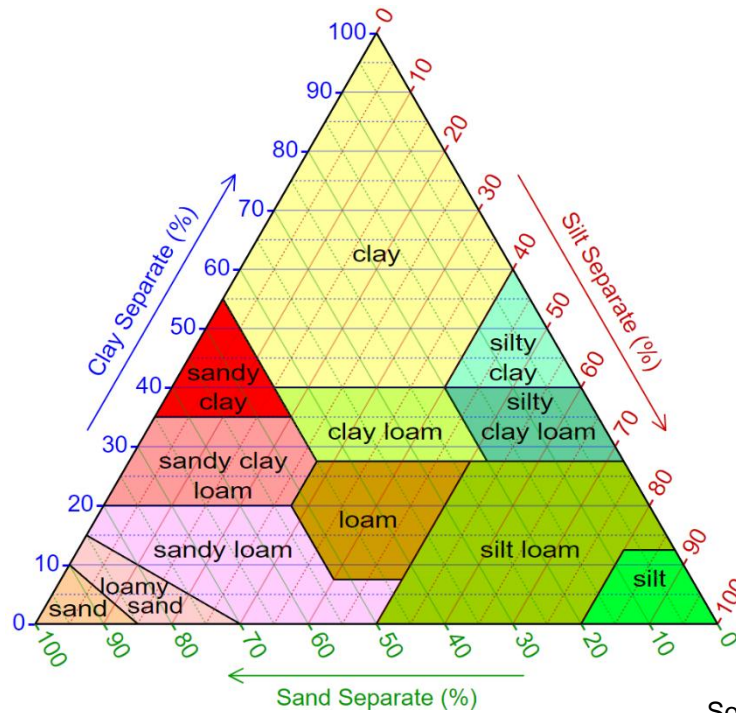
The functional repertoire of soil organisms plays a more critical role than richness alone. Processes such as decomposition exhibit high redundancy, involving numerous organisms capable of maintaining function despite biodiversity loss (Schimel et al.). In contrast, specialized processes like nitrification, carried out by fewer bacteria, or highly specific symbiotic relationships like orchid mycorrhizas, rely on organisms with little or no redundancy (Smith and Read). Biodiversity loss affects these processes differently; redundant functions often remain stable, while unique interactions, when disrupted, can destabilize ecosystems. Although significant declines in soil diversity can impair certain processes, particularly in simplified systems, natural ecosystems typically display resilience due to their inherent biodiversity and functional complexity (Tilman et al.). Generally, 1 gram of soil has over 50,000 protozoa as well as bacteria, algae, fungi, earthworms and nematodes.



### 3.3 SOIL CLASSIFICATION

Soil classification (or soil taxonomy) deals with the systematic categorization of soils based on distinguishing characteristics as well as criteria that dictate choices in use

The grouping of soil is based on chemical, physical and biological properties and World Reference Base for Soil Resources.



Source: Research Gate

Fig: - 3.4 Soil classification chart

### 3.4 SOIL DEGRADATION

Soil degradation is the decline in soil condition caused by its improper use of poor management, usually for agricultural, industrial or urban purposes. It is serious environmental problem. Soils are a fundamental natural resource and are the basis for all terrestrial life. Avoiding soil degradation is crucial to our well-being.

### 3.4.1 Types of soil degradation

**Water Erosion:** The removal of topsoil by surface runoff, forming rills and gullies, significantly reducing soil productivity.

**Wind Erosion:** The detachment and transportation of soil particles by wind, often leading to loss of nutrients and desertification in arid regions.

**Chemical Degradation:** Includes processes like salinization (salt accumulation), acidification (lowering of pH), and nutrient depletion, all of which reduce soil fertility.

**Physical Degradation:** Caused by compaction, crusting, and waterlogging, leading to reduced porosity and aeration, hindering plant growth.

**Deforestation:** The removal of forest cover exposes soil to erosion and depletes organic matter, making the soil prone to degradation.

## 3.5 SOIL EROSION

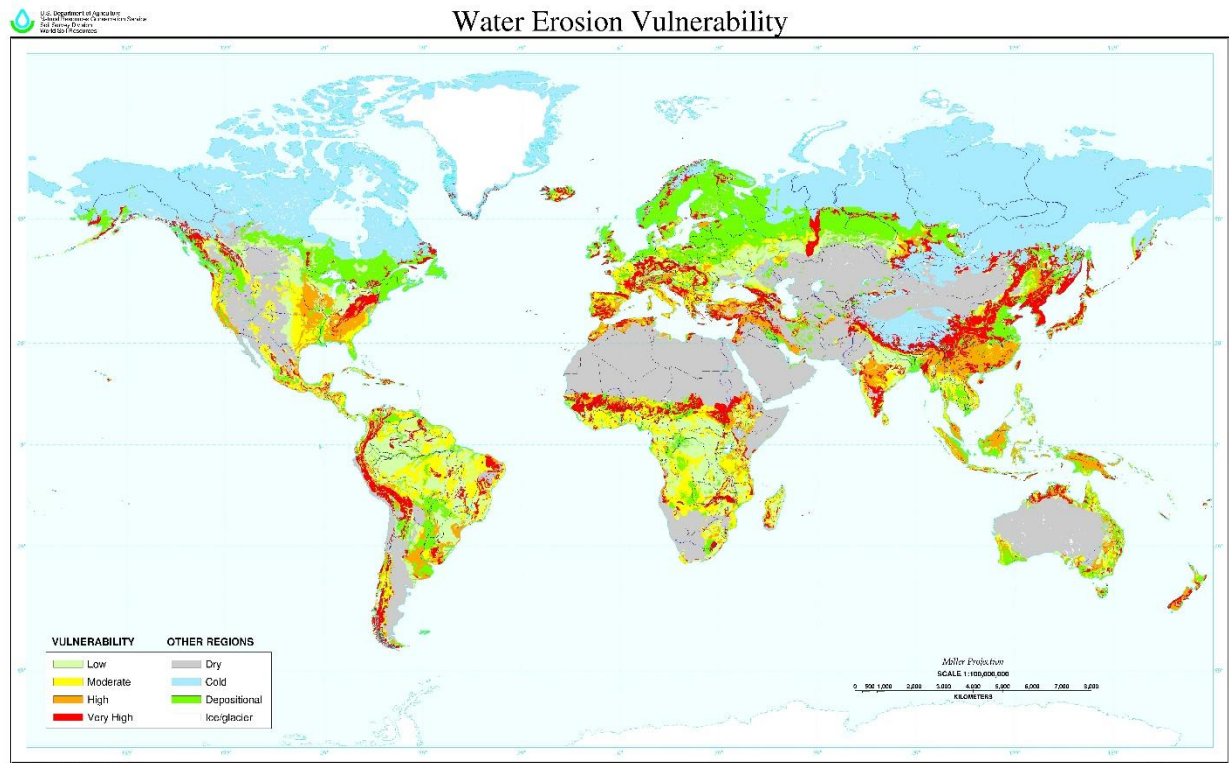
The soil erosion is detachment and subsequent removal of soil particles from terrain surface due to the action of physical forces such as rainfall, runoff and wind.

Soil is naturally removed by the action of water or wind: such **‘background’/‘geological’** soil erosion has been occurring for some 450 million years. In general, background erosion removes soil at roughly the same rate as soil is formed.

**‘Accelerated’** soil erosion – loss of soil at a much faster rate than it is formed – is a far more recent problem. It is always a result of mankind’s unwise actions, such as overgrazing or unsuitable cultivation practices.

- Globally, almost 84% of land loss results from soil erosion processes.
- The estimated mean rates of soil erosion across the world range between 12 and 15 ton/ha/year.

### 3.5.1 SOIL EROSION VULNERABILITY MAP



Source: Google

Fig: - 3.5 Erosion vulnerability map

### 3.5.2 EROSION AND ITS TYPES

- Wind Erosion
- Water Erosion

**Wind erosion** occurs when soil particles are detached and transported by wind, primarily in dry, sparsely vegetated areas. It involves processes like saltation, suspension, and surface creep, driven by factors such as high wind velocity and low soil moisture. Wind erosion depletes topsoil, reduces fertility, and contributes to desertification and dust pollution, impacting agriculture and infrastructure. Effective control measures include maintaining vegetation cover, minimizing soil disturbance, and using windbreaks to reduce erosion.

**Water erosion** is the removal of the top layer of land by water from irrigation, rainfall, snowmelt, runoff and poor irrigation management.

Here rainwater is most frequently to blame when it comes to this issue. The flowing water moves the soil organic and inorganic particles alongside the land surface, depositing them in the lower landscape. The result of this would be flooding in the long run.

### 3.5.2.1 Water Erosion and its Types

Source: Wikipedia

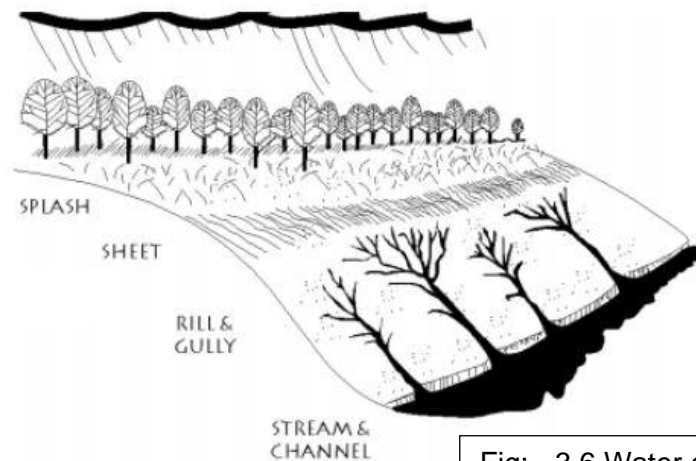


Fig: - 3.6 Water erosion sketch

There are several types of water erosion.

- Sheet and rill erosion
- Scalding
- Gully erosion
- Tunnel erosion
- Stream and bank erosion
- Mass movement

**Sheet erosion** occurs when a thin layer of topsoil is removed over a whole hillside paddock – and may not be readily noticed.

**Scalding** can occur when wind and water erosion removes the top soil and exposes saline or sodic soils.

**Gully erosion** happens when runoff concentrates and flows strongly enough to detach and move soil particles

**Tunnel erosion** is the removal of subsoil. When water penetrates through a soil crack or a hole where a root has decayed the soil disperses and is carried away with the flow to leave a small tunnel.

**Stream bank erosion** is the destruction of vegetation on river banks (generally by clearing, overgrazing, cultivation, vehicle traffic up and down banks or fire) and the removal of sand and gravel from the stream bed.

**Mass movement** occurs on cleared slopes in coastal areas. Gravity moves earth, rock and soil material downslope both slowly (mm per year) and suddenly (eg rock falls)

Here, Streambank erosion is a significant geomorphological process in the Subansiri Basin of Assam, driven by the dynamic nature of the **Subansiri River** and its tributaries. This basin, part of the Brahmaputra River system, experiences intense monsoonal rainfall, which leads to high river discharge and strong hydraulic forces eroding the banks. The erosion is exacerbated by the friable and alluvial nature of the soil, which offers limited resistance to water flow. Human activities, including agriculture and settlement along the riverbanks, further destabilize the soil structure by removing vegetation that would otherwise provide cohesion and reduce erosion. Additionally, fluctuations in river flow due to hydropower projects or sediment transport alter the river's equilibrium, contributing to bank instability. Streambank erosion in the Subansiri Basin not only threatens agricultural land and infrastructure but also disrupts ecosystems and increases sediment load in the river, affecting downstream hydrodynamics and flood patterns. Managing this erosion requires a combination of bioengineering solutions, sustainable land-use practices, and continuous monitoring of hydrological changes.



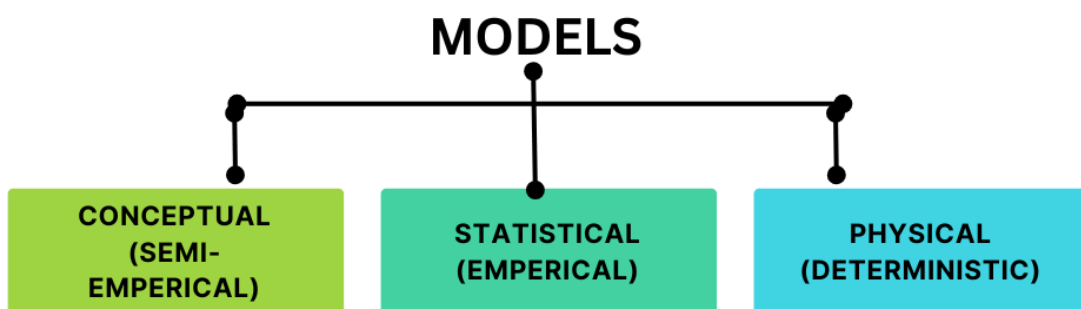
Fig: - 3.7 Soil erosion at study area

SOURCE: THE SENTINEL

### 3.6 EROSION MODEL

An erosion model is a predictive tool designed to estimate soil loss and sediment yield caused by water, wind, or other natural forces. These models are utilized in various fields, including agriculture, civil engineering, and environmental science, to assess the impacts of erosion on landscapes, water quality, and infrastructure. Erosion models simulate the processes that lead to soil detachment, transportation, and deposition. Factors influencing these processes—such as rainfall intensity, soil type, topography, vegetation cover, and land use—are incorporated into the model equations to provide accurate predictions. Common examples include empirical models like the Universal Soil Loss Equation (USLE) and more sophisticated, process-based models like the Soil and Water Assessment Tool (SWAT).

Erosion models play a vital role in land management and environmental conservation by helping to design effective erosion control measures and strategies. They assist policymakers, engineers, and researchers in assessing the risks associated with soil degradation and sedimentation. In particular, these models are crucial for planning agricultural practices, designing sediment retention structures, and mitigating the environmental impacts of construction projects. By understanding the potential extent of erosion, decision-makers can implement preventive actions, such as afforestation, terracing, or improved drainage systems, to preserve soil resources and maintain ecological balance. As there are number of soil erosion models developed in recent decades.



Lists of the top 25 most applied soil erosion prediction models according to the records reported in the GASEMT database

Model	Records	%	References
RUSLE	507	17.1	Renard et al., 1997
USLE	412	13.9	Wischmeier and Smith, 1978
WEPP	191	6.4	Laflen et al., 1991
SWAT	185	6.2	Arnold et al., 2012
WaTEM/SEDEM	139	4.7	Van Oost et al., 2000
RUSLE-SDR	115	3.9	–
USLE-SDR	64	2.2	–
LISEM	57	1.9	De Roo et al., 1996
Customized approach	53	1.8	–
MUSLE	52	1.7	Williams and Berndt, 1977
MMF	48	1.6	Morgan et al., 1984
AnnAGNPS	47	1.6	Young et al., 1989
RHEM	44	1.5	Nearing et al., 2011
Unknown	36	1.2	–
Erosion 3D	29	1	Schmidt, 1991
EPIC	25	0.8	Williams et al., 1983
PESERA	23	0.8	Govers et al., 2003
USPED	22	0.7	Mitasova et al., 1996
GeoWEPP	20	0.7	Renschler, 2003
RUSLE2	20	0.7	Foster et al., 2001
EPM	19	0.6	Gavrilovic, 1962
STREAM	19	0.6	Cerdan et al., 2002
RUSLE/SEDD	16	0.5	Ferro and Porto, 2000
DSESYM	15	0.5	Yuan et al., 2015
EUROSEM	15	0.5	Morgan et al., 1998

Table: - 3.1 GASEMAT database

### 3.6.1 EMPIRICAL MODELS (STATISTICAL)

Empirical models rely on statistical relationships between input and output data without explaining the underlying system. These models address immediate, on-site erosion concerns, particularly related to agricultural productivity and sustainability (e.g., EUROSEM and USLE; Wischmeier and Smith, 1978).

### 3.6.2 PHYSICAL MODELS (DETERMINISTIC)

Physical models, also referred to as formal models, use physical or mathematical analogs to represent erosion processes. They simulate soil particle movement through mathematical equations and aim for universal applicability. Examples such as CREAMS (Knisel, 1980) and WEPP (Laflen et al., 1991) are instrumental in assessing land management impacts under varying conditions, including storms of different intensities.

### **3.6.3 HYBRID MODELS (SEMI-EMPERICAL)**

Hybrid models combine empirical approaches with process-based equations, focusing on spatially distributed water and sediment dynamics. Examples include RUSLE1 and RUSLE2 (Renard et al., 1997; Foster et al., 2001), which enhance predictive capabilities by integrating the strengths of both methods.

### **3.6.4 MODEL AND ITS IMPORTANCE**

#### **3.6.4.1 USLE**

Usle is an empirical model for annual estimate of soil erosion and was further modified as MUSLE and RUSLE. It is a simple model for predicting soil erosion considering rainfall, soil erodibility, land cover, topography and flow rate (for MUSLE) data.

USLE is not event-based and cannot quantify the events that are likely to result in large- scale erosion. The use of slope length factor in RUSLE enables the prediction of soil loss due to overland flow but is mostly applied to agricultural land of gentle slope angle not more than 25° and does not estimate gully or stream channel erosion caused by raindrops.

#### **3.6.4.2 SWAT**

It is a physical model for predicting the impact of land management practices on hydrology, sediment and contaminant transport in large river basins over a long period with integration of drainage, topography, soil, land use and rainfall information

It has different applications such as climate change, land-use change, evapotranspiration assessment, ground or soil water impact, snowmelt process, etc. Although storm event based, high and peak flows are not well simulated by the model.

#### **3.6.4.3 WEPP**

Physical model for predicting spatial and temporal distribution of soil loss, sediment yield, sediment size characteristics, run-off volume, and soil-water balance.

Predictions of the location of sediment deposition and detachment are very effective, but the large computational data requirement of the model limits its applicability.

### 3.6.4.4 EROSION 3D

It is a process-based model for calculating runoff, channel routing and transportation and deposition of sediment.

Its requirement for few data and its compatibility with GIS make it flexible in estimating erosion as its calculation is based on a regular grid, and its disadvantage of this model is similar to the WATEM/SEDEM model.

### 3.6.4.5 MCE (AHP/WIO)

MCE is a qualitative assessment process. It is a probability weighted approach that allows a linear combination of probability weights of several thematic maps. The weightages of individual themes and feature scores are fixed and added to the layer by considering its role in soil erosion.

It is an integrated assessment approach used for identifying a solution with respect to multiple complex problems. It can provide a rationale for making the best decision.

## 3.7 R.U.S.L.E MODEL (REVISED UNIVERSAL SOIL LOSS EQUATION)

RUSLE model is an upgraded version of USLE with higher accuracy. It is an equation that estimates average annual soil loss by sheet and rill erosion on those areas where erosion (but not deposition) is occurring. It estimates long-term average annual soil loss (A) from raindrop impact and runoff on specific slopes under various cropping and management systems (Renard et al., 1997). RUSLE is widely used for planning soil conservation measures, assessing soil erosion impacts, and informing policies on soil management. RUSLE is expressed as

$$A = R * K * (L * S) * C * P$$

where,

- **A**: Average annual soil loss (tons/ha/year)
- **R**: Rainfall and runoff erosivity ( $\text{MJ} \cdot \text{mm} \cdot \text{ha}^{-1} \cdot \text{h}^{-1} \cdot \text{yr}^{-1}$ )
- **K**: Soil erodibility ( $\text{Mg} \cdot \text{h} \cdot \text{MJ}^{-1} \cdot \text{mm}^{-1}$ )
- **LS**: Slope length and steepness factor (dimensionless)
- **C**: Cover-management factor (dimensionless)
- **P**: Support practice factor (dimensionless).

Importance of RUSLE –

- It provides expanded information on soil erodibility.
- A slope length factor that varies with soil susceptibility to rill erosion.
- It improved factor values for the effects of contouring terracing, strip cropping and management practices for rangeland.
- A sub factor method for computing for the cover management factor.

### 3.7.1 COMBINATION OF RUSLE AND GIS

- It contains low availability of input data
- The conventional methods are more reliable and accurate but too expensive and time consuming
- With the help of RS and GIS soil erosion modelling can be fast and cheap on a large scale of territory

## 3.8 RUSLE FATORS

### 3.8.1 RAINFALL EROSIIVITY (R) FACTOR

The rainfall erosivity factor (**R**)\_quantifies rain's ability to detach soil particles based on the amount and intensity of rainfall (Wischmeier and Smith, 1978; Arnoldus, 1980). It accounts for the impact of raindrops on the soil and the associated runoff, requiring detailed, continuous precipitation data. Annual rainfall erosivity represents the cumulative erosivity of all rainfall events within a year.

This factor is crucial for assessing soil erosion risks, particularly under varying land-use practices and climate change scenarios. Rainfall, being a primary driver of water erosion, makes **R** an essential parameter in evaluating soil conservation needs and understanding erosion processes at specific locations.

equation –

$$\mathbf{R} = \sum_{i=1}^{12} 1.735 * 10 (1.5 * \log_{10} \left( \frac{P_i^2}{P} \right) - 0.08188 )$$

where:

**P<sub>i</sub>** is a monthly rainfall (mm)

**P** annual rainfall (mm)

Here are some data where R values is implemented according to countries specification.

Country	R Formula
Zimbabwe	$R = 38.5 + 0.35 M$
Marrocco	$R = 2.8959X * 0.002983 M$
USA	$R = 1.24 * M^{1.36}$
Central Asia	$R = 0.04830 M^{1.61}$

Table: - 3.2 R formula as per locations

### 3.8.2 SOIL ERODIBILITY (K) FACTOR

The soil erodibility which reflects the rate of soil loss depending on the erosion (R factor), and calculated on the basis of soil textures, is an empirical measure of soil erosion and represents the susceptibility of the soil to erosion.

The structure and permeability of the soil profile and organic matter are the main soil properties affecting K, and the value of K is characterized by the soil texture and permeability of organic compounds depending on the soil type and is modeled with the aid of an equation.

It quantifies the potential and rate of soil erosion caused by rainfall under typical conditions. It also indicates how easily soil can be eroded and its ability to transport sediment (Ganasri and Ramesh, 2016). A key component of erosion models like the RUSLE (Revised Universal Soil Loss Equation), the K factor is essential for estimating soil loss (Hudson, 1981).

Factors such as soil organic matter, texture, structure, and permeability influence soil erodibility. Unlike many earlier studies that relied on secondary data, this research took a more precise approach by conducting field measurements. Soil samples were collected from various physiographic zones in the Kurumali watershed to analyze parameters like organic matter content, texture, structure, and permeability.

The K factor was calculated using **Wischmeier's (1974)** equation in an Excel spreadsheet

$$K = \frac{2.1 \times 10^{-4} \cdot (12 - a) \cdot M^{1.14} + 3.25 \cdot (b - 2) + (c - 3)}{759.4}$$

where:

**K = soil erodibility (tons·yr/MJ·mm)**

**M = (% silt + % very fine sand) × (100 - % clay)**

**a = percentage of organic matter in the soil**

**b = structural class value**

**c = permeability class value**

Soil structure codes (b) range from 1 (fine granular) to 4 (blocky or massive), while permeability (c) ranges from 1 (rapid) to 6 (very slow). Laboratory analyses were conducted to determine soil texture and organic carbon, using the Walkley-Black method for organic carbon and the international pipette method for texture. The results were input into the formula to compute the K factor, which was further integrated into a spreadsheet and linked with sample location data in ArcGIS for spatial analysis.

Another formula proposed by **Merzouk (1985)**

$$K = 311.63 - 4.48 * (SG \% + S\%) + 613.4 + 6.45 * EC,$$

where,

SG is the coarse sand content (in %)

S is the sand content (in %)

EC is the electrical conductivity

Formula proposed by **Williams (1995)**

$$K_{USLE} = K_W = F_{csand} * F_{cl-si} * F_{orgc} * F_{hisand}$$

$$F_{csand} = ( 0.2 + 0.3 \exp [ -0.256 * m_s * (1 - \frac{m_{silt}}{100}) ] )$$

$$F_{cl-si} = ( \frac{m_{silt}}{m_c + m_{silt}} )^{0.3}$$

$$F_{orgc} = ( 1 - \frac{0.250egC}{orgC + \exp[3.72 - 2.95 X orgC]} )$$

$$F_{hisand} = ( 1 - \frac{0.7 X (1 - \frac{m_s}{100})}{(1 - \frac{m_s}{100}) + \exp[-5.51 + 22.9 (1 - \frac{m_s}{100})]} )$$

## Defined K factor

<i>Utilized K factor for different soil groups (adopted from Dogan et al., 2000)</i>	
<b>Soil types</b>	<b>K factor (tons/MJ h/mm)</b>
Basaltic soils	0.014
Lime - free brown soils	0.021
Red mediterranean soils	0.017
Lime - free brown forest soils	0.031
Brown forest soils	0.024
Reddish brown soils	0.027
Red - brown mediterranean soils	0.022
Brown soils	0.023
Colluvium soils	0.021
Alluvium soils	0.043
Coal pit	0.052
Settlement	0.001
Bareland	0.0065

Table: - 3.3 K-factor data as per soil properties

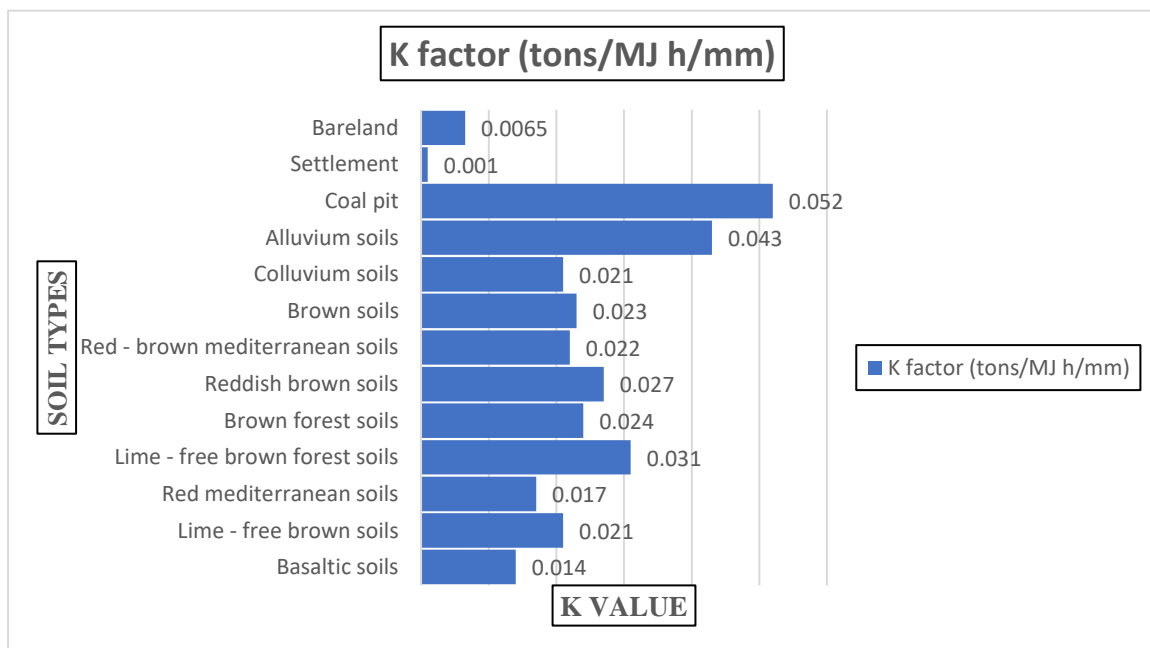


Fig: - 3.8 K - FACTOR CHART

### 3.8.3 SLOPE LENGTH AND SLOPE STEEPNESS (LS) FACTOR

The **L** (slope length) and **S** (slope steepness) factors in the RUSLE represent topographic influences on soil erosion, accounting for the effects of slope length and gradient on sheet and rill erosion (Renard et al., 1997). The slope length factor (**L**) is defined as the horizontal distance from the point where overland flow begins to where runoff either starts deposition or enters a defined channel. The slope steepness factor (**S**) quantifies the impact of slope gradient on erosion intensity. Together, these factors determine the **LS** topographic factor, which reflects how slope length and steepness influence soil loss.

As slope length and steepness increase, soil loss per unit area also rises, emphasizing their significance in soil erosion modeling. For instance, the ratio of soil loss under specific conditions, such as a 9% slope gradient and a 22.13-meter slope length, illustrates the combined effect of these factors. The **LS** factor is typically calculated using digital elevation models (DEMs) and geospatial tools like ArcGIS hydrology functions (Desmet and Govers, 1996). High-resolution DEMs, such as those created from Cartosat-1 satellite imagery with 30-meter resolution (USGS), enable precise assessment of topography's role in erosion modeling and runoff transport capacity. The slope-length factor (**L**) was determined using the following equation:

$$L = \left(\frac{\lambda}{22.13}\right)^m$$

where 22.13 are the RUSLE unit plot length (in metres) and *m* is the exponent of a variable slope length. Slope length exponent *m* can be calculated as

$$m = \frac{\beta}{(1+\beta)}$$

$$\beta = \frac{\frac{\sin \theta}{0.0896}}{3.0(\sin \theta)0.8+0.56}$$

where,  $\theta$  is the slope angle

The slope steepness factor (**S**) is estimated using the relationships given by McCool *et al.*, (1987, 1993)

$$S = 10.8 \sin \theta + 0.03 \quad S < 9\% \text{ (i. e. } \tan \theta < 0.09)$$

$$S = \left(\frac{\sin \theta}{\sin 5.143}\right)^{0.6} \quad S \geq 9\% \text{ (i. e. } \tan \theta \geq 0.09)$$

Using the hydrology tools in the spatial analyst tool of ArcGIS, the DEM data was used to create flow fill, flow direction, and flow accumulation. Operations for fill, flow direction, and flow accumulation were produced one at a time. The flow accumulation raster obtained was then used for the estimation of the L factor by using the following formula-

$$L = \left( \frac{\text{Flow accumulation} * \text{cell size}}{22.13} \right)^m$$

or,

$$LS = [\text{flow accumulation} * \frac{\text{Cell Size}}{22.13}]^{0.4} * \left[ \frac{\sin \text{Slope}}{0.00896} \right]^{1.3}$$

### 3.8.4 COVER MANAGEMENT (C) FACTOR

The cover-management factor (C) is a fundamental component in estimating soil erosion rates, particularly within models like the Revised Universal Soil Loss Equation (RUSLE). It reflects the influence of vegetation cover, cropping systems, and land management practices on soil erosion, serving as a key indicator of how human activities and natural land cover affect the soil's vulnerability to erosive forces. As highlighted by Koirala et al. (2019), the significance of the C factor lies in its ability to quantify the protective role of vegetation in mitigating soil erosion, ranking second only to topography as a determinant of erosion risk. Vegetation cover functions as a natural barrier, reducing the erosive impact of raindrops on the soil surface. This minimizes the detachment of soil particles and simultaneously enhances the soil's capacity to absorb rainfall, reducing surface runoff and, consequently, the potential for erosion.

The C factor is defined as the ratio of soil loss from a particular land use condition to the soil loss from continuously tilled bare land, which represents the most vulnerable scenario. This makes it a direct measure of the erosion-reducing capability of vegetation cover and management practices. The values of the C factor range from 0 to 1, with lower values indicating better soil protection and reduced erosion. The factor is highly dynamic, as it can change with seasonal variations in vegetation and land use practices. This adaptability emphasizes its importance, as it offers a quantifiable means for assessing the effectiveness of soil conservation measures.

Calculation of the C factor typically involves deriving the weighted average of soil loss ratios (SLRs) associated with different land use types. However, more advanced approaches involve the use of remote sensing techniques and vegetation indices like the Normalized Difference Vegetation Index (NDVI). NDVI is a widely recognized metric for assessing vegetation health and density, and it provides spatially and temporally explicit data.

It is calculated using satellite imagery, such as from Landsat 8 OLI/TIRS, based on the spectral difference between the near-infrared (NIR) and red (R) bands. The formula for NDVI is

$$\text{NDVI} = \frac{\text{NIR} - \text{RED}}{\text{NIR} + \text{RED}}$$

where NIR corresponds to Band 5 and Red corresponds to Band 4 in Landsat 8 imagery.

NDVI is calculated, the C factor can be derived using the empirical relationship

$$C = 0.431 - 0.805 \times \text{NDVI}, \text{ as proposed by Vatandaslar et al. 2017.}$$

This formula establishes an inverse relationship between vegetation density and the C factor. Higher NDVI values, indicative of denser and healthier vegetation, result in lower C values, signifying reduced soil erosion potential. This integration of NDVI into soil erosion studies allows for the generation of high-resolution C factor maps, capturing spatial and temporal variations in vegetation cover and land use.

Also, another formula proposed by *De Jong, 1994*

**If NDVI < 0**

$$C = 0$$

**Else**

$$C = -1.25 (\text{NDVI}) + 1$$

Formula proposed by *Durgion et al, 2014*

$$C = \frac{(-\text{NDVI} + 1)}{2}$$

Other equations mainly for EU climate, proposed by *Knijff et al., 2000*

$$C = e^{-2.5 * \frac{\text{NDVI}}{1 - \text{NDVI}}}$$

The corresponding C factor values for each land use category were assigned by using Table below -

Table: - 3.4 C – factor data as per LU/LC

SL NO	LAND USE/LAND COVER	C FACTOR
1	CROP LAND	0.5
2	DENSE FOREST	0.005
3	MODERATE DENSE FOREST	0.006
4	DEGRADED FOREST	0.05
5	DENSE SCRUB	0.05
6	OPEN SCRUB	0.07
7	RIVER	0
8	HABITATION	0
9	PLANTATION	0.05

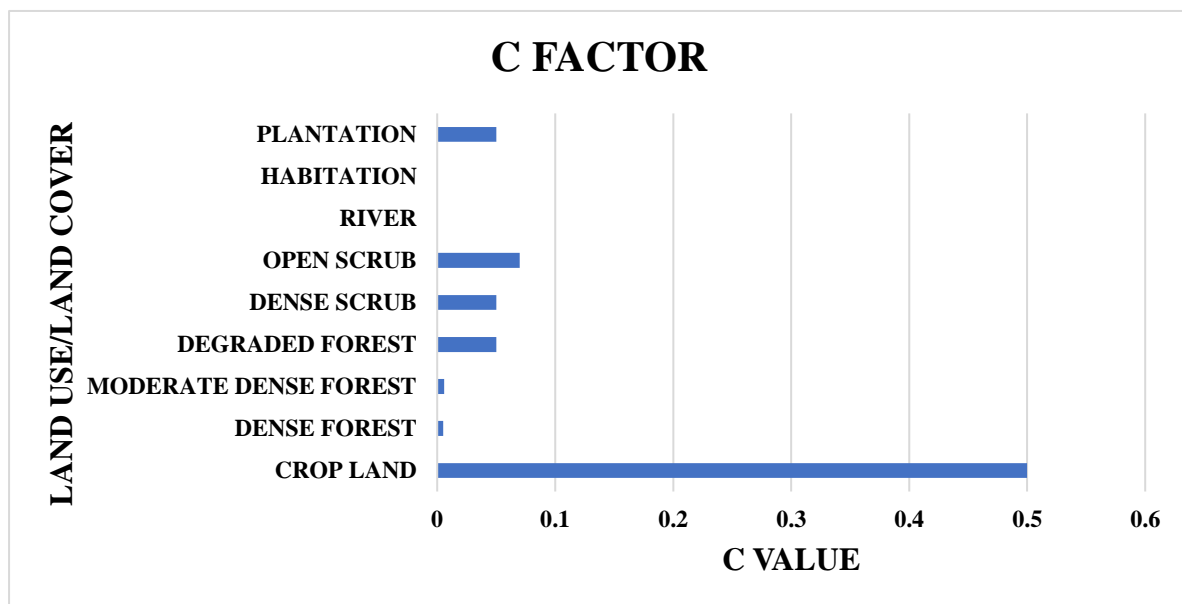


Fig: - 3.9 C- FACTOR CHART

The application of NDVI and satellite-based assessments in deriving the C factor underscores the growing importance of remote sensing in soil erosion modeling and conservation planning. These tools enable researchers and land managers to monitor changes in vegetation and erosion risk dynamically, offering actionable insights for implementing sustainable land use practices. In addition, the C factor's sensitivity to human interventions makes it a valuable parameter for evaluating and optimizing conservation strategies, such as afforestation, cover cropping, and other soil protection measures. Overall, the C factor is not only a critical theoretical parameter but also a practical tool in understanding and mitigating the impacts of soil erosion on environmental and agricultural systems.

### 3.8.5 SUPPORT PRACTICE (P) FACTOR

The support practice factor P express the effects of surface practices that are applied to reduced soil loss through erosion processes.

These practices include among others terracing strip cropping and contour ploughing the P factor value ranges between 0 and 1, where 0 shows the highest effectiveness of the conservation practice and 1 indicates that there are no support practices or measures implemented. Conservation practices mostly applied for agricultural areas or artificial pastures.

Common conservation practices include –

- Terracing
- Strip Cropping
- Contour Clothing
- Planting tress across agricultural areas

**Table for different practices in conjunction with slope (Shin and Pesaran 1999)**

Slope %	Contour	Strip cropping	Terraces
0 - 7	0.55	0.27	0.1
7 - 11.3	0.6	0.3	0.12
11.3 - 17.6	0.8	0.4	0.16
17.6 - 27	0.9	0.45	0.18
27>	1	0.52	0.2

Table: - 3.5 C – value as per slope, and different practice work

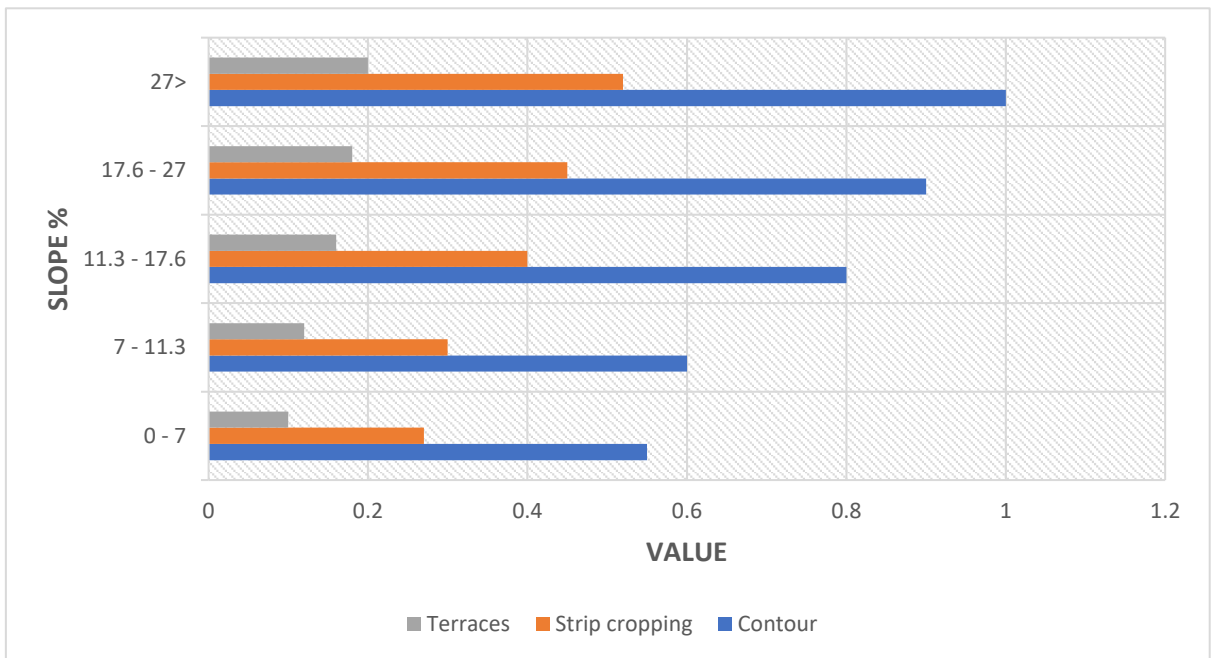


Fig: - 3.10 P – FACTOR CHART WITH SLOPE %

Land use type	Slope %	P factor
Agricultural land	0 to 5	0.1
	5 to 10	0.12
	10 to 20	0.14
	20 to 30	0.19
	30 to 50	0.25
	50 to 100	0.33
Other Land	All	1

Table: - 3.6 P – factor as per slope

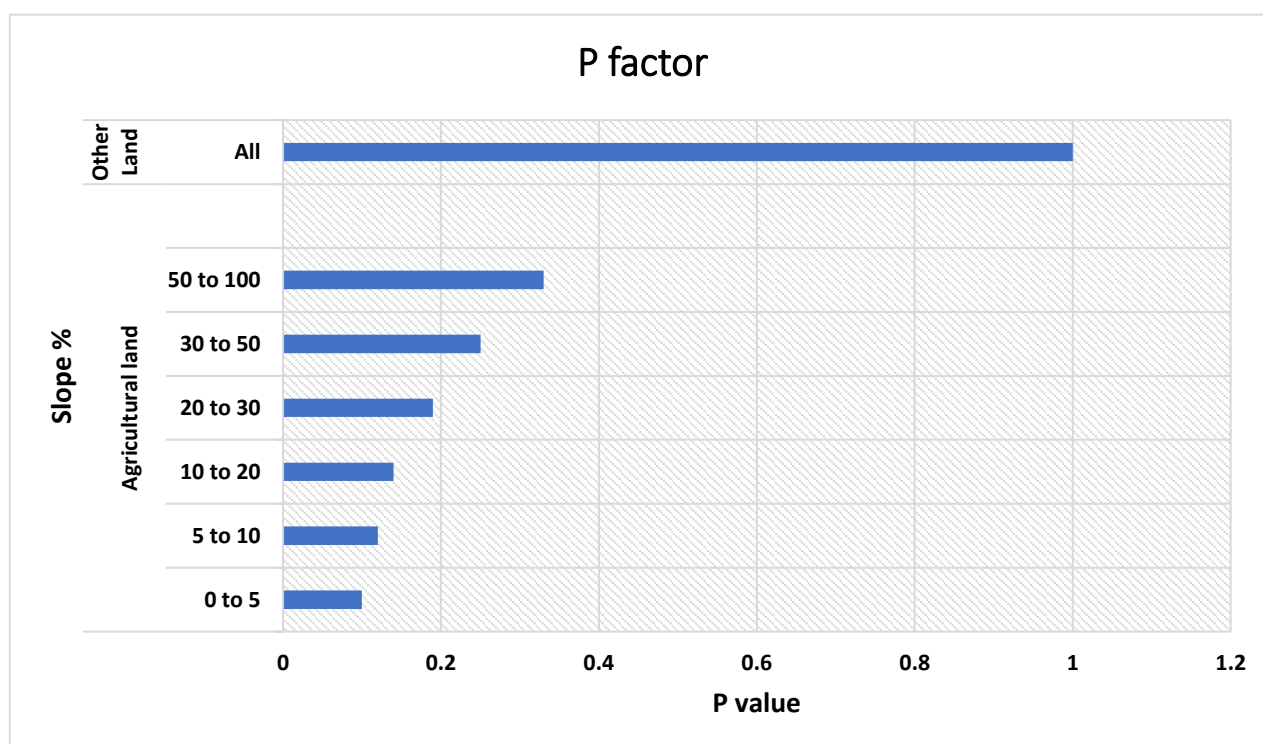


Fig: - 3.11 P – FACTOR OF DIFFERENT LAND SLOPE %

As from the above proposed table, the modeling of the study area is not calculated because, for instance water area doesn't have erosion or urban areas doesn't have erosion as there is no soil in water and as well as urban construction area are just commercially used.

Also given proposed equation is not taken for calculation as it takes only slope factor on account without considering and land change factor.

So, a modified table from given data is taking under consideration for P factor study.

<b>LAND USE TYPE</b>	<b>SLOPE %</b>	<b>P FACTOR</b>
Agricultural land	0-5	0.1
	5 to 10	0.12
	10 to 20	0.14
	20-30	0.19
	30-50	0.25
	50-100	0.7
Water	0-100	0
Urban Land	0-100	0
Forest	0-5	0.03
	5 to 10	0.05
	10 to 20	0.1
	31-30	0.2
	50-100	0.5
Range land	0-5	0.1
	5-10	0.13
	10 to 20	0.15
	20-30	0.2
	30-50	0.4
	51-100	0.7
Bare soil	0-5	0.25
	5 to 10	0.35
	10 to 20	0.45
	20-30	0.55
	30-50	0.75
	50-100	1

Table: - 3.7 P – factor as per slope & LU/LC

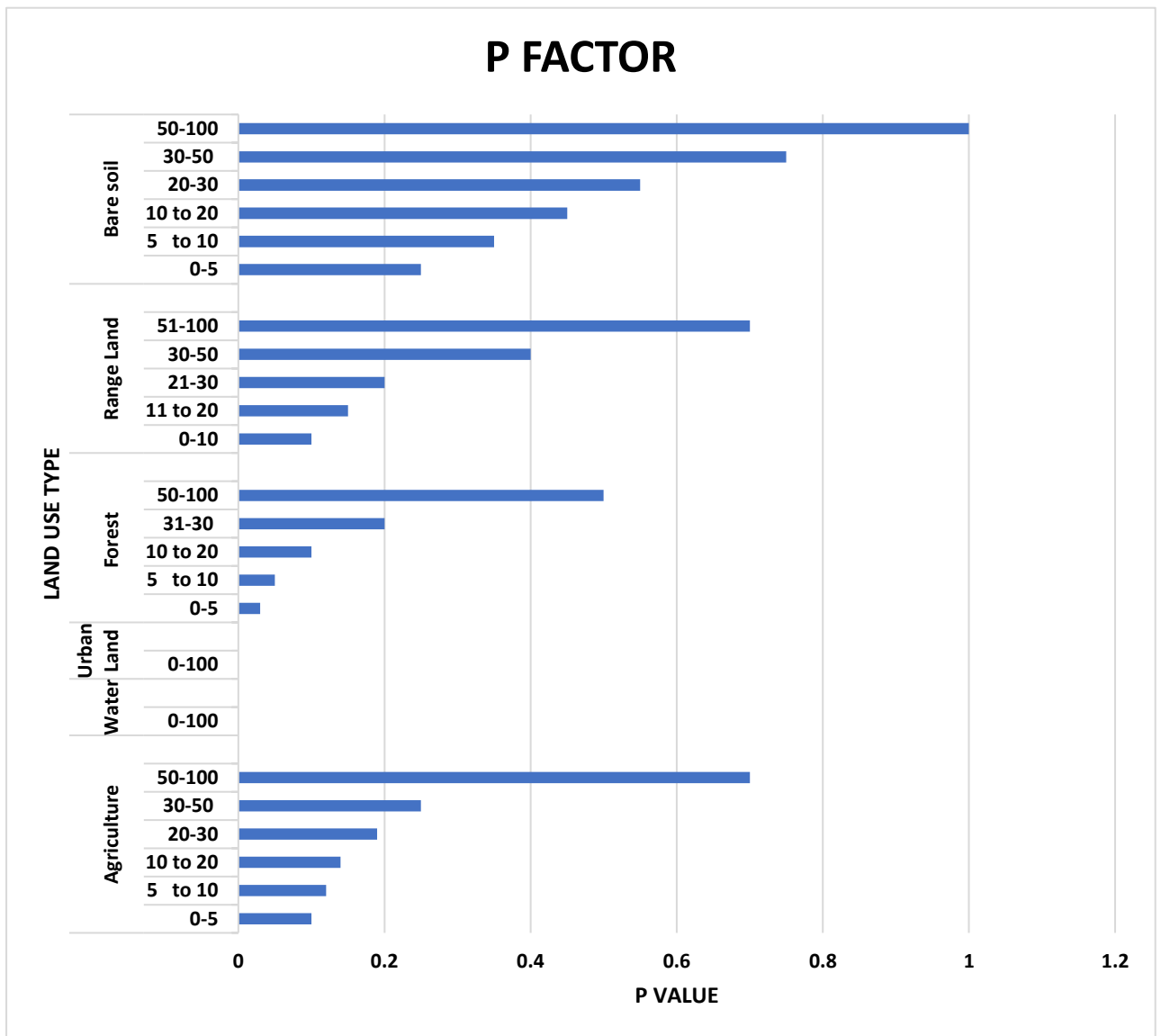


Fig: - 3.12 P – FACTOR OF DIFFERENT LAND USE TYPE

Here, P factor is slightly changed as for high slope it is reduces because agriculture cannot protect from water erosion is there is high slopes.

Water and Urban area are always 0 P factor regardless of the slope and forest area is good protected from soil erosion specially in low slope area and in high slope area there are moderately protected from erosion.

For rangelands, area is mostly close to agriculture area as there not exist any furrows or empty lands. Mostly they are covered by small percent of vegetation.

Bare soils cannot protect from water erosion as it doesn't cover by vegetation.

## CHAPTER 4

### METHODOLOGY

---

#### 4.1 THE RUSLE MODEL

The spatio-temporal variation of soil erosion in the Subansiri River Basin was assessed using the Revised Universal Soil Loss Equation (RUSLE) model, which predicts average annual soil erosion rates under varying scenarios involving cropping systems, management techniques, and erosion control practices (Renard et al., 1997; Wischmeier & Smith, 1978). In a GIS environment, the RUSLE model estimates soil loss using raster-based data representations, which allow for efficient processing and analysis of continuous spatial data through overlay operations. Soil erosion rates for **2014, 2022, and 2023** were calculated using RUSLE parameters derived from corresponding LANDSAT imagery and precipitation data provided as CRU files for the respective periods.

The RUSLE model, an improved version of the USLE model, calculates annual soil loss using five parameters: rainfall erosivity (**R**), soil erodibility (**K**), slope length and steepness factor (**LS**), cover management factor (**C**), and conservation practice factor (**P**) (Renard et al., 1997).

The model is expressed as -

$$A = R \times K \times LS \times C \times P$$

Where **A** ( $t\ ha^{-1}\ y^{-1}$ ) represents the total annual soil loss; **R** ( $MJ\ mm\ ha^{-1}\ h^{-1}\ y^{-1}$ ) is the rainfall erosivity factor; **K** ( $t\ ha\ h\ ha^{-1}\ MJ^{-1}\ mm^{-1}$ ) is the soil erodibility factor; **LS** is the slope length and steepness factor (dimensionless); **C** is the cover-management factor (dimensionless); and **P** is the conservation practice factor (dimensionless). The methods for estimating these parameters were adapted from studies by Bamutaze et al. (2010), Pilesjö et al. (1992), and Prasannakumar et al. (2012), ensuring robust and reliable calculations. The work flow is shown in the flow chart below –

#### Process of SOIL EROSION ESTIMATION



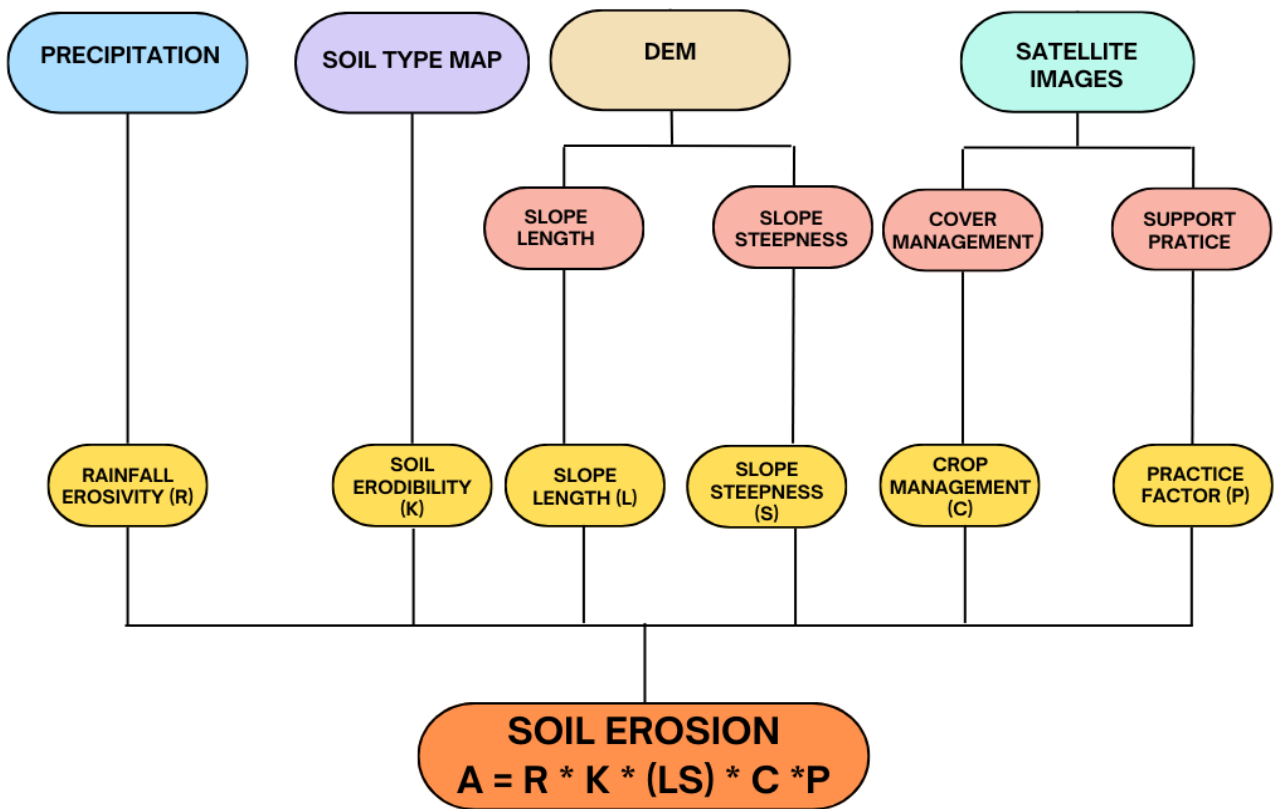


Fig: - 4.1 RUSLE FLOW DIAGRAM

## 4.2 RUSLE FACTORS

### 4.2.1 RAINFALL EROSIIVITY FACTOR (R)

The rainfall erosivity factor indicates the erosive force of a specific rainfall (Prasannakumar et al., 2012). The relationship between rainfall erosivity and rainfall depth developed by Wischmeier & Smith (1978) and modified by Arnoldus (1980) was used to translate the rainfall depth to rainfall erosivity. The calculation formula was as follows:

$$R = \sum_{i=1}^{12} 1.735 * 10 (1.5 * \log_{10} \left( \frac{P_i^2}{P} \right) - 0.08188 )$$

where:

**P<sub>i</sub>** is a monthly rainfall (mm)

**P** annual rainfall (mm)

Here, for evaluation of rainfall erosivity (R) factor data acquired from Climatic Research Unit (CRU) of NETCDF file with extension name (.pre.dat.nc.gz) of Dataset Name **CRU TS v4.08 Precipitation Data** of File name **cru\_ts4.08.2021.2023.pre.dat.nc.gz** and **cru\_ts4.08.2011.2020.pre.dat.nc.gz** for research work.

As in NeTCDF file it contains Monthly Rainfall Data of 10 years (2011 – 2020) and other file contains 3 years data (2021 – 2023) of file **cru\_ts4.08.2011.2020** & **cru\_ts4.08.2021.2023** respectively, where the precipitation data are categorized with their individual bands.

Hence, **cru\_ts4.08.2011.2020** contains 120 Bands i.e.,

[ 1 year = 12 months],

and, 1 Month = 1 Bands

Therefore, 10 years = 12 \* 10 = 120 Months = 120 \* 1 = 120 Bands

Table: - 4.1 BAND as per month with different period

YEAR	JANUARY	FEBRUARY	MARCH	APRIL	MAY	JUNE	JULY	AUGUST	SEPTEMBER	OCTOBER	NOVEMBER	DECEMBER
2011	BAND 1	BAND 2	BAND 3	BAND 4	BAND 5	BAND 6	BAND 7	BAND 8	BAND 9	BAND 10	BAND 11	BAND 12
2012	BAND 13	BAND 14	BAND 15	BAND 16	BAND 17	BAND 18	BAND 19	BAND 20	BAND 21	BAND 22	BAND 23	BAND 24
2013	BAND 25	BAND 26	BAND 27	BAND 28	BAND 29	BAND 30	BAND 31	BAND 32	BAND 33	BAND 34	BAND 35	BAND 36
2014	BAND 37	BAND 38	BAND 39	BAND 40	BAND 41	BAND 42	BAND 43	BAND 44	BAND 45	BAND 46	BAND 47	BAND 48
2015	BAND 49	BAND 50	BAND 51	BAND 52	BAND 53	BAND 54	BAND 55	BAND 56	BAND 57	BAND 58	BAND 59	BAND 60
2016	BAND 61	BAND 62	BAND 63	BAND 64	BAND 65	BAND 66	BAND 67	BAND 68	BAND 69	BAND 70	BAND 71	BAND 72
2017	BAND 73	BAND 74	BAND 75	BAND 76	BAND 77	BAND 78	BAND 79	BAND 80	BAND 81	BAND 82	BAND 83	BAND 84
2018	BAND 85	BAND 86	BAND 87	BAND 88	BAND 89	BAND 90	BAND 91	BAND 92	BAND 93	BAND 94	BAND 95	BAND 96
2019	BAND 97	BAND 98	BAND 99	BAND 100	BAND 101	BAND 102	BAND 103	BAND 104	BAND 105	BAND 106	BAND 107	BAND 108
2020	BAND 109	BAND 110	BAND 111	BAND 112	BAND 113	BAND 114	BAND 115	BAND 116	BAND 117	BAND 118	BAND 119	BAND 120

Here yellow marked row is considered for calculating Rainfall erosivity factor of period **2014**.

Similarly,

For **cru\_ts4.08.2021.2023** contains 36 Bands i.e.,

[ 1 year = 12 months],

and, 1 Month = 1 Bands

Therefore, 3 years = 12 \* 3 = 36 Months = 36 \* 1 = 36 Bands

YE AR	JANU ARY	FEBRU ARY	MAR CH	APR IL	MA Y	JUN E	JUL Y	AUG UST	SEPTEM BER	OCTO BER	NOVEM BER	DECEM BER
202 1	BAND 1	BAND 2	BAN D 3	BAN D 4	BA ND 5	BA ND 6	BA ND 7	BAND 8	BAND 9	BAND 10	BAND 11	BAND 12
202 2	BAND 13	BAND 14	BAN D 15	BAN D 16	BA ND 17	BA ND 18	BA ND 19	BAND 20	BAND 21	BAND 22	BAND 23	BAND 24
202 3	BAND 25	BAND 26	BAN D 27	BAN D 28	BA ND 29	BA ND 30	BA ND 31	BAND 32	BAND 33	BAND 34	BAND 35	BAND 36

Table: - 4.2 BAND as per month with period 2022, 2023

Here yellow marked row is considered for calculating Rainfall erosivity factor of **period 2022 and 2023**.

#### 4.2.1.1 Working with precipitation in NetCDF file of CRU of period 2014

Firstly, create a blank page in ArcMap and add file name **cru\_ts4.08.2011.2020.pre.dat.nc.gz** by clicking ArcToolbox, a drop-down menu appears then **go to > Multidimensional Tools > Make NetCDF Raster Layer**

A dialog box appears, then add all credentials and corresponding file for calculation.

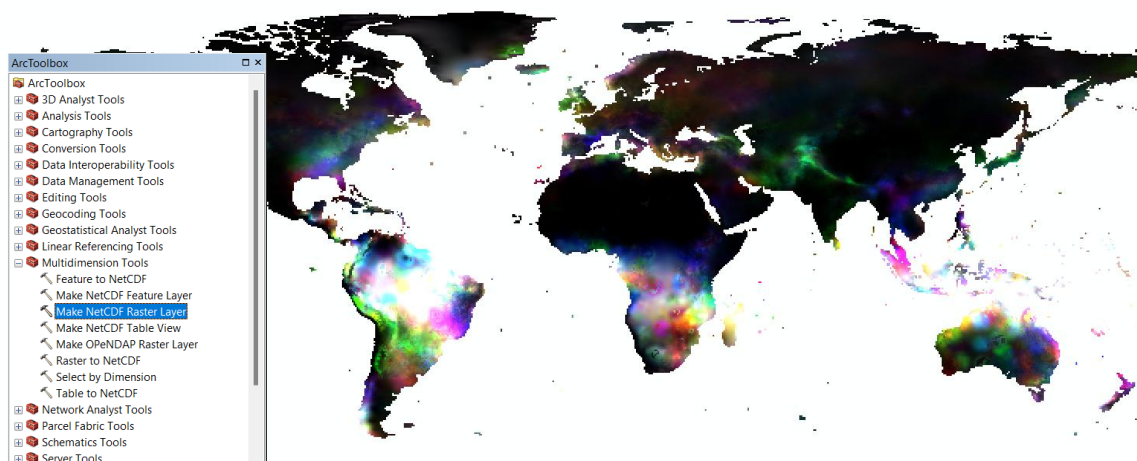
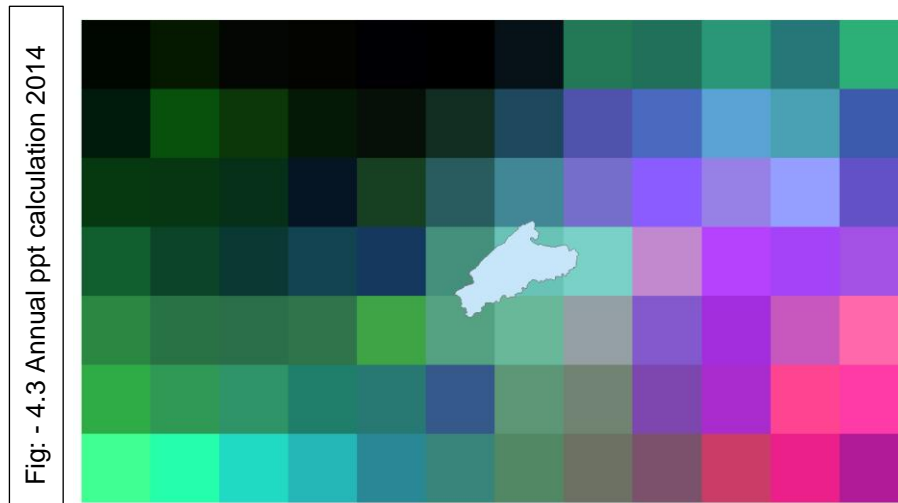


Fig: - 4.2 NetCDF MAP 2014

After, preparing the NetCDF file to precipitation layer format the file has been exported to Current Data Frame of **WGS 1984** for calculation of monthly precipitation map.



Now, for calculation of annual precipitation of study area above map Fig [ 4.3] is converted by using following step –

### Spatial Analyst Tool > Local > Cell Statistics

A dialog box appears where required band of corresponding period 2014 is considered on adding **Band 37 to Band 48** as earlier highlighted in above table [ ] and at **Overlay statistic option > SUM**, is being selected for chosen bands.

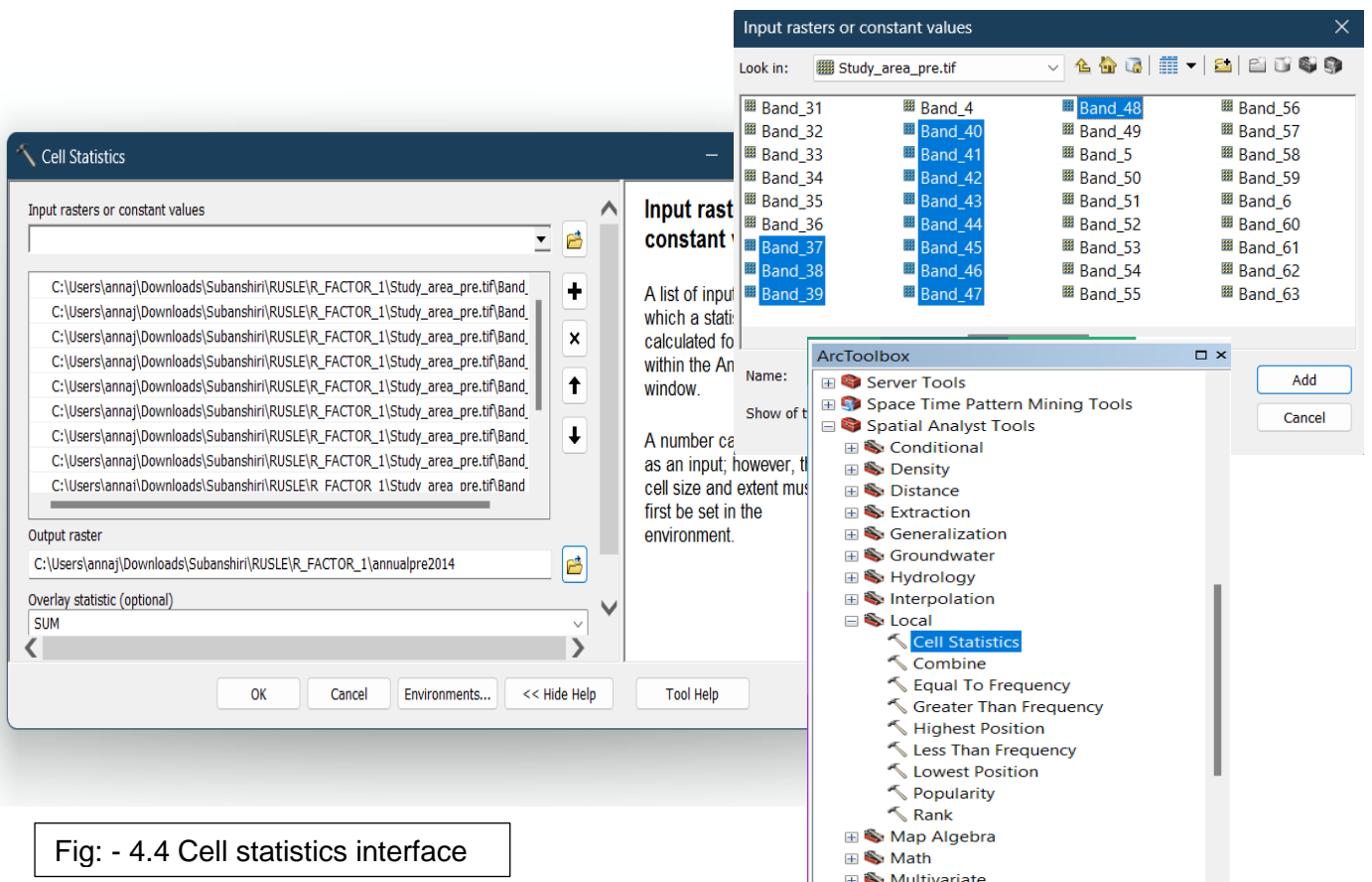


Fig: - 4.4 Cell statistics interface

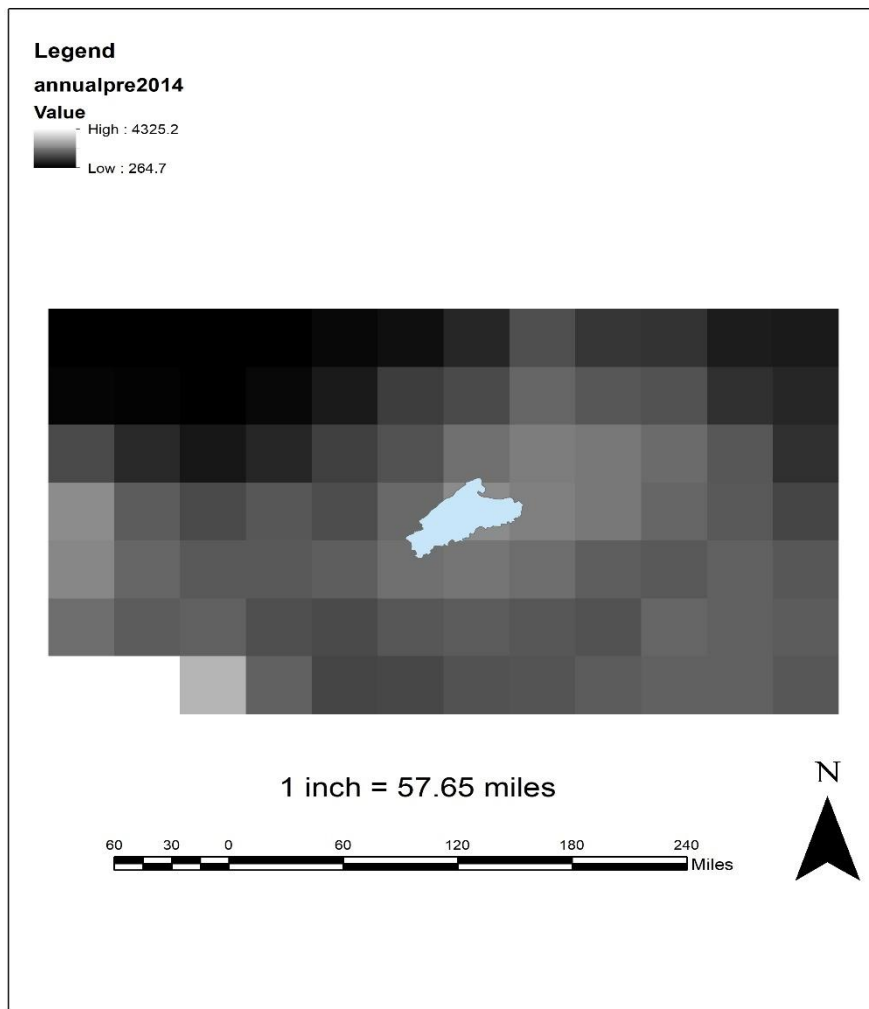


Fig: - 4.5 Annual precipitation map of 2014

Above Fig [4.5] presented that for period 2014 annual precipitation is shown from **264.7 mm** to **4325.2mm** of **Projected Coordinate System WGS 1984 UTM Zone 43N** as file name **annualpre\_2014\_UTM.tif**

Now converting Raster format to point where points are defined as empirical rain-gauge station for calculation of varying precipitation intensity of the study area.

Steps are as follows –

ArcToolbox > Conversion Tools > From Raster > Raster to Point, as shown in below

A dialog box adds all the credentials and insert **annualpre\_2014\_UTM.tif** in Input Option and point map is created Fig [4.6]

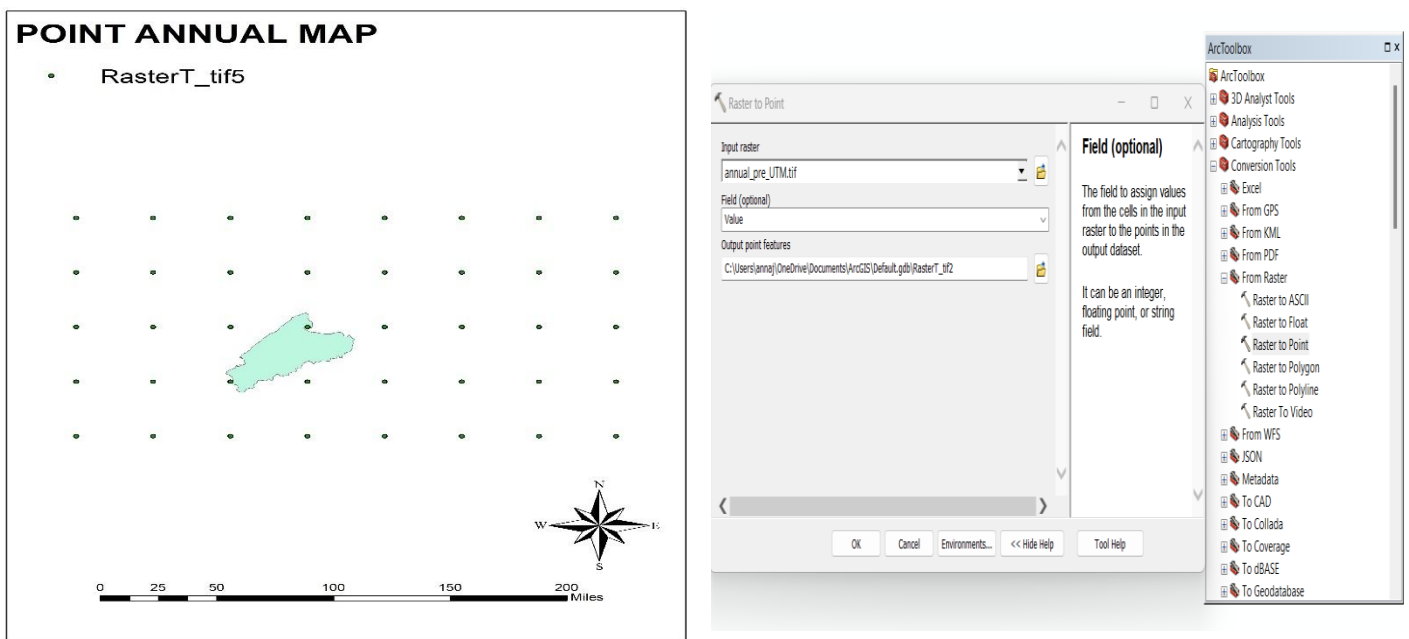


Fig: - 4.6 Annual precipitation point map of 2014

Here, for spatial distribution of annual precipitation in the study area is estimated by using **Kriging Interpolation** technique by converting output cell size into 30 \* 30 resolutions.

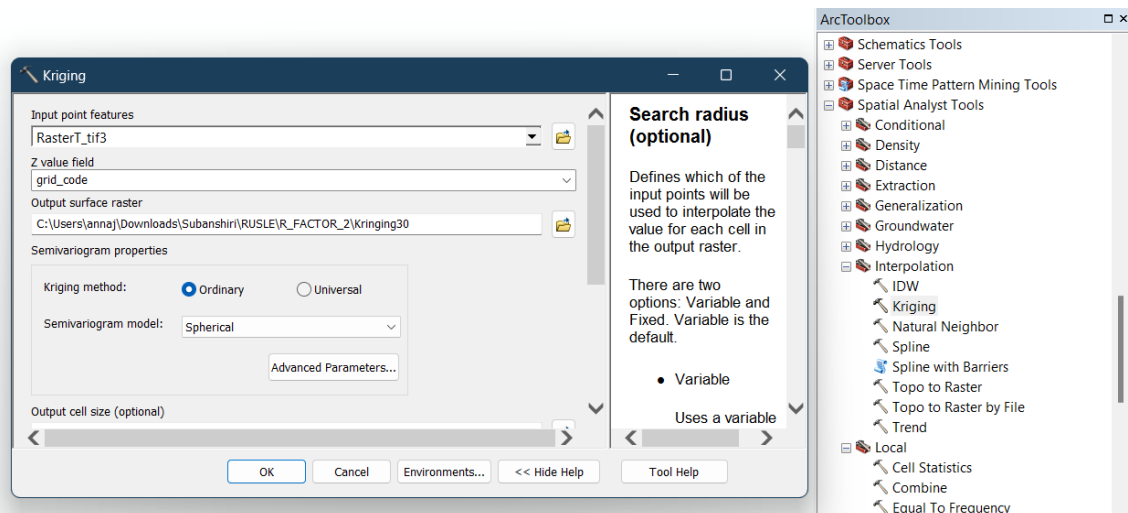


Fig: - 4.7 Kriging Interpolation dialog box

After interpolation technique is applied the required interpolated map is being generated as Fig [4.8]

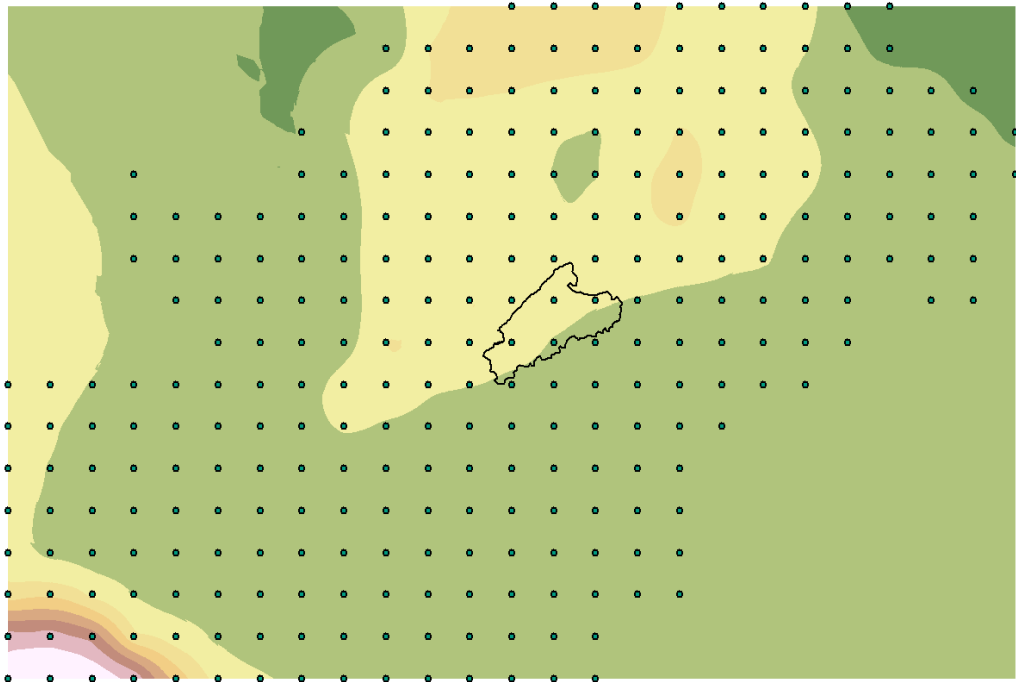
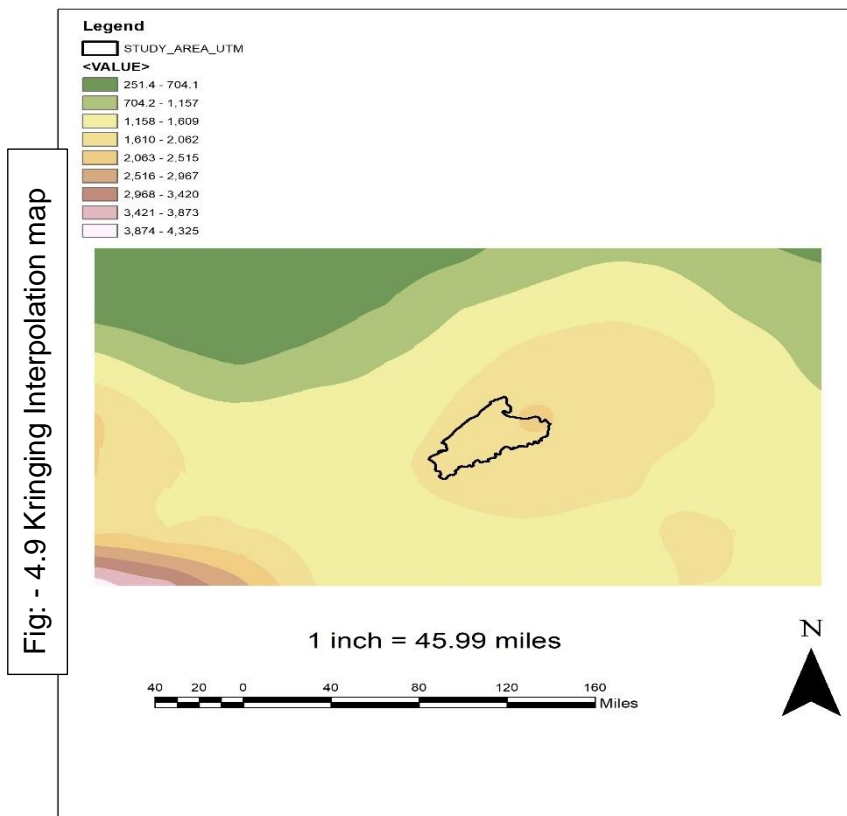


Fig: - 4.8 Kriging Interpolation interface

And exported of above Fig [4.9] of Kriging Interpolation Technique applied map as below where maximum value is ranged from [2,063 – 2,515]



#### 4.2.1.1.1 Reproject of Monthly Rainfall Data of period 2014

Again, reprojection of monthly data is performed for calculation of rainfall erosivity using Model Builder where the selected band i.e., Band 37 to Band 48 is converted to Band UTM respectively.



After selecting the **Model Builder** option, as shown in Fig. [4.10], a new window opens. Add the required band for conversion to UTM Zone 46N. Once the process runs successfully, a dialog box confirming completion will appear.

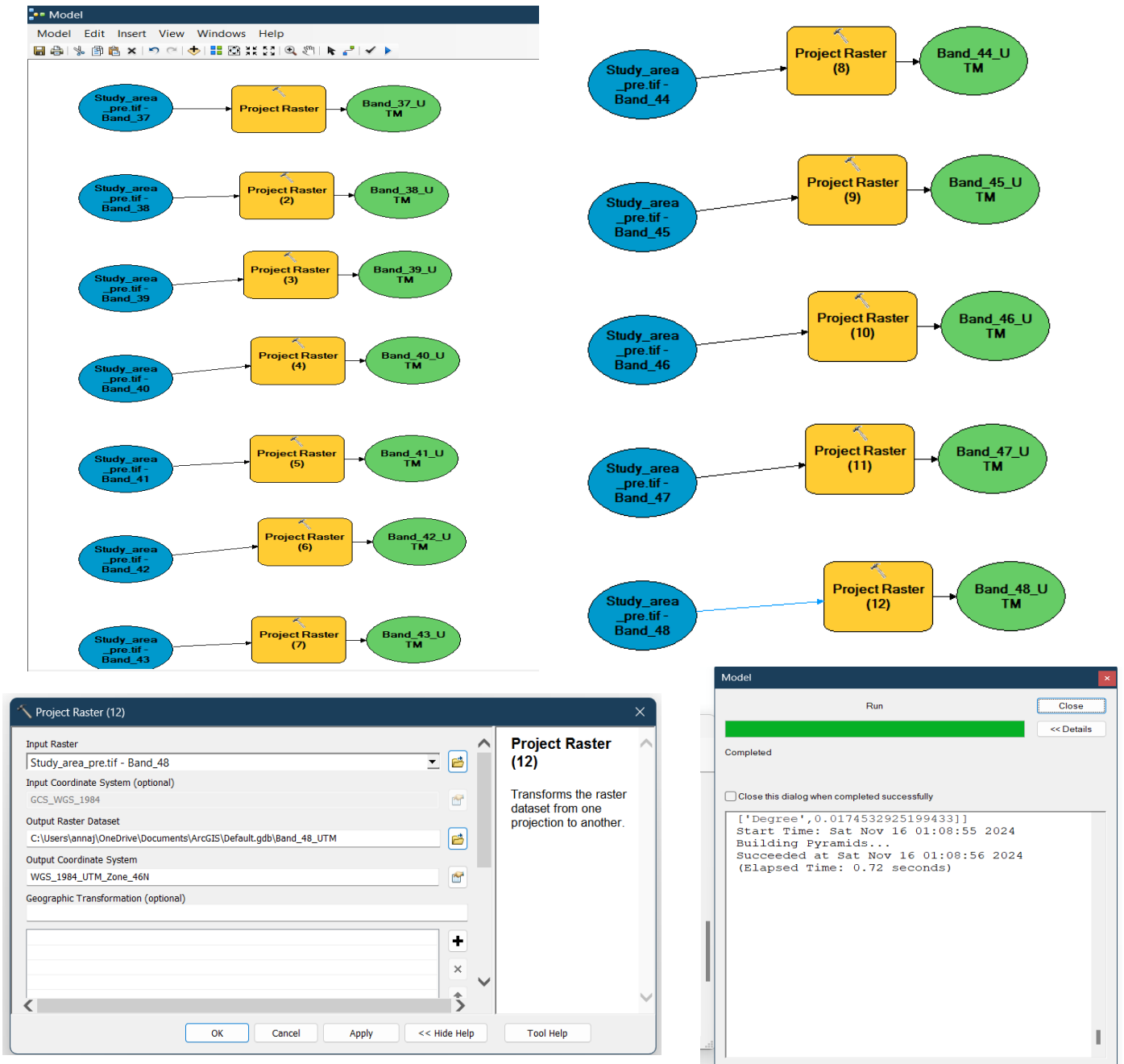


Fig - 4.10 Model building of raster projection

#### 4.2.1.1.2 Calculation of R factor using projected Rainfall data of period 2014

$$\text{Here, } R = \sum_{i=1}^{12} 1.735 * 10 (1.5 * \log_{10} \left( \frac{P_i^2}{P} \right) - 0.08188 )$$

where:

$P_i$  is a monthly rainfall (mm)

$P$  annual rainfall (mm)

Above equation is used for calculation R value as proposed by Wischmeier and Smith, 1978; Arnoldus, 1980 where evaluation will be done on Model Builder as shown in Fig [4.11]

Steps as follows –

After adding Bands\_UTM file in Model Builder window then drag **Raster Calculator** option from **Spatial Analyst** option and then add **Cell Statistics Option** for Summation of Bands Value as present in the above equation in Fig [4.12]

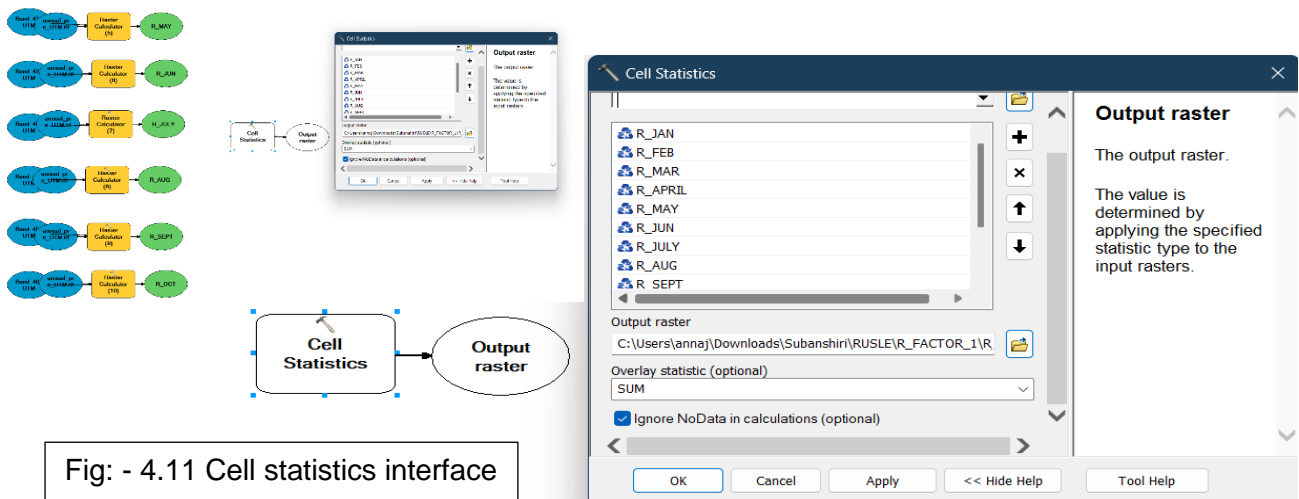


Fig - 4.11 Cell statistics interface

Here in Raster Calculator box given equation is used for evaluation of monthly rainfall data as shown in Fig [1.30]

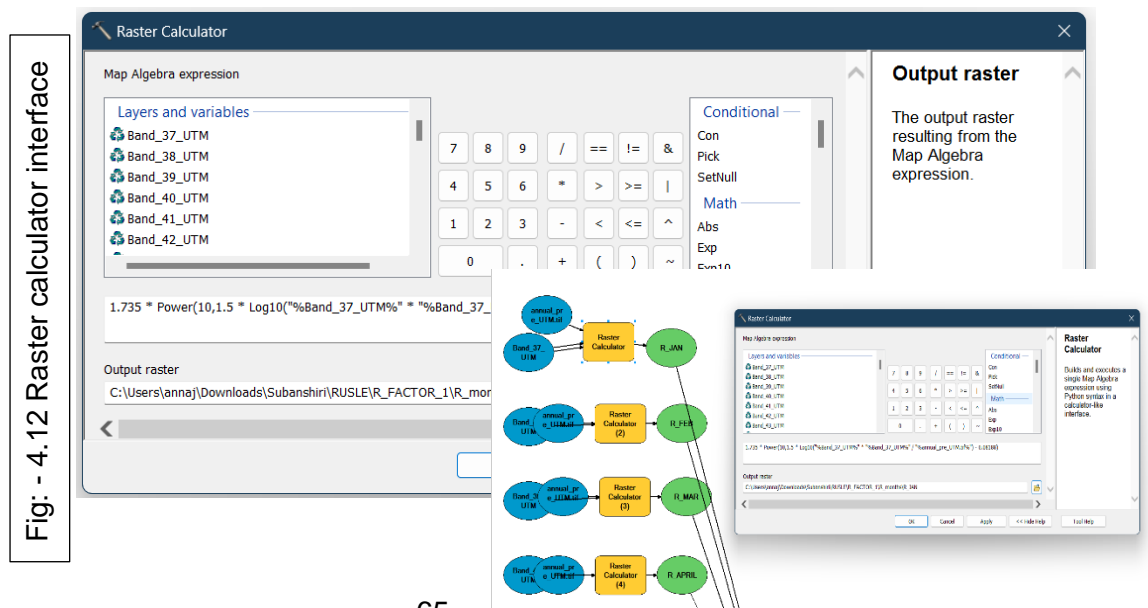


Fig - 4.12 Raster calculator interface

#### 4.2.1.2 Working with precipitation in NetCDF file of CRU of period 2022

Similar method is applied with period 2022 but file name taken as **cru\_ts4.08.2022.2023.pre.dat.nc.gz** by clicking ArcToolbox, a drop-down menu appears then go to **> Multidimensional Tools > Make NetCDF Raster Layer**

A dialog box appears, then add all credentials and corresponding file for calculation.

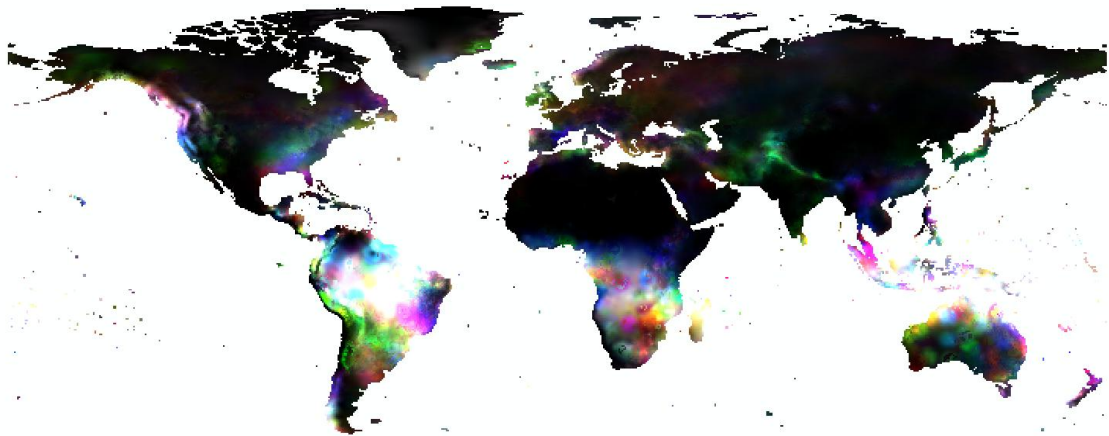


Fig: - 4.13 NetCDF MAP 2022

After converting NetCdf file to raster calculation of annual precipitation is performed in similar manner but bands are considered as Band 13 to Band 24

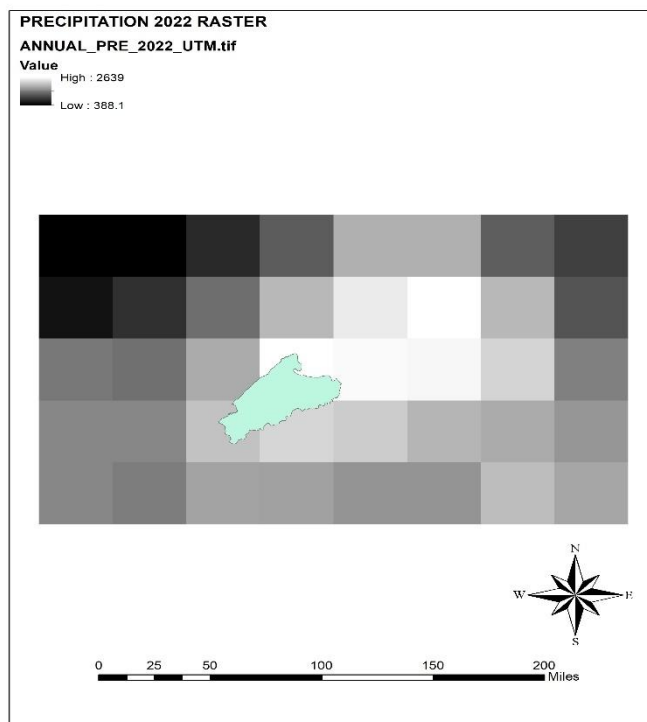


Fig: - 4.14 Annual precipitation map of 2022

for period 2022 annual precipitation is shown from **388.1 mm to 2639mm** of **Projected Coordinate System WGS 1984 UTM Zone 43N** as file name **annualpre\_2022\_UTM.tif**

Again, converting Raster format to point where points are defined as empirical rain-gauge station for calculation of varying precipitation intensity of the study area.

Steps are as follows –

ArcToolbox > Conversion Tools > From Raster > Raster to Point

A dialog box adds all the credentials and insert **annualpre\_2022\_UTM.tif** in Input Option and point map is created Fig [4.15]

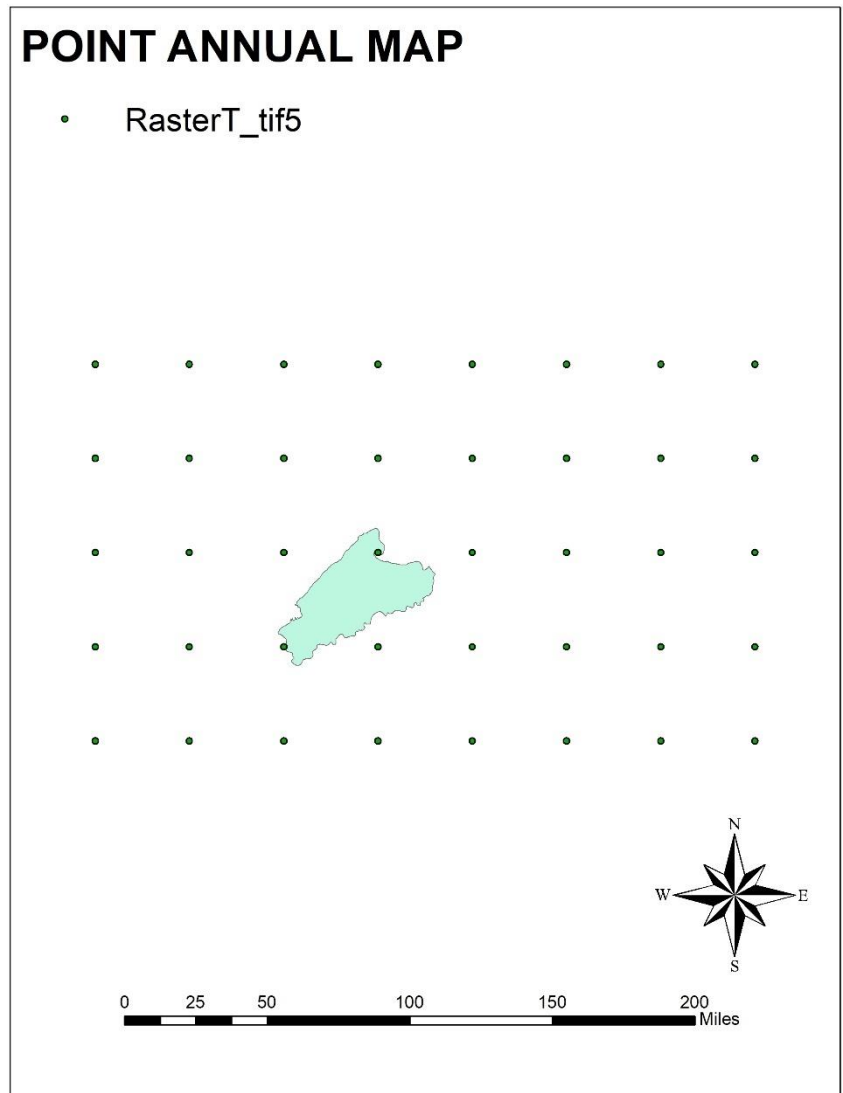


Fig: - 4.15 Annual precipitation point map of 2022

Then, spatial distribution of annual precipitation in the study area was estimated using the Kriging Interpolation technique, with the output cell size set to a  $30 \times 30$  resolution. After applying the interpolation method, the required precipitation map was generated and exported, as shown in Fig. [4.16], representing the interpolated values derived from the Kriging Interpolation Technique with interval data as [2103.29 – 2638.93] in fig[4.17]

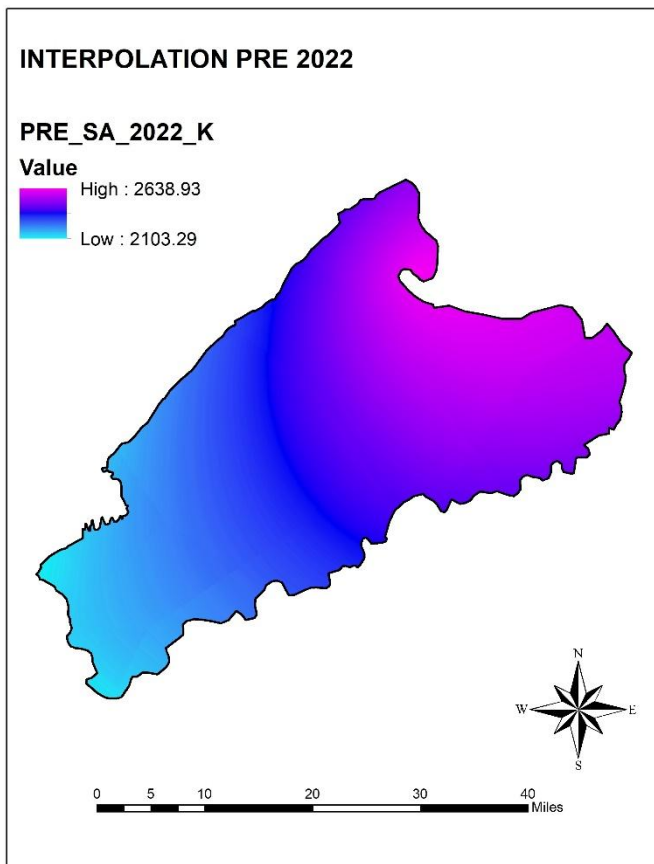


Fig: - 4.16 Interpolation precipitation map of 2022

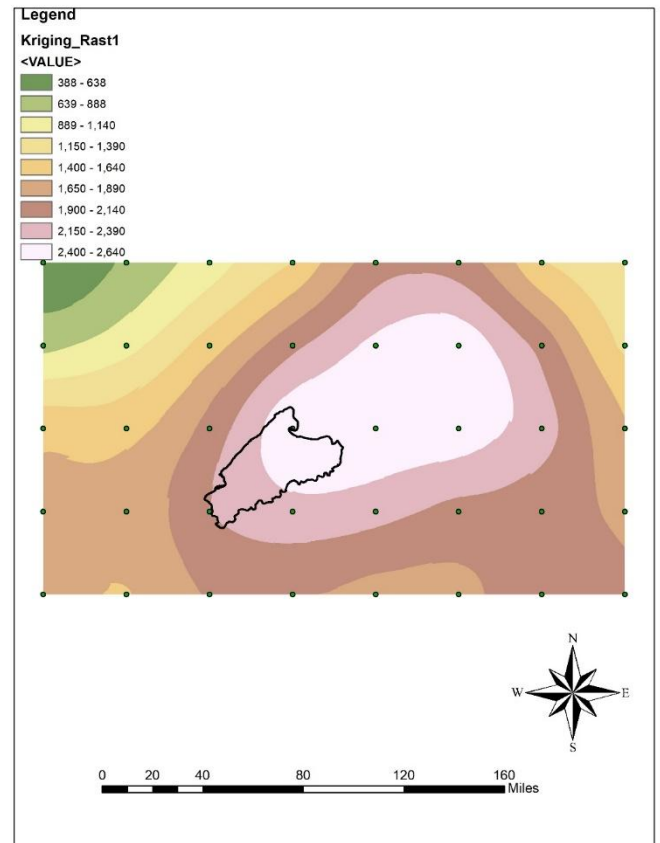


Fig: - 4.17 Kriging Interpolation map of 2022

#### 4.2.1.2.1 Reproject of Monthly Rainfall Data of period 2022

Again, reprojection of monthly data is performed for calculation of rainfall erosivity using Model Builder where the selected band i.e., Band 13 to Band 24 is converted to Band UTM respectively.



After selecting the **Model Builder** option, as shown in Fig. [4.18], a new window opens. Add the required band for conversion to UTM Zone 46N. Once the process runs successfully, a dialog box confirming completion will appear.

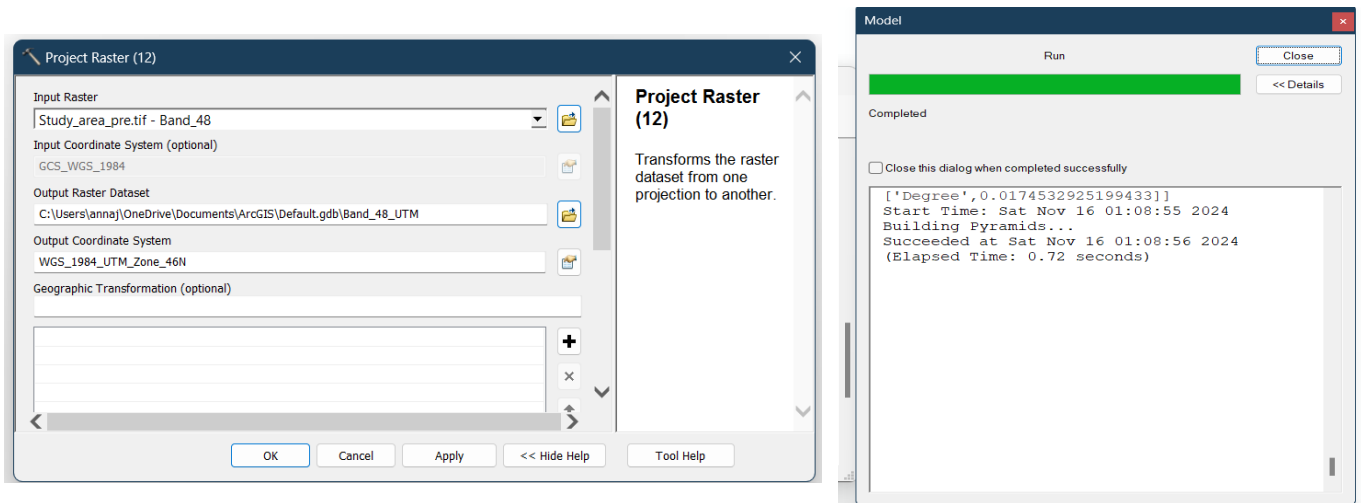


Fig: - 4.18 Model building of raster projection

#### 4.2.1.2.2 Calculation of R factor using projected Rainfall data of period 2022

$$\text{Here, } R = \sum_{i=1}^{12} 1.735 * 10 (1.5 * \log_{10} \left( \frac{P_i^2}{P} \right) - 0.08188 )$$

where:

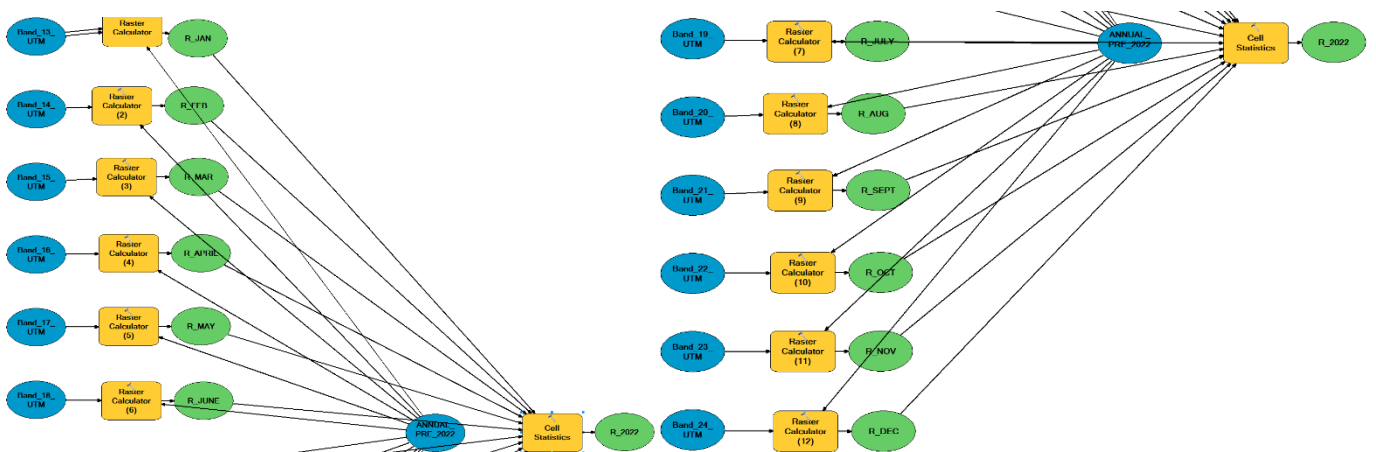
$P_i$  is a monthly rainfall (mm)

$P$  annual rainfall (mm)

Above equation is used for calculation R value as proposed by Wischmeier and Smith, 1978; Arnoldus, 1980 where evaluation will be done on Model Builder as shown in Fig [4.19]

Steps as follows –

After adding Bands\_UTM file in Model Builder window then drag **Raster Calculator** option from **Spatial Analyst** option.



Here in Raster Calculator box given equation is used for evaluation of monthly rainfall data.

Fig: - 4.19 Model building of raster projection

### 4.2.1.3 Working with precipitation in NetCDF file of CRU of period 2023

Similar method is applied with period 2023 but file name taken as **cru\_ts4.08.2022.2023.pre.dat.nc.gz** by clicking ArcToolbox, a drop-down menu appears then go to **> Multidimensional Tools > Make NetCDF Raster Layer**

A dialog box appears, then add all credentials and corresponding file for calculation.

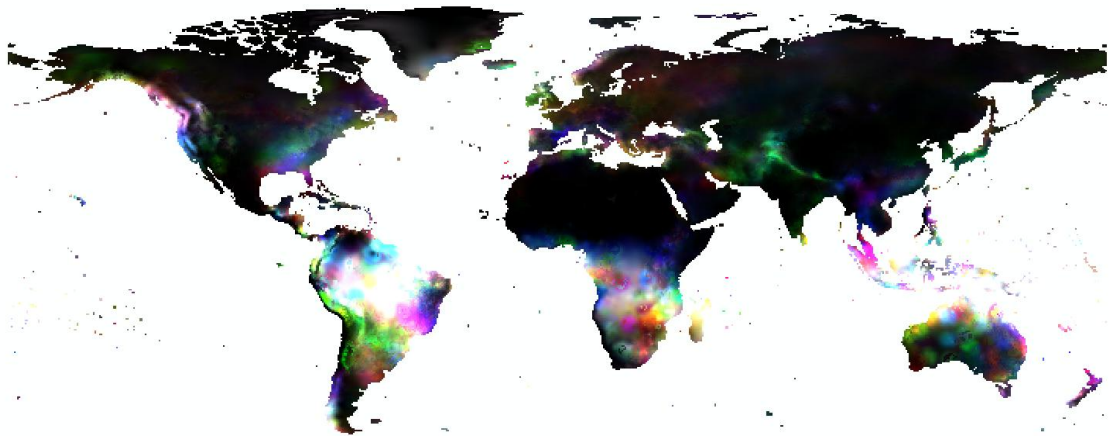


Fig: - 4.20 NetCDF MAP 2023

After converting NetCdf file to raster calculation of annual precipitation is performed in similar manner but bands are considered as Band 13 to Band 24

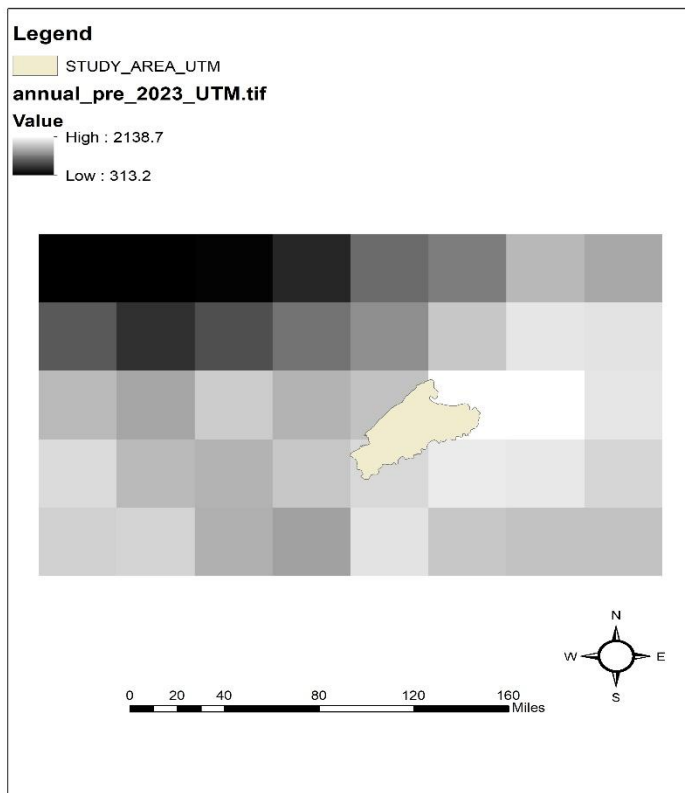


Fig: - 4.21 Annual precipitation map of 2023

for period 2022 annual precipitation is shown from 313.2 mm to 2138.7 mm of Projected Coordinate System WGS 1984 UTM Zone 43N as file name **annualpre\_2023\_UTM.tif**

Again, converting Raster format to point where points are defined as empirical rain-gauge station for calculation of varying precipitation intensity of the study area.

Steps are as follows –

ArcToolbox > Conversion Tools > From Raster > Raster to Point

A dialog box adds all the credentials and insert **annualpre\_2023\_UTM.tif** in Input Option and point map is created Fig [4.22]

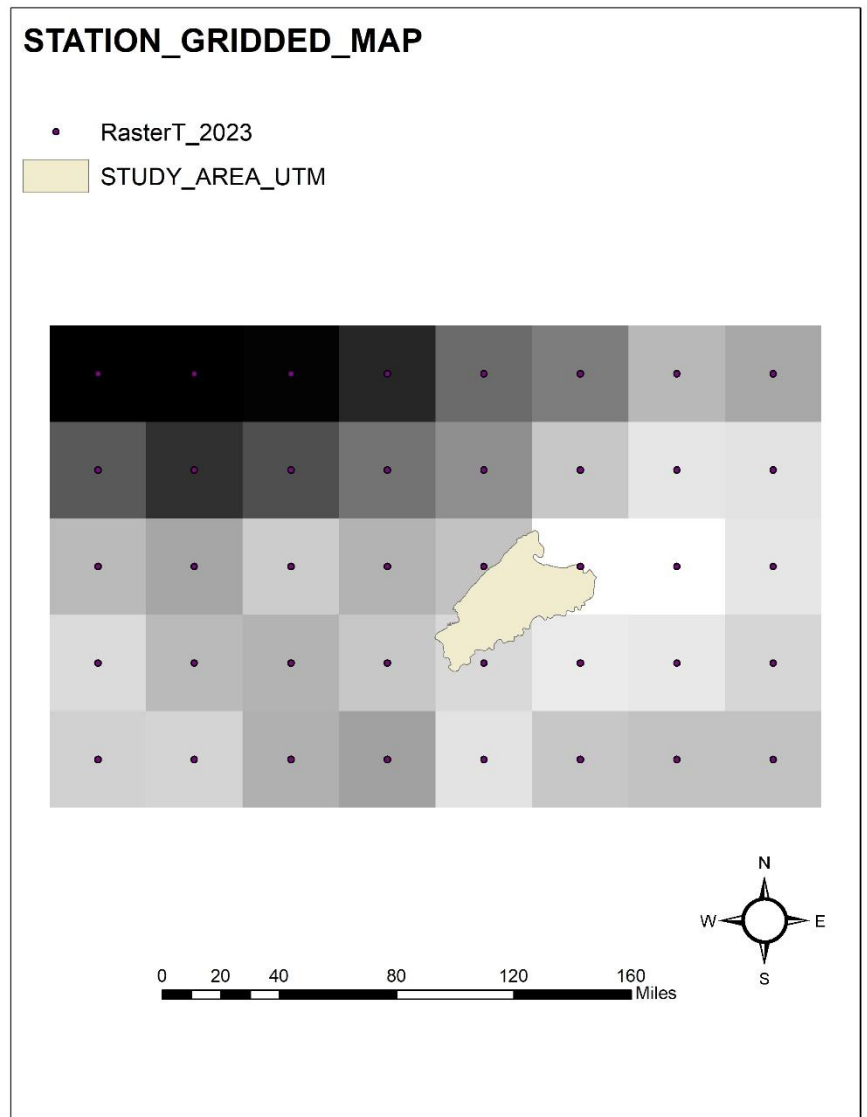


Fig: - 4.22 Annual precipitation point map of 2023

Then, spatial distribution of annual precipitation in the study area was estimated using the Kriging Interpolation technique, with the output cell size set to a  $30 \times 30$  resolution. After applying the interpolation method, the required precipitation map was generated and exported, as shown in Fig. [4.23], representing the interpolated values derived from the Kriging Interpolation Technique with interval data as [1699.47 – 2138.68]

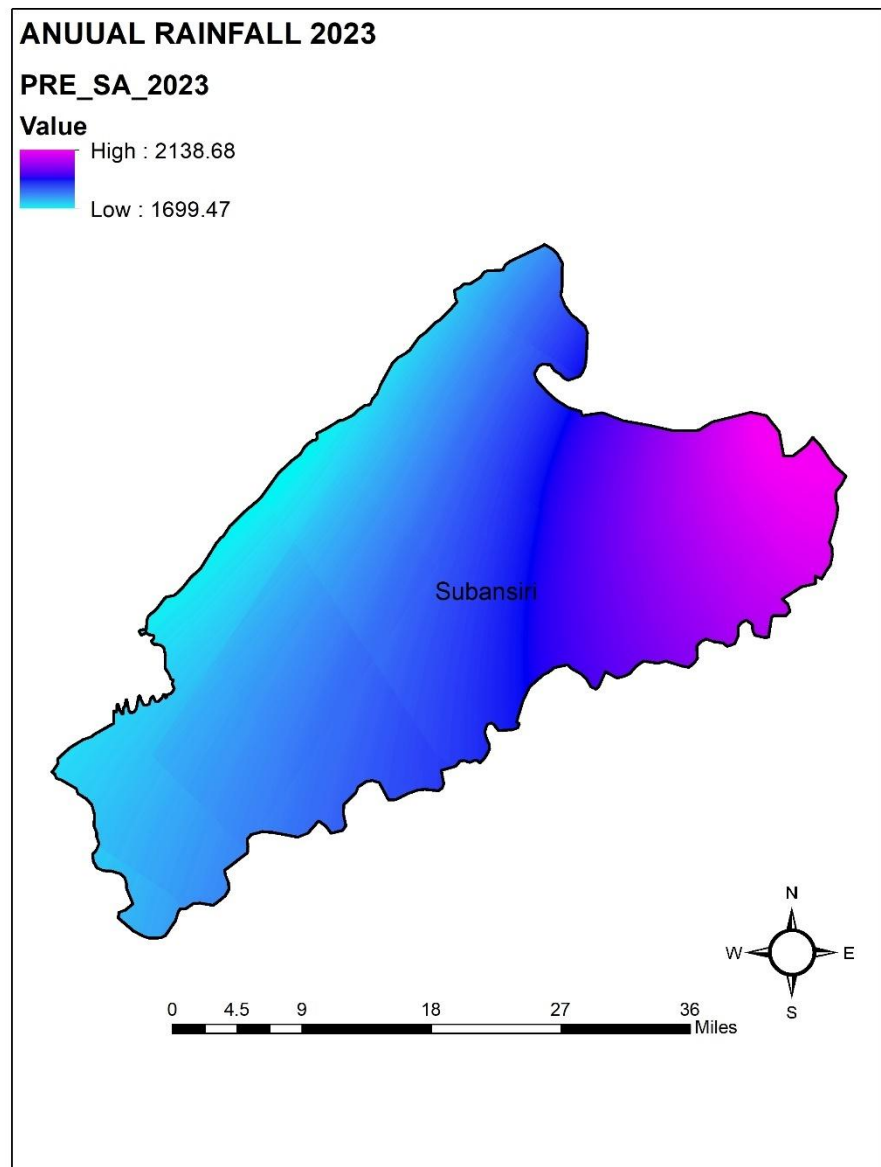


Fig: - 4.23 Interpolation precipitation map of 2023

### 4.2.1.3.1 Reproject of Monthly Rainfall Data of period 2023

Again, reprojection of monthly data is performed for calculation of rainfall erosivity using Model Builder where the selected band i.e., Band 25 to Band 36 is converted to Band UTM respectively.



After selecting the **Model Builder** option, as shown in Fig. [4.24], a new window opens. Add the required band for conversion to UTM Zone 46N. Once the process runs successfully, a dialog box confirming completion will appear.

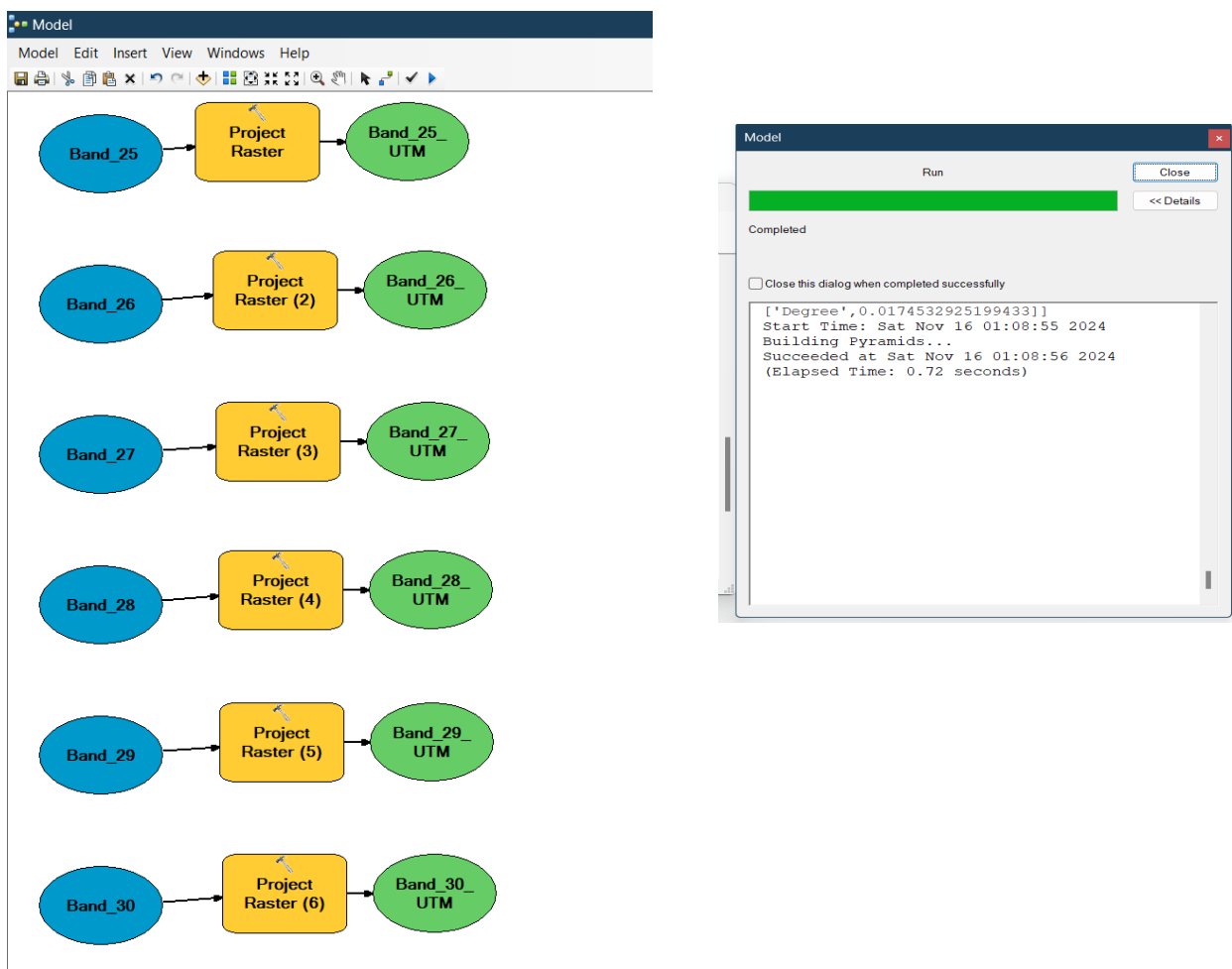


Fig: - 4.24 Model building of raster projection - 1

#### 4.2.1.3.2 Calculation of R factor using projected Rainfall data of period 2023

$$\text{Here, } R = \sum_{i=1}^{12} 1.735 * 10 (1.5 * \log_{10} \left( \frac{P_i^2}{P} \right) - 0.08188 )$$

where:

$P_i$  is a monthly rainfall (mm)

P annual rainfall (mm)

Above equation is used for calculation R value as proposed by Wischmeier and Smith, 1978; Arnoldus, 1980 where evaluation will be done on Model Builder as shown in Fig [4.25]

Steps as follows –

After adding Bands\_UTM file in Model Builder window then drag **Raster Calculator** option from **Spatial Analyst** option and then add **Cell Statistics Option** for Summation of Bands Value as present in the above equation

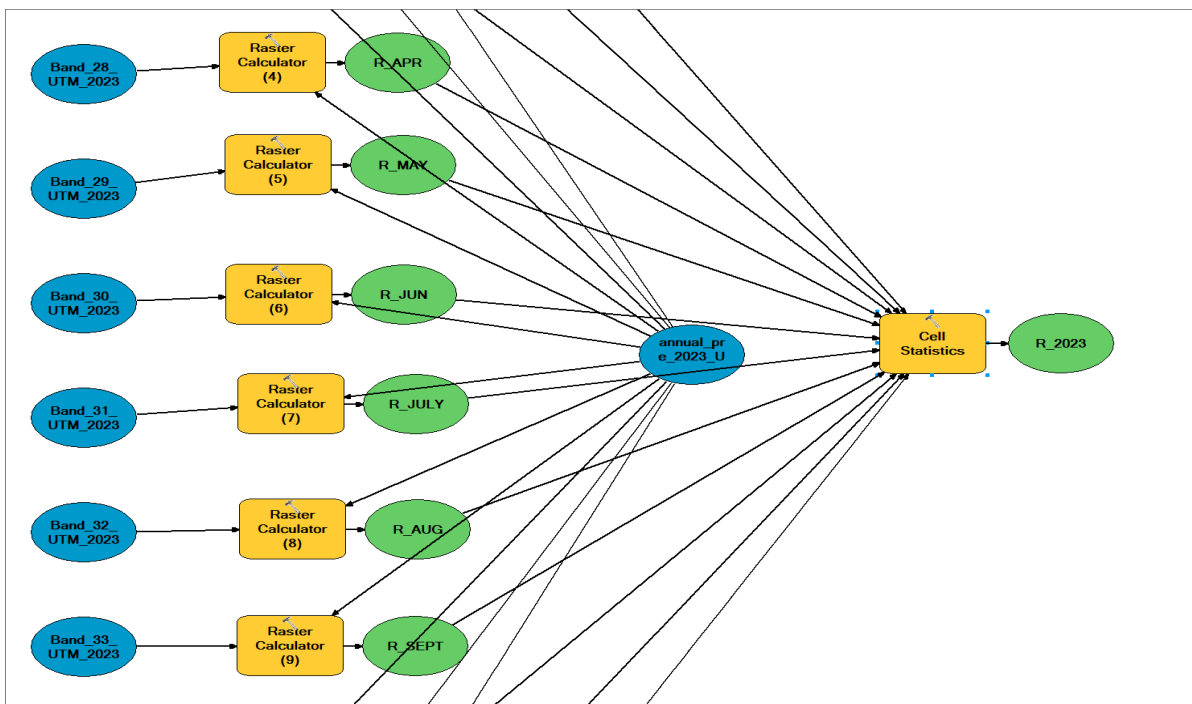


Fig: - 4.25 Model building of raster projection - 2

Here in Raster Calculator box given equation is used for evaluation of monthly rainfall data.

## 4.2.2 SOIL ERODIBILITY (K)

The soil erodibility which reflects the rate of soil loss depending on the erosion (R factor), and calculated on the basis of soil textures, is an empirical measure of soil erosion and represents the susceptibility of the soil to erosion.

Formula used for analyzing soil characteristics proposed by Williams (1995)

$$K_{USLE} = K_W = F_{csand} \times F_{cl-si} \times F_{orgc} \times F_{hisand}$$

$$F_{csand} = \left( 0.2 + 0.3 \exp \left[ -0.256 \times m_s \times \left( 1 - \frac{m_{silt}}{100} \right) \right] \right)$$

$$F_{cl-si} = \left( \frac{m_{silt}}{m_c + m_{silt}} \right)^{0.3}$$

$$F_{orgc} = \left( 1 - \frac{0.25 \text{ orgC}}{\text{orgC} + \exp[3.72 - 2.95 \times \text{orgC}]} \right)$$

$$F_{hisand} = \left( 1 - \frac{0.7 \times \left( 1 - \frac{m_s}{100} \right)}{\left( 1 - \frac{m_s}{100} \right) + \exp[-5.51 + 22.9 \left( 1 - \frac{m_s}{100} \right)]} \right)$$

### 4.2.2.1 USE OF FAO (FOOD AND AGRICULTURAL ORGANISATION) FOR SOIL STUDIES CONDUCTED IN THE YEAR 2014, 2022 AND 2023

Initially, the FAO soil data is downloaded from ( <https://data.apps.fao.org/map/catalog> ) where desired study area will be overlaid in ArcGIS for soil characteristics study.

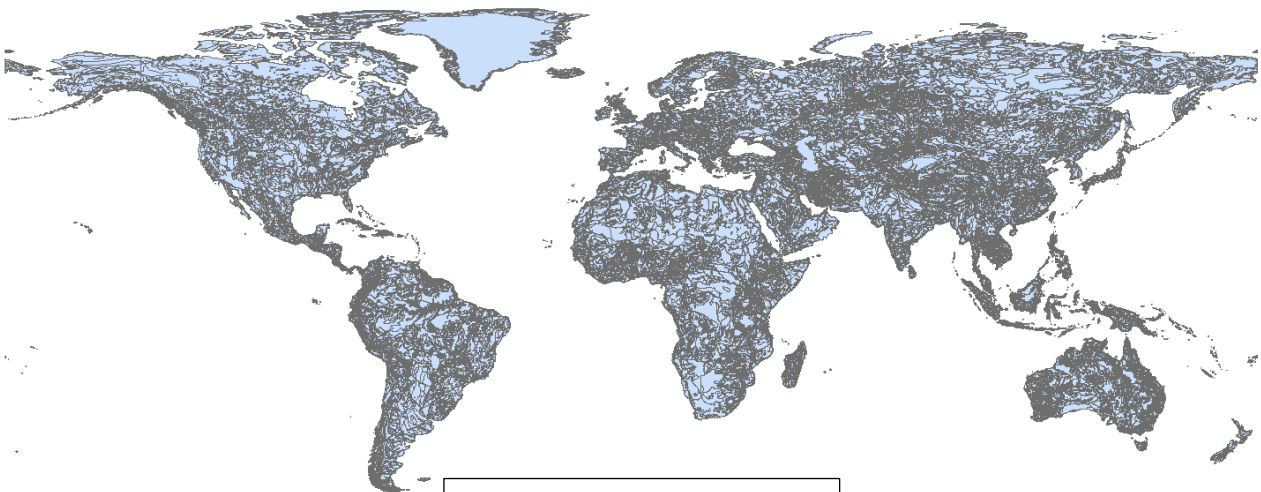


Fig: - 4.26 FAO SOIL MAP

Since the same DEM is used as the input file for different years, the soil types would remain consistent across the study area. As a result, the soil types derived from the FAO soil map would not vary for different years.

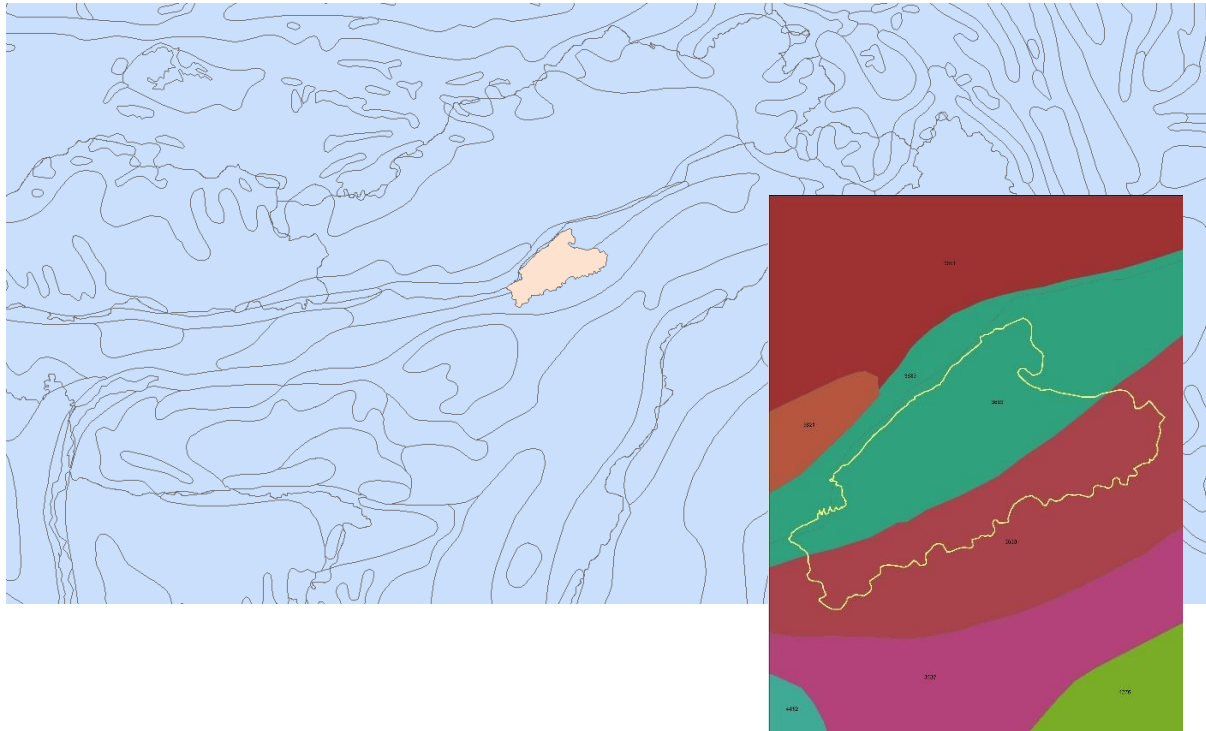


Fig: - 4.27 FAO SOIL WITH STUDY AREA MAP

Here, after overlapped two different soil types is observed from the selected area with different SNUM (soil number) as per FAO attribute table

#### 4.2.2.2 K factor extracted from FAO soil data for dominant soil

Firstly, extracted the study area shape file from soil map in ArcGIS where dominant soil of the required area will be visible in the corresponding attribute table.

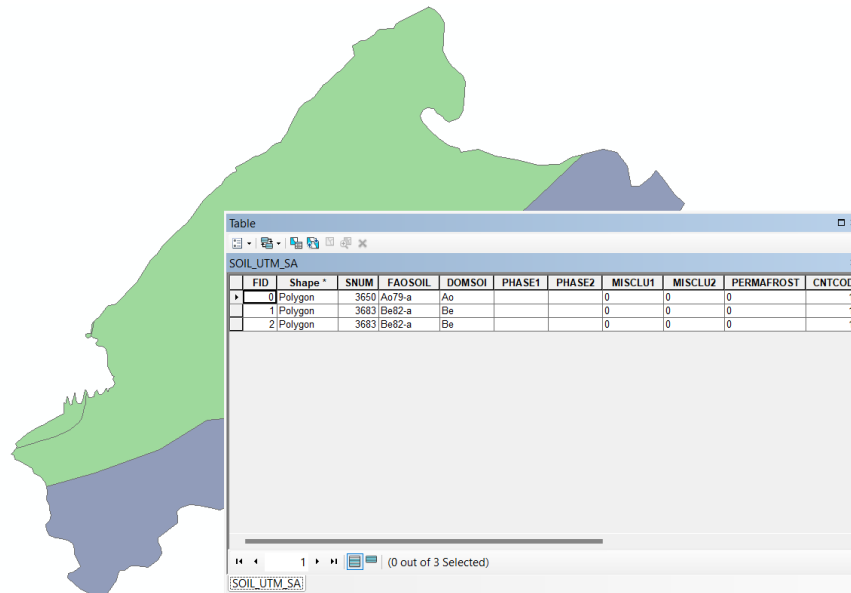


Fig: - 4.28 K\_FACTOR ATTRIBUTE CHART

From the above Fig [4.28] the FAOSOIL type is marked and look into the soil map data for requirements of **Williams.et.al** proposed formula for calculation.

Soil unit symbol	sand % topsoi	sand % subsoi	silt % topsoi	silt% subsoi	clay % topsoi	clay % subsoi	pH water topsoi	pH water subsoi	OC % topsoi
Ao	53.6	43.4	15.8	16	30.6	40.6	5.1	5.2	2.25
Be	36.4	41.7	37.2	32.1	26.4	26.3	6.9	7.1	1.07

Table: - 4.3 FAO SOIL MAP DATA FOR DOMINANT SOIL

Above table [4.3] is the FAO soil map data from where yellow marked column is prioritized for evaluation.

Here, soil unit symbol for the study area is **Ao and Be**

From the table [3.3] K factor is being calculated which will displayed in Chapter [3] for detailed analysis.

### 4.2.2.3 CONVERSION OF K FACTOR MAP TO RASTER IMAGE

Since the K-factor map is in shapefile format, it needs to be converted into raster format using the K-factor attribute data to ensure accuracy.

So, Go To

Arc Toolbox > Conversion Tools > To Raster > Polygon to Raster,

A dialog box appears after filling all credentials desired raster map Fig [4.29] and Fig[4.30] classification soil raster map is obtained by keeping value field option as K\_factor and cell size as 30m

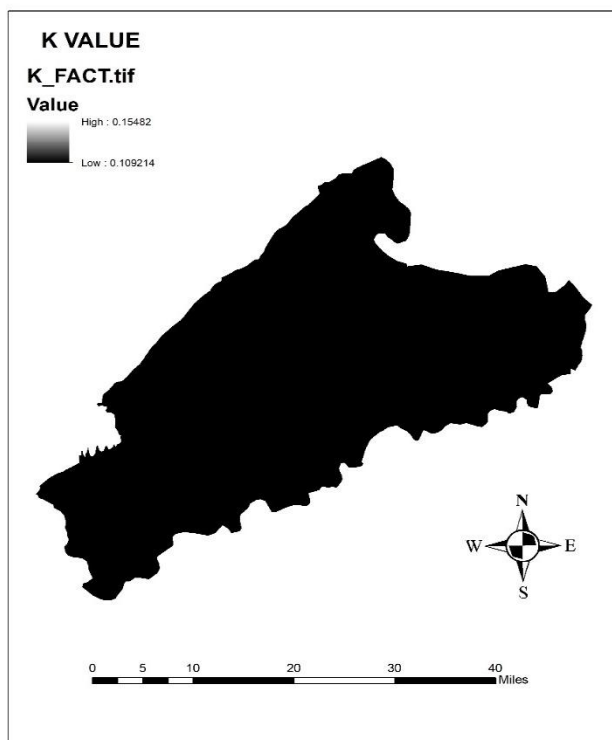


Fig - 4.29 K\_FACTOR RASTER MAP

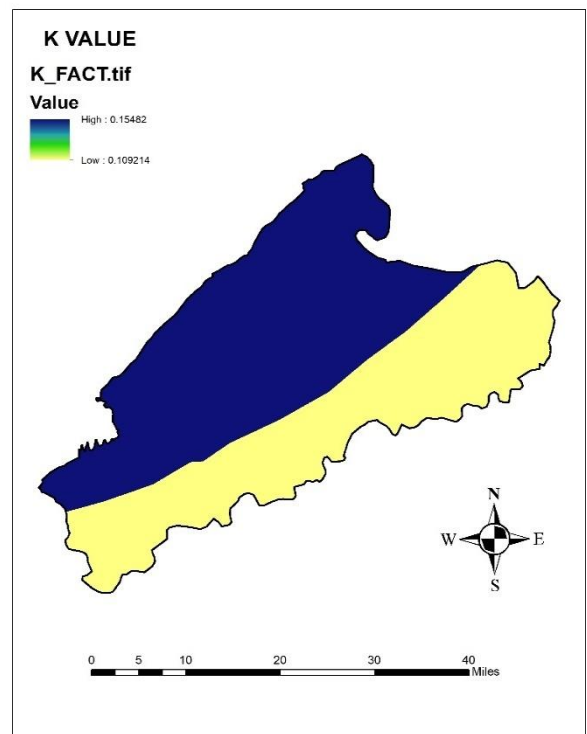


Fig - 4.30 K\_FACTOR SOIL MAP

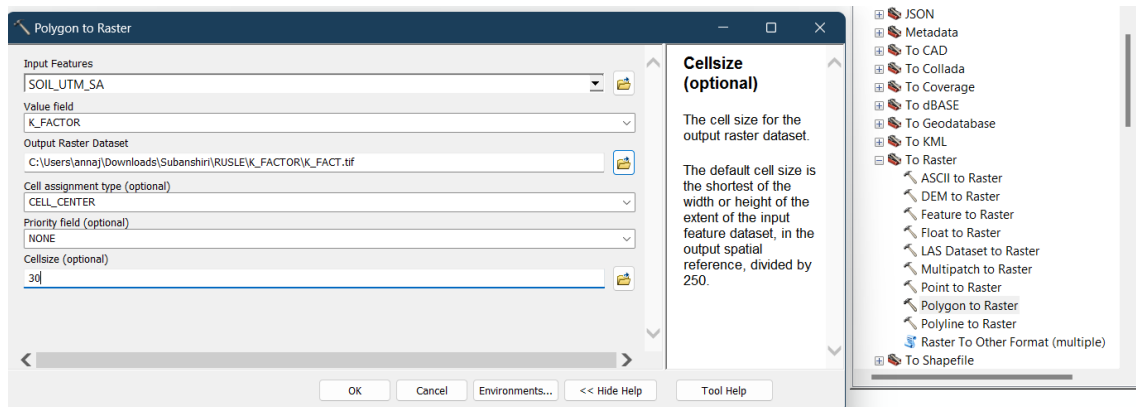


Fig - 4.31 CONVERSION OF POL TO RASTER

### 4.2.3 SLOPE LENGTH (LS) FACTOR FOR SOIL STUDIES CONDUCTED IN THE YEAR 2014, 2022 AND 2023

Topographic factor – Slope Length and Steepness (LS) is a combination of slope gradient factor (S) and a slope – length (L), which are determined from the DEM

Slope – length factor is a vital parameter in soil erosion modeling and computing transport capacity of surface runoff.

An increase in the slope length of area indicates the steepness in which soil loss per unit area increases.

The flow accumulation raster obtained was then used for the estimation of the L factor by using the following formula

$$L = \left( \frac{\text{Flow accumulation} * \text{cell size}}{22.13} \right)^m$$

generalised LS formula is –

$$LS = [\text{flow accumulation} * \frac{\text{Cell Size}}{22.13}]^{0.4} * \left[ \frac{\sin \text{Slope}}{0.00896} \right]^{1.3}$$

#### 4.2.3.1 FLOW DIAGRAM FOR LS FACTOR CALCULATION

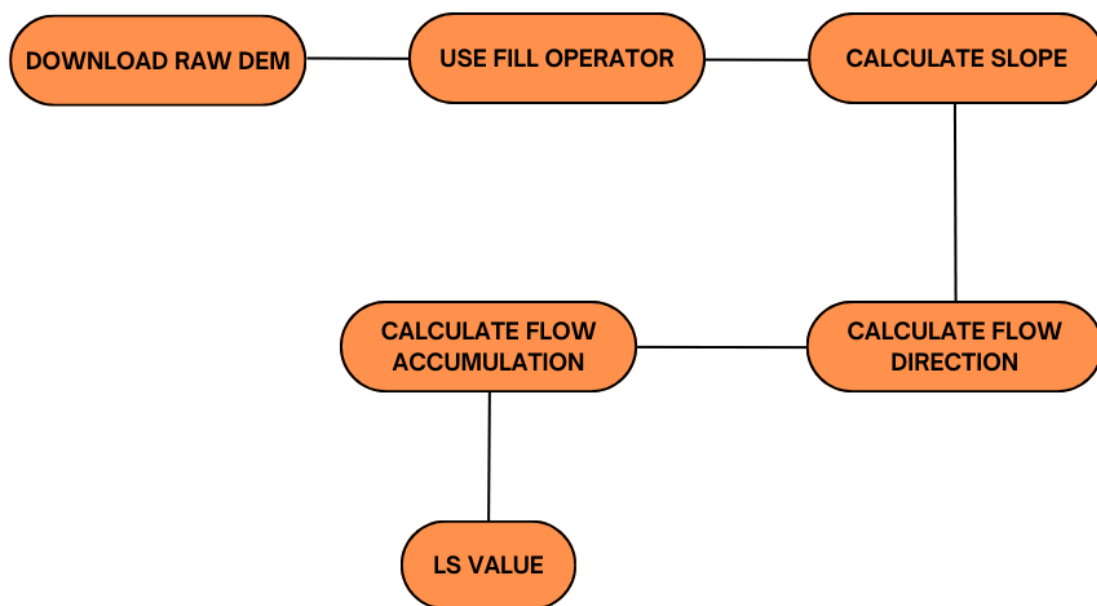


Fig: - 4.32 FLOW CHART OF LS WORKS

### 4.2.3.2 CREATION OF FILL AND FLOW DIRECTION

After downloading DEM (Data Elevation Model) from USGS earth explorer corresponding Fill and flow direction map have been created in ArcGIS for measuring slope length.

From above generalised equation, required parameters for calculation is *flow accumulation* and *Sin Slope* value with cell size as 30m

Steps for creating fill and flow direction map in Model Builder

Go to Model builder tool > Drag the .tif file > Arc Toolbox > Spatial Analyst Tools > Hydrology > Fill & Flow Direction

**Defination of Fill** – *Fill sinks in a surface raster to remove small imperfections in the given data*

Put all the credentials in the pop-up box on Fill menu.

Similarly, drag the Flow Direction option in the model builder menu for operation.

Connect the data .tif file to fill and flow option and create corresponding flow and fill file in the desired folder for further operation.

Now for merging Fill and Flow direction map, Mosaic is better way to merged the file in new raster map

Steps are as follows –

Go to Data Management Tools > Raster > Raster Dataset > Mosaic to New Raster,

Drag the Mosaic option to builder and run the model for validation outcome.

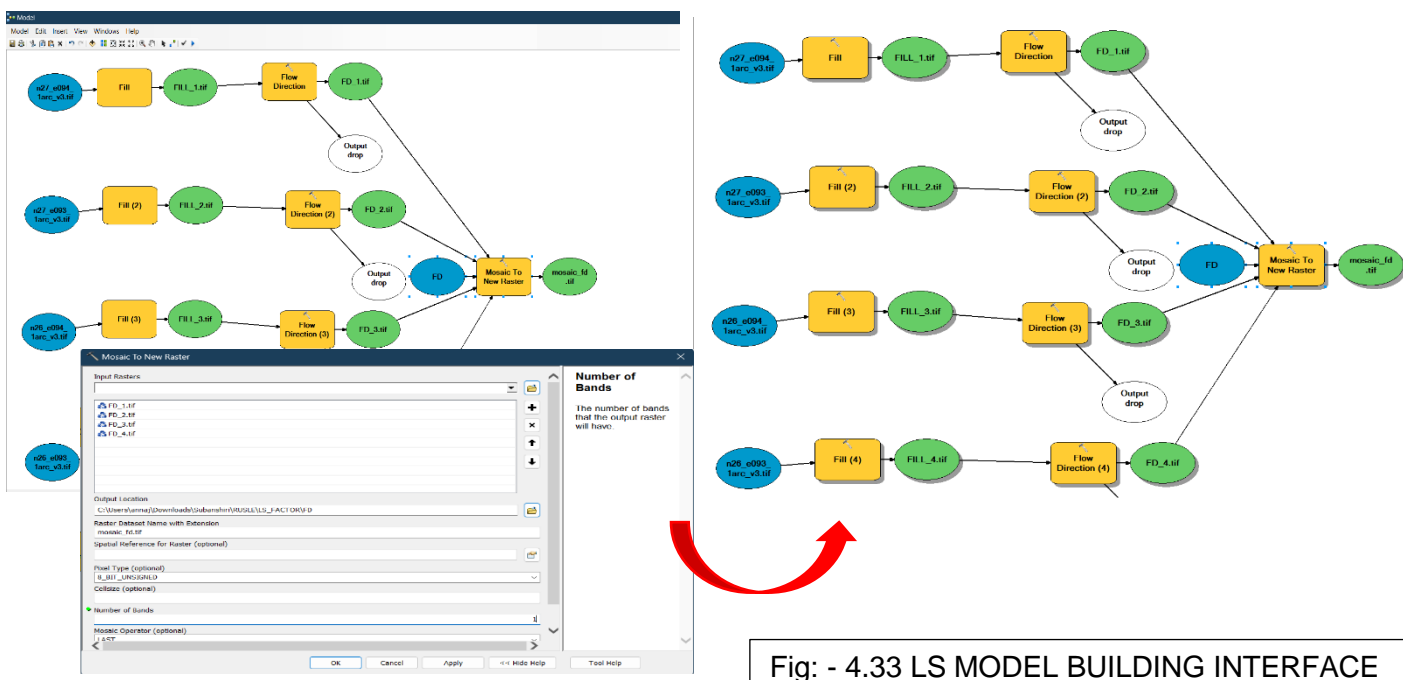


Fig: - 4.33 LS MODEL BUILDING INTERFACE

Below figure [4.34] is the mosaic flow direction map of value ranged from (1 – 128) where low is 1 and high is 128

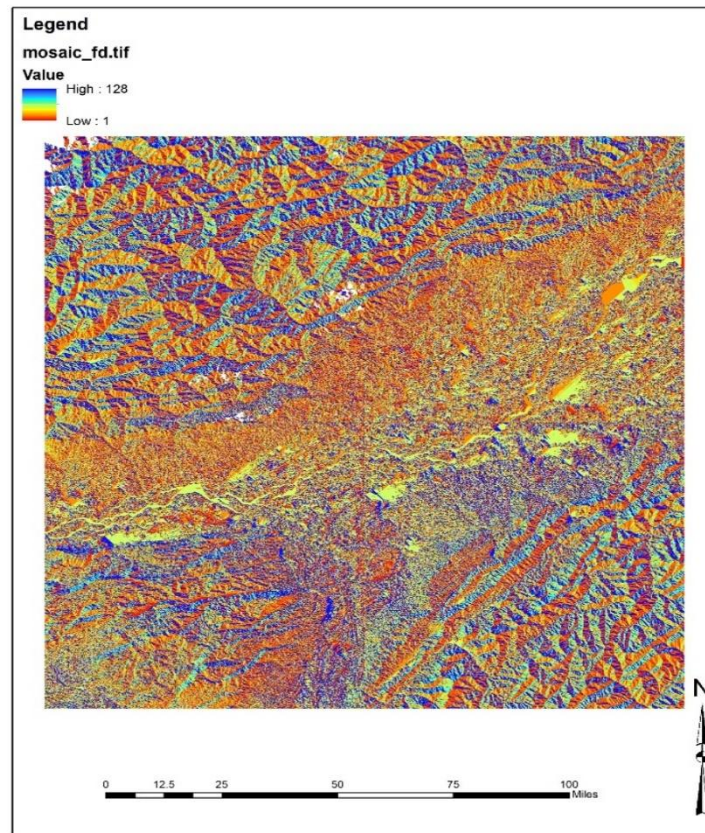


Fig: - 4.34 FLOW DIRECTION MOSAIC MAP

#### 4.2.3.3 CREATION OF FLOW ACCUMULATION MAP

As Flow direction map is obtained, now flow accumulation map will be created from the FD map for LS calculation which is being mosaic by model builder.

Steps to create *flow accumulation* map by following ways –

Method 1 –

Go to Arc Toolbox > Spatial Analyst Tools > Hydrology > Flow Accumulation,

A dialog box appears where after filling all the credentials with flow direction type D8.

Method 2 –

Go to Toolbar and select Geoprocessing > Environments Settings > Parallel processing > Parallel processing factor = 0; by turning off the Background Processing disabled

Here method 2 is taken into account for smooth interpretation of the data.

After then add all the FD (flow direction) map in ArcGIS and drag to model builder window

Then, Go to Arc Toolbox > Spatial Analyst tools > Hydrology > Flow Accumulation

Drag the flow accumulation option in Model Builder window for Mosaic the FD.tif files as shown in fig [4.35] by connecting each FD file

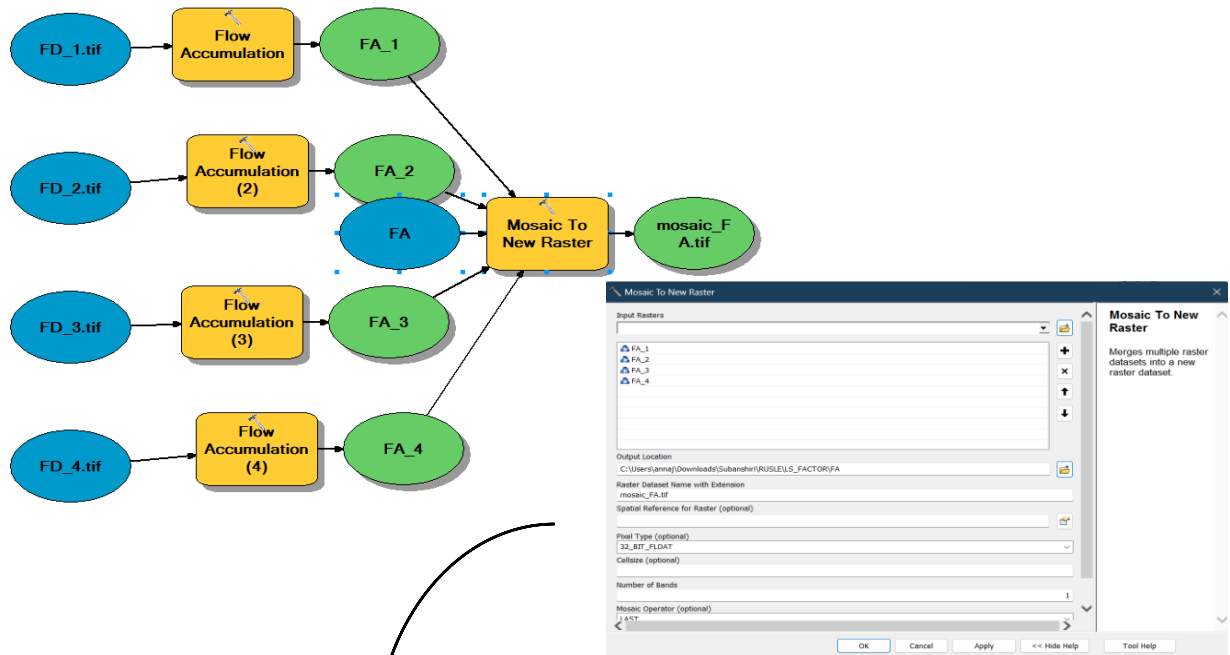
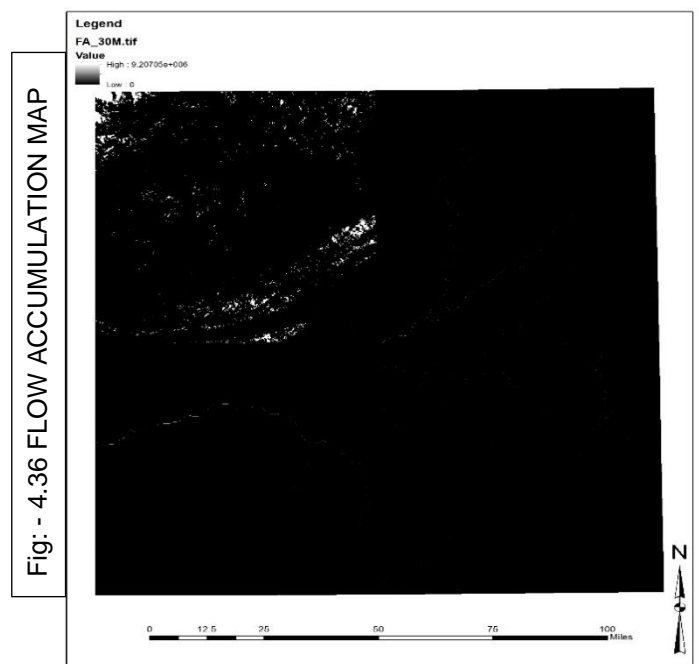


Fig: - 4.35 FLOW ACCUMULATION MODEL BUILDER

After validation run the model, where required flow accumulation map is being generated.

At Mosaic new Raster window,  
Pixel Type = **32-bit Float**  
Cell Size = **30**  
No of bands as **1**



#### 4.2.3.4 CALCULATION OF SLOPE IN RADIANS

Initially, add all the Fill Map in ArcGIS under layers at Table of contents bar.

Now mosaic the fill maps by following ways –

Go to Arc Toolbox > Data Management tools > Raster > Raster Dataset > Mosaic to New Raster

A dialog box appears add all the credentials and changed pixel type as **16-BIT UNSIGNED** and No of bands as 1

Then to calculate slope of the area

Go to Arc Toolbox > Spatial Analyst Tools > Surface > Slope

Add mosaic\_fill maps as in input in the surface dialog box and unchanged output measurements as DEGREE with Z- factor as 1 as shown in fig [4.38]

Again, change slope of the area from degree to radian as per requirements of **Williams.et.al** proposed formula

As we know, **1 degree = 0.0174533 radians**

Hence, above conversion will be perform in **Raster Calculator** followed by Spatial Analyst tools under Map Algebra option as shown below Fig [4.37] and formula used for evaluation with Spatial reference as WGS 1984 UTM Zone 46N

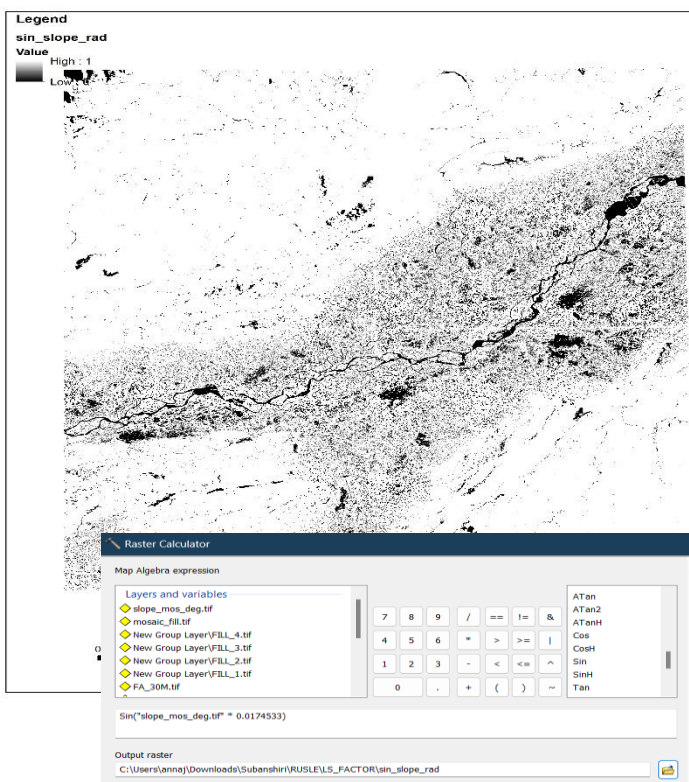


Fig: - 4.37 SIN\_SLOPE\_RADIAN MAP

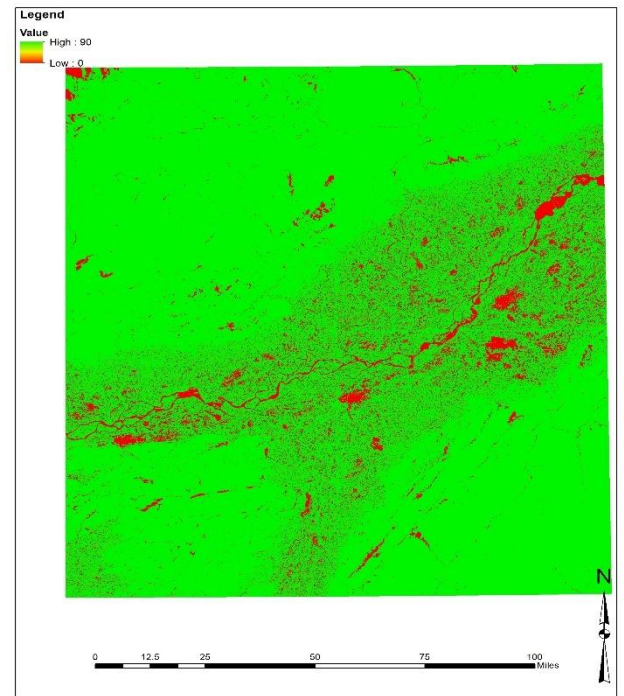


Fig: - 4.38 RADIAN MAP

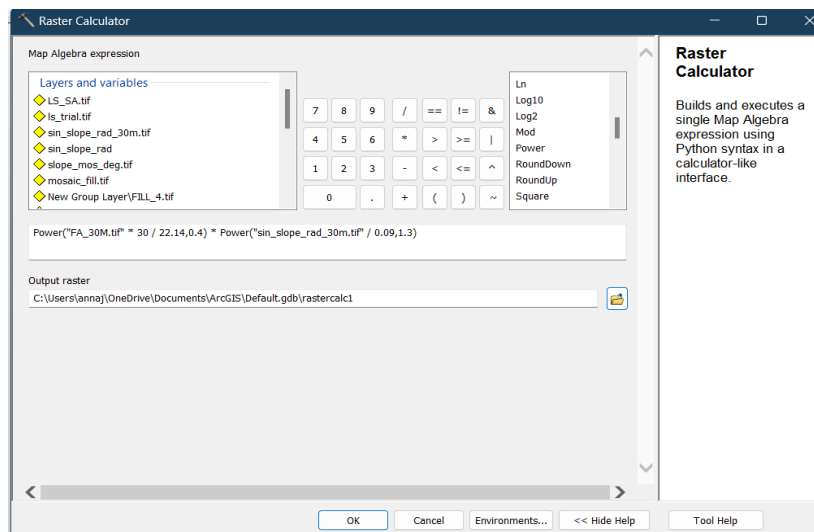
#### 4.2.3.5 EVALUATION OF LS MAP

After conversion of slope and flow accumulation generation, add the above data in ArcGIS window and then perform Raster Calculation in Map Algebra option

$$\text{Add formula } \mathbf{LS} = [\mathbf{flow\ accumulation} * \frac{\mathbf{Cell\ Size}}{22.13}]^{0.4} * \left[ \frac{\mathbf{sin\ Slope}}{0.00896} \right]^{1.3}$$

Add map algebra expression as –

- SIN\_SLOPE\_RAD map
- FLOW\_ACCU map, as shown in fig [4.38]



As per various research papers and from researchers LS value cannot exceed 100, but due to unavailability of field data it's difficult to evaluate correct LS value map

So, SAGA GIS is the useful software for finding LS factor which is more accurate than ArcGIS evaluated map independent of any field data (Šimůnek et al. (2017), Panagos et al. (2015), Mitasova et al. (1996). Hence, with accurate LS map overall evaluation of desired result will be appropriate to present where value range from (0 – 74.4633) which is accurate as shown in Fig [4.39]

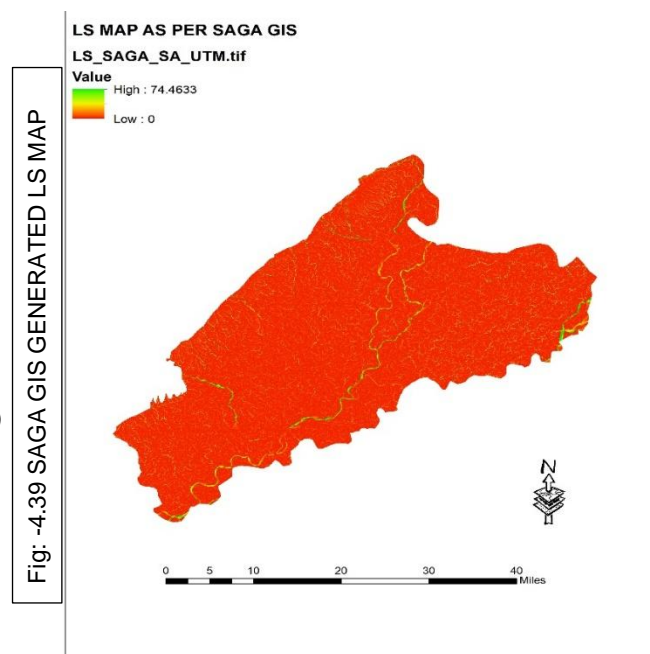


Fig: -4.39 SAGA GIS GENERATED LS MAP

#### 4.2.4 C – FACTOR (LAND USE AND LAND COVER)

The cover-management factor (C) is a fundamental component in estimating soil erosion rates, particularly within models like the Revised Universal Soil Loss Equation (RUSLE). It reflects the influence of vegetation cover, cropping systems, and land management practices on soil erosion, serving as a key indicator of how human activities and natural land cover affect the soil's vulnerability to erosive forces. As highlighted by **Koirala et al. (2019)**, the significance of the C factor lies in its ability to quantify the protective role of vegetation in mitigating soil erosion, ranking second only to topography as a determinant of erosion risk.

The values of the C factor range from 0 to 1, with lower values indicating better soil protection and reduced erosion.

Formula proposed by *Durgion et al, 2014*

$$C = \frac{(-NDVI+1)}{2}$$

Another one proposed by *Vatandaslar et al. 2017*.

$$C = 0.431 - 0.805 * NDVI$$

Above equations are taken into account for evaluation of C – factor

##### 4.2.4.1 WORKING WITH LANDSAT IMAGE OF 2014 FOR C- FACTOR CALCULATION

Firstly, Landsat image of 2014 is downloaded from USGS earth explorer of file name as – **LC08\_L2SP\_135041\_2014** of 30m resolution of Cloud Coverage percentage 30% as shown in fig [4.50]

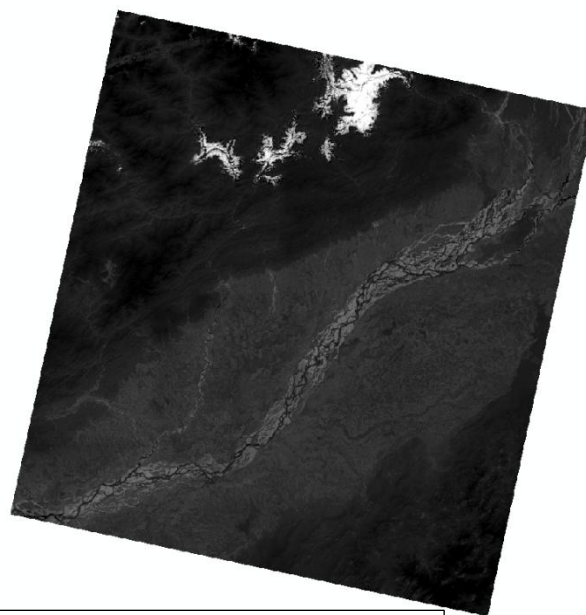


Fig: - 4.40 LANDSAT IMAGE OF YEAR 2014

#### 4.2.4.1.1 EVALUATION OF COMPOSITE BAND OF YEAR 2014

After downloading Landsat gridded image from USGS, add the file in ArcGIS window of band (.tif) file from zip file of the gridded file.

Steps for generating composite band –

Go to Arc Toolbox > Data Management Tools > Raster > Raster Processing > Composite Bands

A dialog box appears, add only band no 5, 4, 3, 2

Where Band No = 5 (Near Infrared) for Landsat 8 & Band No = 4 for Landsat 7

**Red, Green and Blue** for Band 3, 2, 1 respectively of Landsat 7 & Band 4, 3, 2 for Landsat 8

After following above steps composite band image generated of 30 m resolution as shown in Fig [4.41] & band for 4, 3, 2 of RGB map is defined as True Color Composite map fig [4.42]

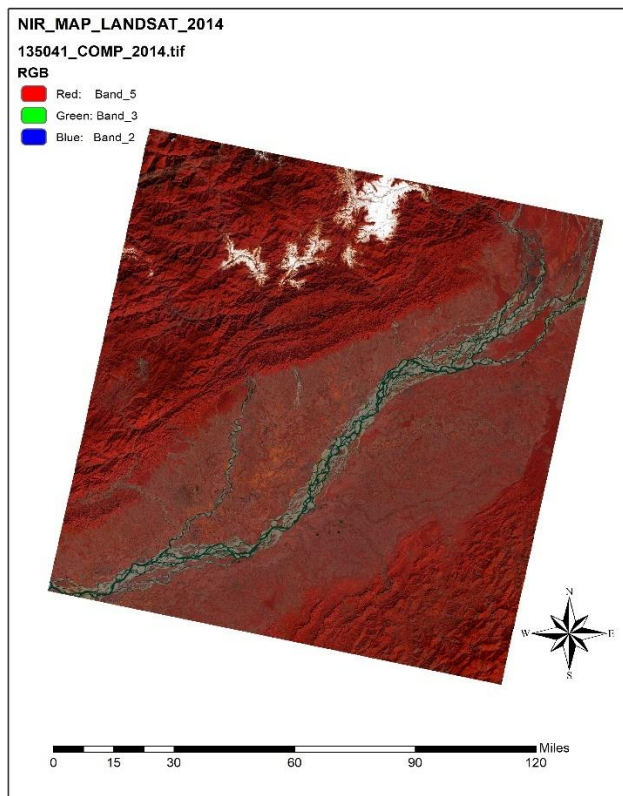


Fig: - 4.41 COMPOSITE BAND FCC 2014

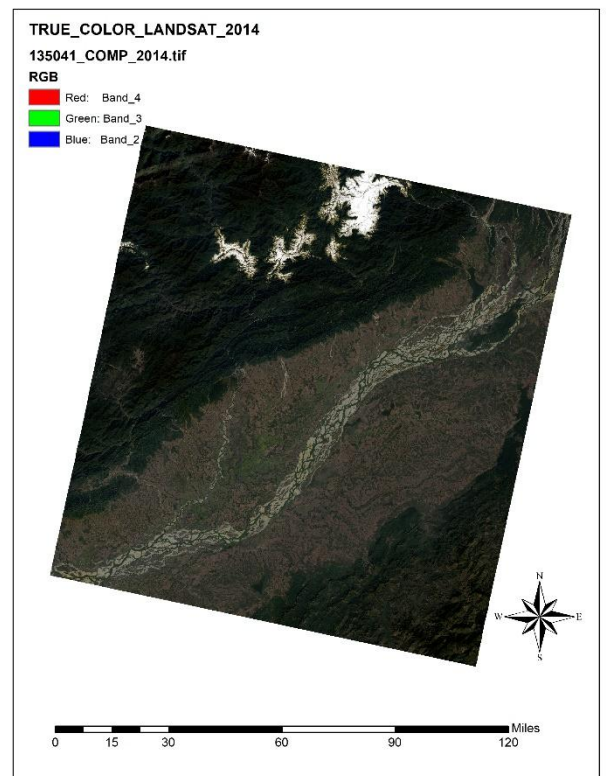


Fig: - 4.42 COMPOSITE BAND TRUE COLOR 2014

#### 4.2.4.1.2 EVALUATION OF NDVI MAP OF YEAR 2014

Here, NDVI (Normalized Difference Vegetation Index) is generated from composite band which mentioned in above Fig [4.41]

Steps of NDVI generation –

Go to Toolbar > Windows > Image Analysis

A side menu appears, Go to Image analysis option and changed Red bands as 4 and Infrared bands as 5

Then, go to processing bar and click NDVI button

A new NVDI map is being generated as shown in fig [4.43]

Here, fluctuation of value is due to variability of intensity of vegetation on that area

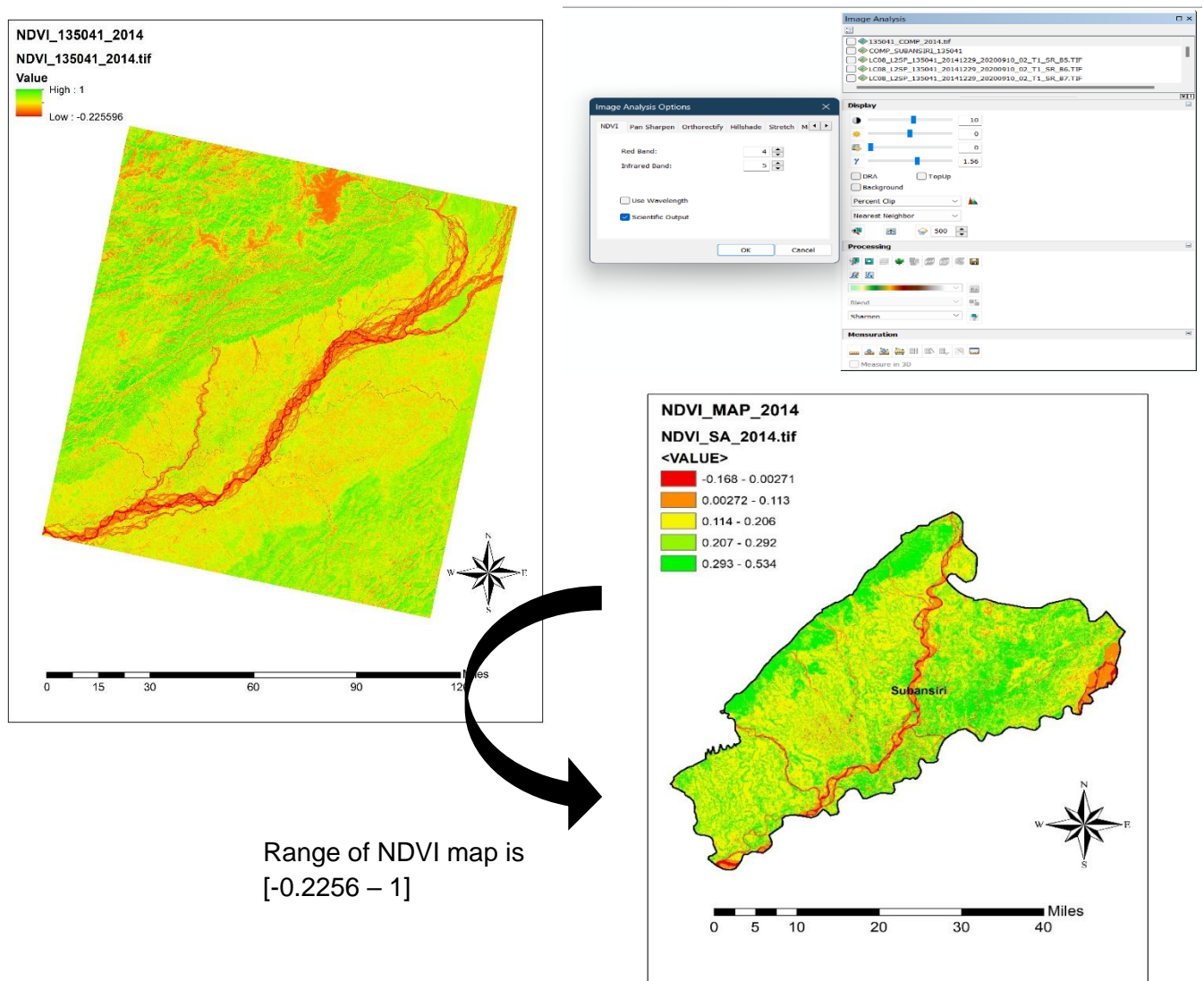


Fig: - 4.43 NDVI MAP OF 2014

### 4.2.4.1.3 EVALUATION OF C – FACTOR MAP OF YEAR 2014

Here, after above mentioned steps now calculation of C – factor is done with considered parameters as per **Vatandaslar.et.al** and **Durgion.et.al** proposed formula and considered appropriate map for further calculation

- Considered **Vatandaslar.et.al,2017** proposed formula –  
 $C = 0.431 - 0.805 * NDVI$

Go to Arc Toolbox > Spatial Analyst tool > Map Algebra > Raster Calculation

At map algebra expression added **Vatandaslar.et.al** formula as shown in fig [4.44] where value ranges from (0.00132 – 0.566143).

- Considered **Durgion.et.al** proposed formula –  
 $C = \frac{(-NDVI+1)}{2}$

Go to Arc Toolbox > Spatial Analyst tool > Map Algebra > Raster Calculation

At map algebra expression added **Durgion.et.al** formula as shown in fig [4.45] where value ranges from (0.233122 – 0.58394).

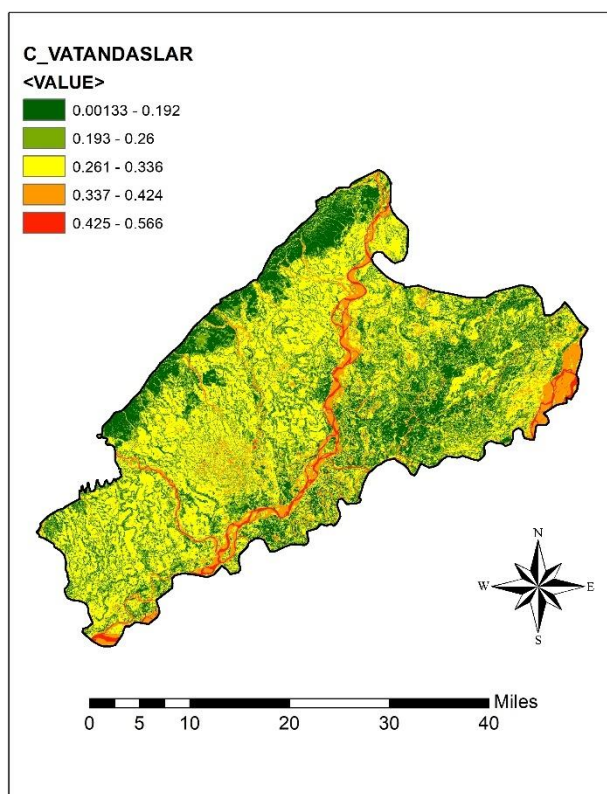


Fig - 4.44 C-FACTOR MAP BY VATANDASLAR.ET.AL 2014

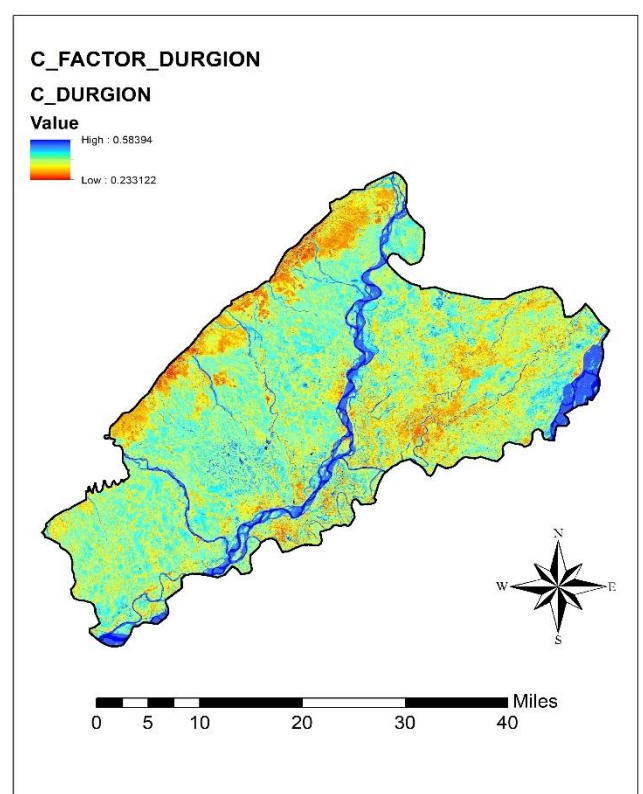


Fig - 4.45 C-FACTOR MAP BY DURGION.ET.AL 2014

#### 4.2.4.2 WORKING WITH LANDSAT IMAGE OF 2022 FOR C- FACTOR CALCULATION

Firstly, Landsat image of 2022 is downloaded from USGS earth explorer of file name as – **LC08\_L2SP\_135041\_2022** of 30m resolution of Cloud Coverage percentage 30%

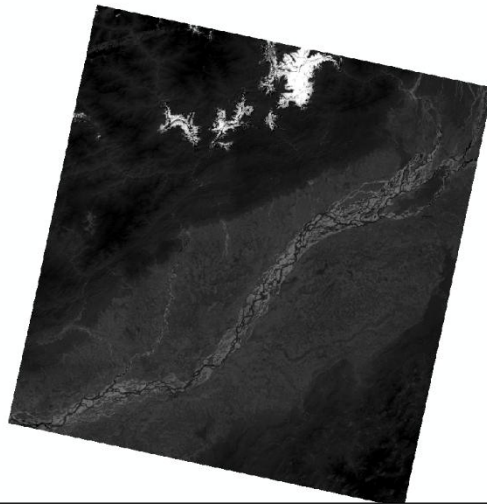


Fig: - 4.46 LANDSAT IMAGE OF YEAR 2022

##### 4.2.4.2.1 EVALUATION OF COMPOSITE BAND OF YEAR 2022

After downloading Landsat gridded image from USGS, add the file in ArcGIS window of band (.tif) file from zip file of the gridded file.

Steps for generating composite band –

Go to Arc Toolbox > Data Management Tools > Raster > Raster Processing > Composite Bands

A dialog box appears, add only band no 5, 4, 3, 2

Where Band No = 5 (Near Infrared) for Landsat 8 & Band No = 4 for Landsat 7

**Red, Green and Blue** for Band 3, 2, 1 respectively of Landsat 7 & Band 4, 3, 2 for Landsat 8

After following above steps composite band image generated of 30 m resolution

#### 4.2.4.2.2 EVALUATION OF NDVI MAP OF YEAR 2022

Here, NDVI (Normalized Difference Vegetation Index) is generated from composite band

Steps of NDVI generation –

Go to Toolbar > Windows > Image Analysis

A side menu appears, Go to Image analysis option and changed Red bands as 4 and Infrared bands as 5

Then, go to processing bar and click NDVI button. A new NVDI map is being generated of value ranges from (-0.244963 – 0.539822) as shown in fig [4.47]

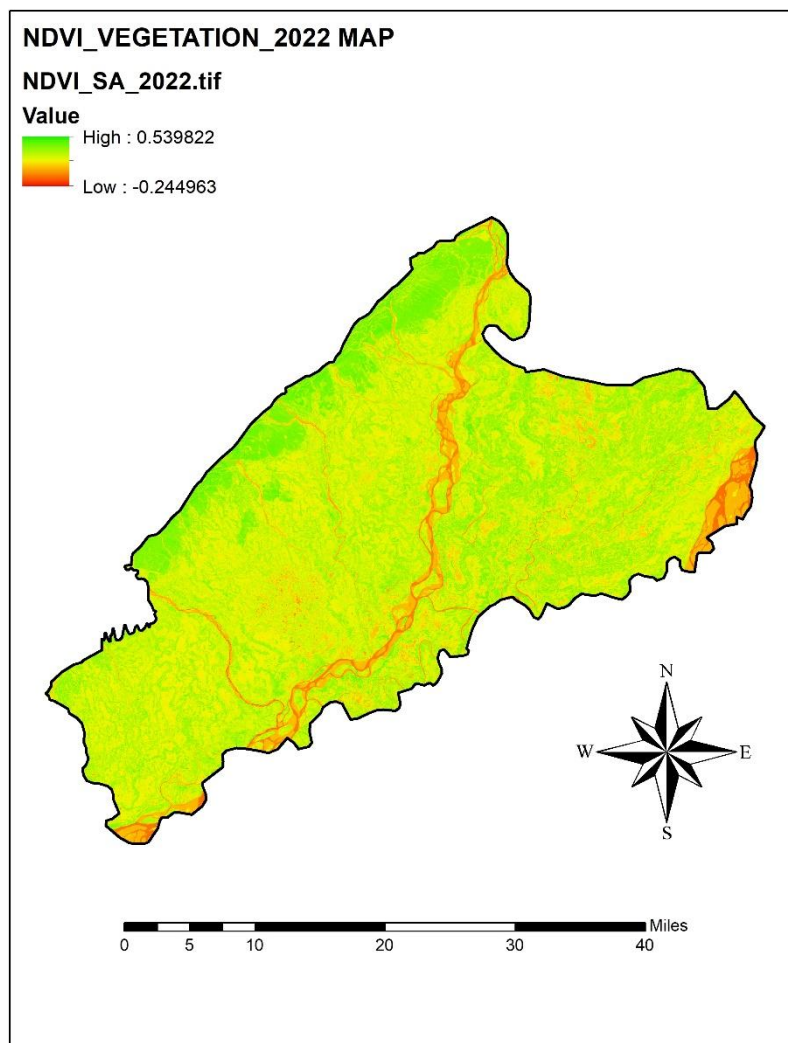


Fig: - 4.47 NDVI MAP OF 2022

#### 4.2.4.2.3 EVALUATION OF C – FACTOR MAP OF YEAR 2022

Here, after above mentioned steps now calculation of C – factor is done with considered parameters as per **Vatandaslar.et.al** and **Durgion.et.al** proposed formula and considered appropriate map for further calculation

- Considered **Vatandaslar.et.al,2017** proposed formula –  
 $C = 0.431 - 0.805 * NDVI$

Go to Arc Toolbox > Spatial Analyst tool > Map Algebra > Raster Calculation

At map algebra expression added **Vatandaslar.et.al** formula as shown in fig [4.48] where value ranges from (-0.00355 – 0.628195).

- Considered **Durgion.et.al** proposed formula –  
 $C = \frac{(-NDVI+1)}{2}$

Go to Arc Toolbox > Spatial Analyst tool > Map Algebra > Raster Calculation

At map algebra expression added **Durgion.et.al** formula as shown in fig [4.49] where value ranges from (0.230089 – 0.622481)

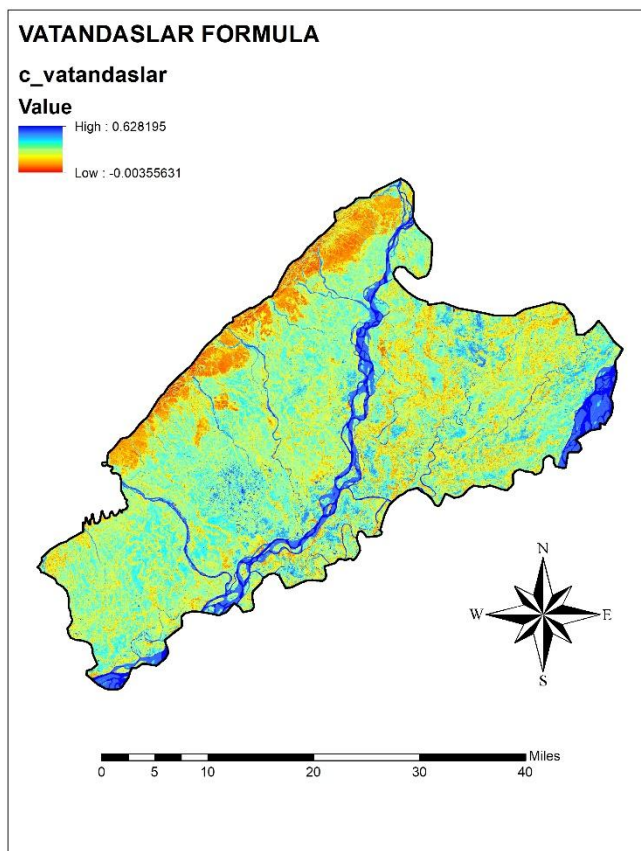


Fig: - 4.48 C-FACTOR MAP BY VATANDASLAR.ET.AL 2022

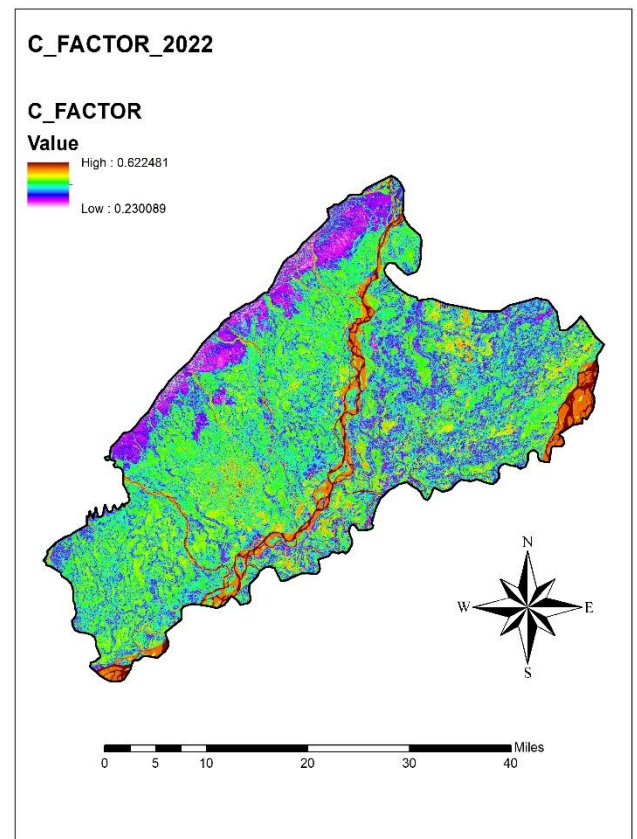


Fig: - 4.49 C-FACTOR MAP BY DURGION.ET.AL 2022

#### 4.2.4.3 WORKING WITH LANDSAT IMAGE OF 2023 FOR C- FACTOR CALCULATION

Firstly, Landsat image of 2023 is downloaded from USGS earth explorer of file name as – **LC08\_L2SP\_135041\_2023** of 30m resolution of Cloud Coverage percentage 30%

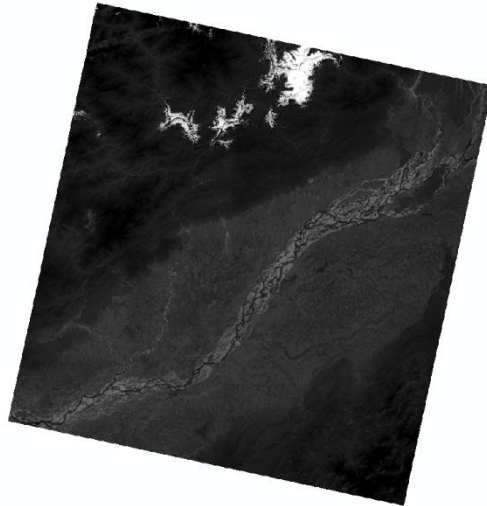


Fig: - 4.50 LANDSAT IMAGE OF YEAR 2023

##### 4.2.4.3.1 EVALUATION OF COMPOSITE BAND OF YEAR 2023

After downloading Landsat gridded image from USGS, add the file in ArcGIS window of band (.tif) file from zip file of the gridded file.

Steps for generating composite band –

Go to Arc Toolbox > Data Management Tools > Raster > Raster Processing > Composite Bands

A dialog box appears, add only band no 5, 4, 3, 2

Where Band No = 5 (Near Infrared) for Landsat 8 & Band No = 4 for Landsat 7

**Red, Green and Blue** for Band 3, 2, 1 respectively of Landsat 7 & Band 4, 3, 2 for Landsat 8

After following above steps composite band image generated of 30 m resolution

#### 4.2.4.3.2 EVALUATION OF NDVI MAP OF YEAR 2023

Here, NDVI (Normalized Difference Vegetation Index) is generated from composite band

Steps of NDVI generation –

Go to Toolbar > Windows > Image Analysis

A side menu appears, Go to Image analysis option and changed Red bands as 4 and Infrared bands as 5

Then, go to processing bar and click NDVI button. A new NVDI map is being generated of value ranges from (-0.237862 – 0.556076) as shown in fig [4.51]

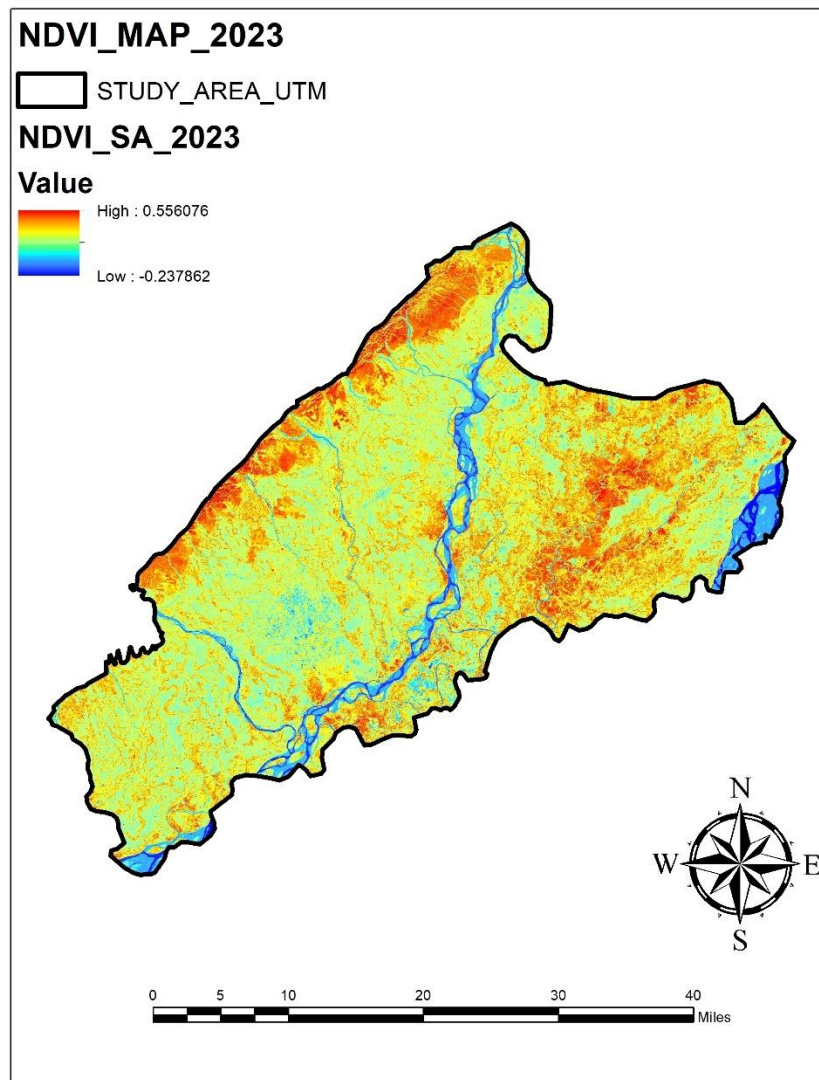


Fig: - 4.51 NDVI MAP OF 2023

#### 4.2.4.3.3 EVALUATION OF C – FACTOR MAP OF YEAR 2023

Here, after above mentioned steps now calculation of C – factor is done with considered parameters as per **Vatandaslar.et.al** and **Durgion.et.al** proposed formula and considered appropriate map for further calculation

- Considered **Vatandaslar.et.al,2017** proposed formula –  
 $C = 0.431 - 0.805 * NDVI$

Go to Arc Toolbox > Spatial Analyst tool > Map Algebra > Raster Calculation

At map algebra expression added **Vatandaslar.et.al** formula as shown in fig [4.52] where value ranges from (-0.01664 – 0.62247)

- Considered **Durgion.et.al** proposed formula –  
 $C = \frac{(-NDVI+1)}{2}$

Go to Arc Toolbox > Spatial Analyst tool > Map Algebra > Raster Calculation

At map algebra expression added **Durgion.et.al** formula as shown in fig [4.53] where value ranges from (0.2219 – 0.618931)

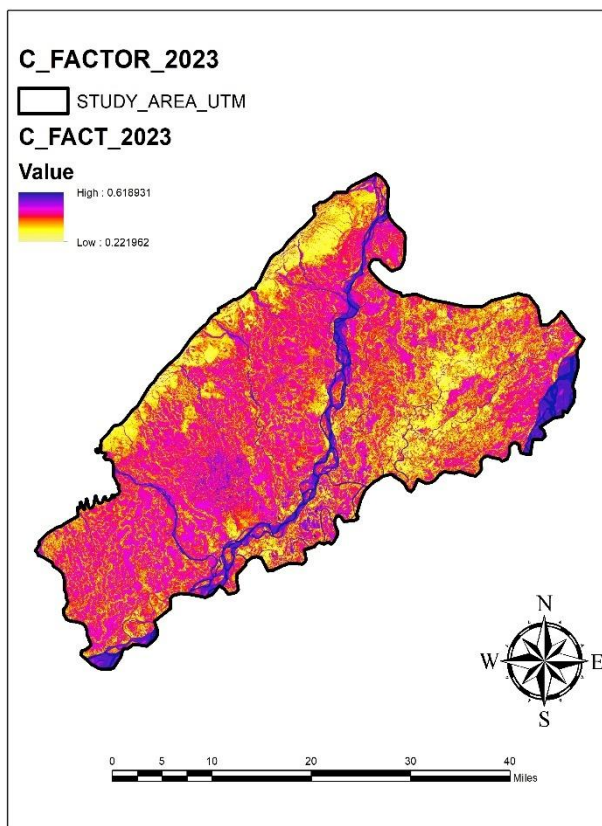


Fig: - 4.52 C-FACTOR MAP BY VATANDASLAR.ET.AL 2023

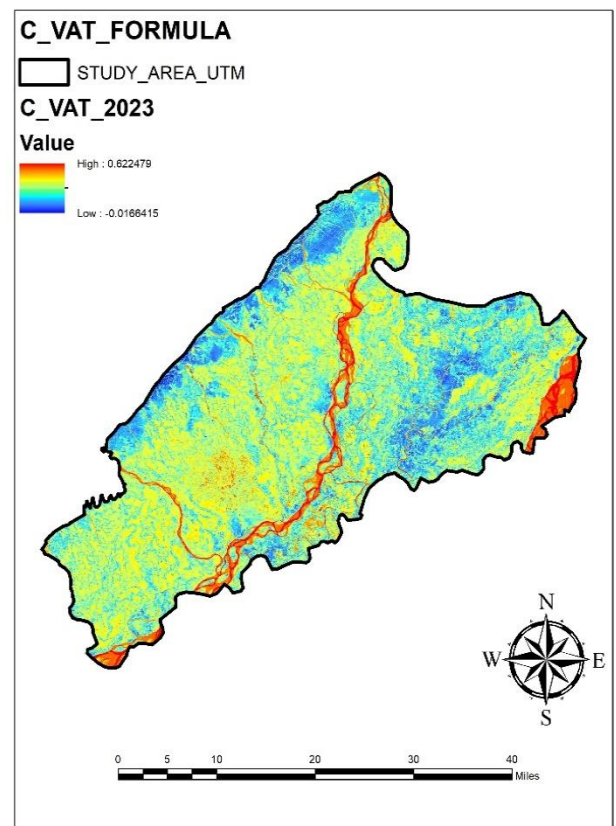


Fig: - 4.53 C-FACTOR MAP BY DURGION.ET.AL 2023

## 4.2.5 P – FACTOR (CONSERVATION PRACTICE FACTOR)

The conservation practice factor (P), also known as the support factor, represents the soil-loss ratio after implementing specific conservation practices, indicating their effectiveness in reducing soil and water loss. The P-factor ranges from 0 to 1, with lower values signifying more effective practices. For this study, a value of 1 was assigned across the entire study area in the RUSLE model due to the absence of significant conservation practices. In regions like Manafwa, conservation efforts, primarily tree planting, are more relevant to the cover management factor (C) rather than the P-factor.

### 4.2.5.1 P – FACTOR WORKING FOR STUDY AREA 2014

#### 4.2.5.1.1 SUPERVISED CLASSIFICATION FOR THE YEAR 2014

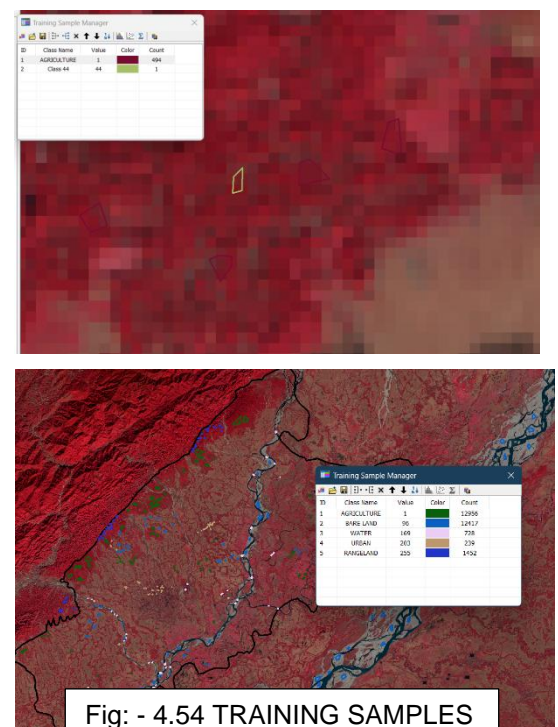
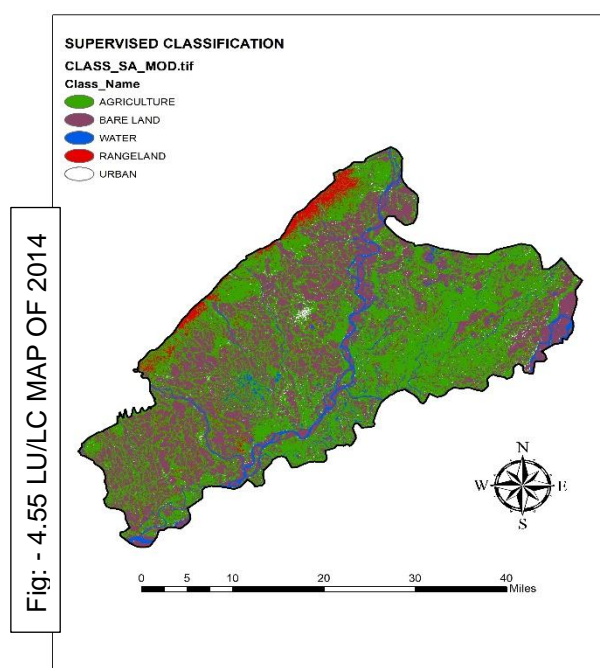
Initially, add the composite band tif file in the ArcGIS under layers bar for classification.

Extract the study area from composite band tif file by using extract by mask in Arc Toolbox followed by Spatial Analyst tools > Extraction

Before classification, changed the colour Red to band 5 as NIR for convenient identification of vegetation while training samples.

Now, from classification bar select polygon option and start collecting samples from the study area as shown in fig [4.55] (*collecting agricultural samples*) and value will be recorded on Training sample manager.

In this way samples are selected of different types for supervised classification where final land cover image is generated Fig [4.54]



#### 4.2.5.1.2 RECLASSIFY SLOPE AND COMBINE WITH CLASSIFICATION MAP

Here, slope is converted to percentage for evaluation of P – FACTOR. As P values varied with slope percentage which will be validate for study land use/land cover factor of the study area.

Steps for operation –

At first add Mosaic\_fill.tif files into ArcGIS window followed by layer column.

Go to Arc Toolbox > Spatial Analyst Tools > Surface > Slope

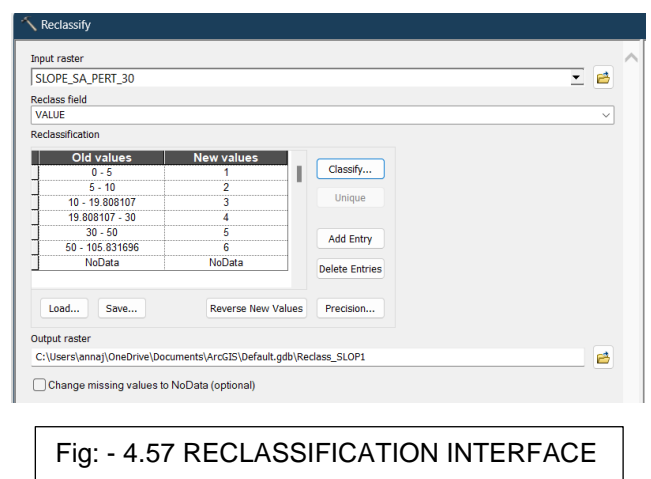
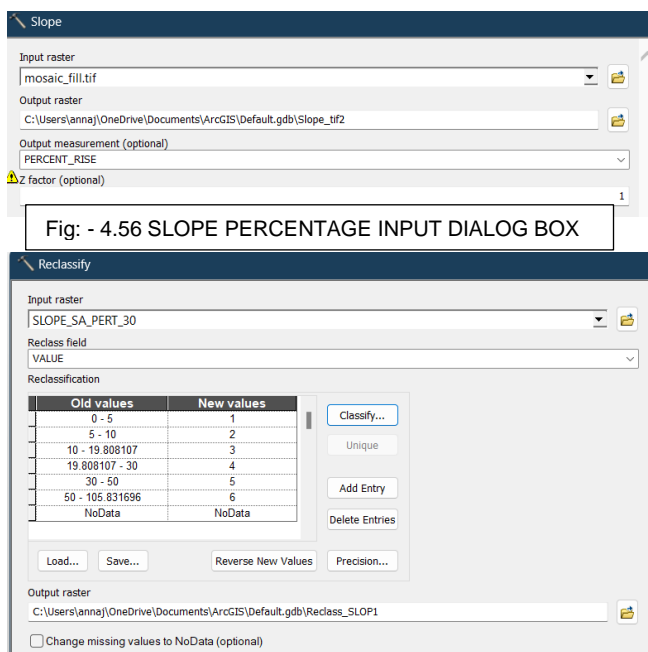
A dialog box appears add all the credentials followed by Output Measurement as Percent\_Rise with unchanged Z – factor as 1 and extract the study area followed by Extract by Mask under Extraction option in Arc Toolbox.

Now in slope percentage map, from continue dataset it converts to discrete dataset as in discrete dataset contains integer values.

So, in order to make both map discrete i.e, classification map fig [1.72] & slope percentage map combine operation is required

Go to Arc Toolbox > Spatial Analyst Tools > Reclass > Reclassify

Put slope percentage map as an input and classify the existing table with modification on table [3.7] and figure is shown Fig [4.56] & Fig [4.57] interface of the reclassify window for editing the slope value manually for accurate calculation without any error due to unavailability of filed data.



After reclassification and combining the two discrete entities following map is generated for further analysis as shown in fig [4.58] & fig [4.59] respectively where 30 different classes is obtained for accurate identification.

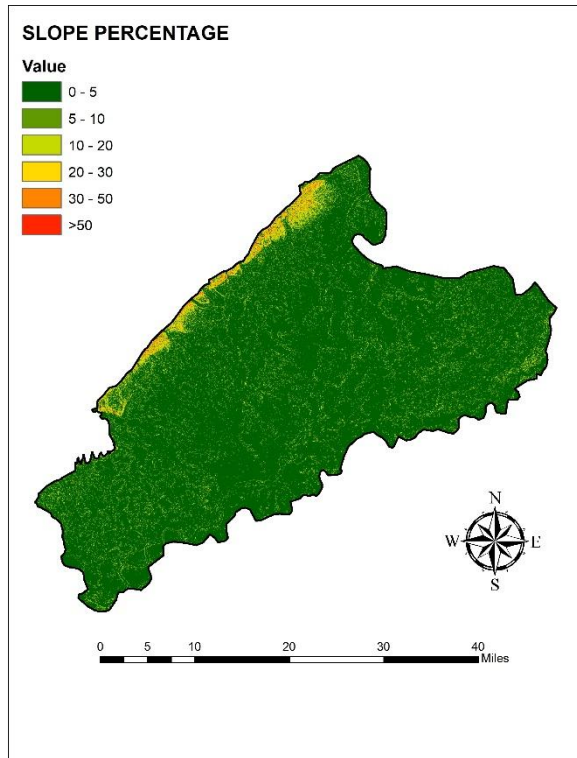


Fig: - 4.58 SLOPE PERCENTAGE MAP 2014

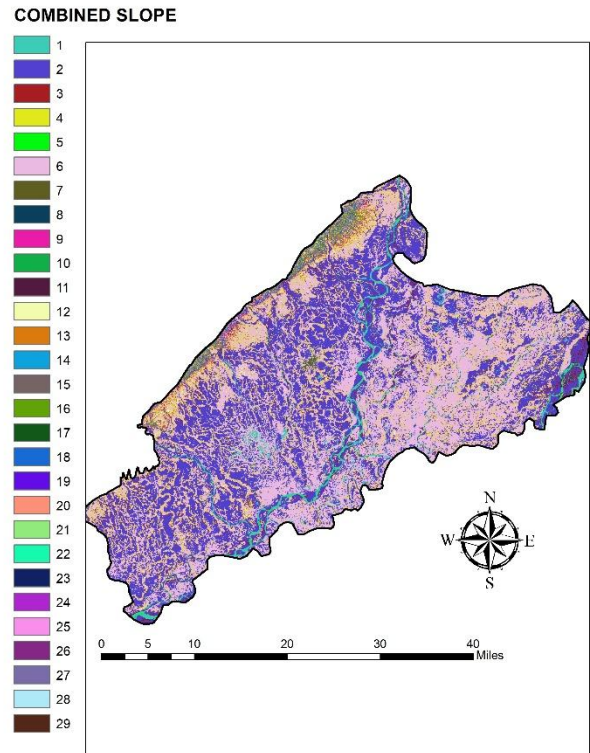


Fig: - 4.59 COMBINED SLOPE MAP 2014

#### 4.2.5.1.3 ASSIGNING P – FACTOR VALUES FOR CLASSES IN ATTRIBUTE TABLE

Here, combined map that have generated earlier is technically a P – factor map without any assigned P – values.

So, assigning P -values is mandatory for classification of the P – FACTOR map.

Hence, assigning is done by the following steps –

Right Click on combined\_map at Layers column > click on Attribute Table

A table will pop up > Click Add field from toolbar > Name the field as P\_Factor; Type changed to Float

Now, assigned the value according to its class number by taking reference from table [3.7] for accurate outcome and assigned table of 2014 P -factor is table [4.4]

ATTRIBUTE TABLE OF COMBINED SLOPE CLASS 2014				
Value	Count	Reclass_SL	CLASS_SA_M	P_factor
1	121204	1	169	0.00
2	1194075	1	96	0.25
3	108639	2	96	0.35
4	271554	2	1	0.12
5	14847	2	169	0.00
6	1332474	1	1	0.10
7	32677	1	256	0.00
8	2744	3	169	0.00
9	48119	3	1	0.14
10	4758	2	256	0.00
11	12339	3	96	0.45
12	39167	1	255	0.10
13	26630	2	255	0.13
14	10235	4	1	0.19
15	505	3	256	0.00
16	23351	3	255	0.15
17	613	4	96	0.55
18	15673	4	255	0.20
19	5077	5	1	0.25
20	11396	5	255	0.40
21	1659	6	255	0.70
22	388	6	1	0.70
23	169	5	96	0.75
24	45	4	256	0.00
25	102	4	169	0.00
26	19	5	169	0.00
27	7	6	169	0.00
28	9	5	256	0.00
29	14	6	96	1.00

Table: - 4.4 Attribute table of period 2014

After assigning the value Go to Layer properties and changed Fields Value as P\_factor and classes to 5. Here, fig [4.60] is assigned P\_factor map and fig [4.61] P factor map in UTM format.

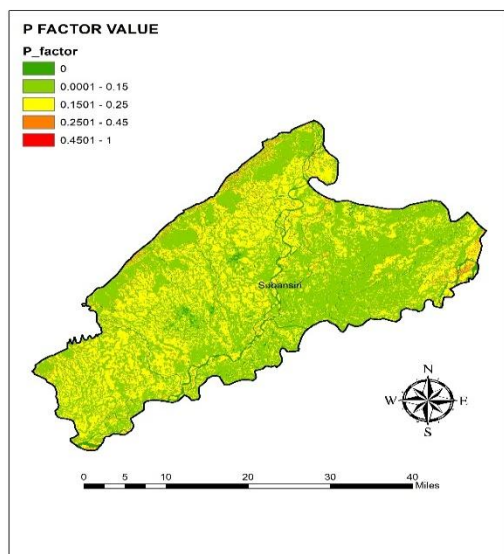


Fig: - 4.60 P\_FACTOR VALUE MAP 2014

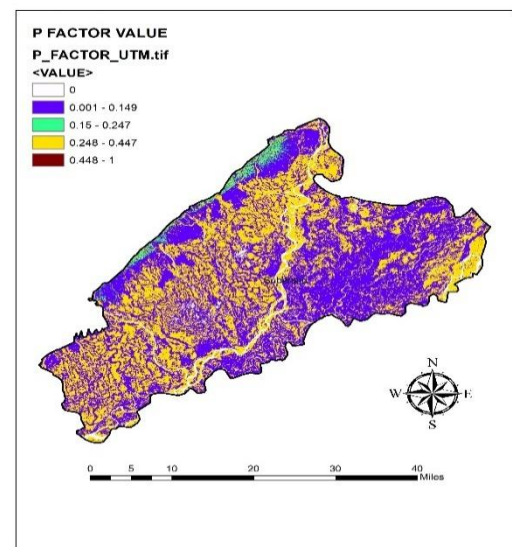


Fig: - 4.61 P\_FACTOR UTM MAP 2014

## 4.2.5.2 P – FACTOR WORKING FOR STUDY AREA 2022

### 4.2.5.2.1 SUPERVISED CLASSIFICATION FOR THE YEAR 2022

Initially, add the composite band tif file in the ArcGIS under layers bar for classification.

Extract the study area from composite band tif file by using extract by mask in Arc Toolbox followed by Spatial Analyst tools > Extraction

Before classification, changed the colour Red to band 5 as NIR for convenient identification of vegetation while training samples.

Now, from classification bar select polygon option and start collecting samples from the study area as shown in fig [4.63] (*collecting agricultural samples*) and value will be recorded on Training sample manager.

In this way samples are selected of different types for supervised classification where final land cover image is generated Fig [4.62]

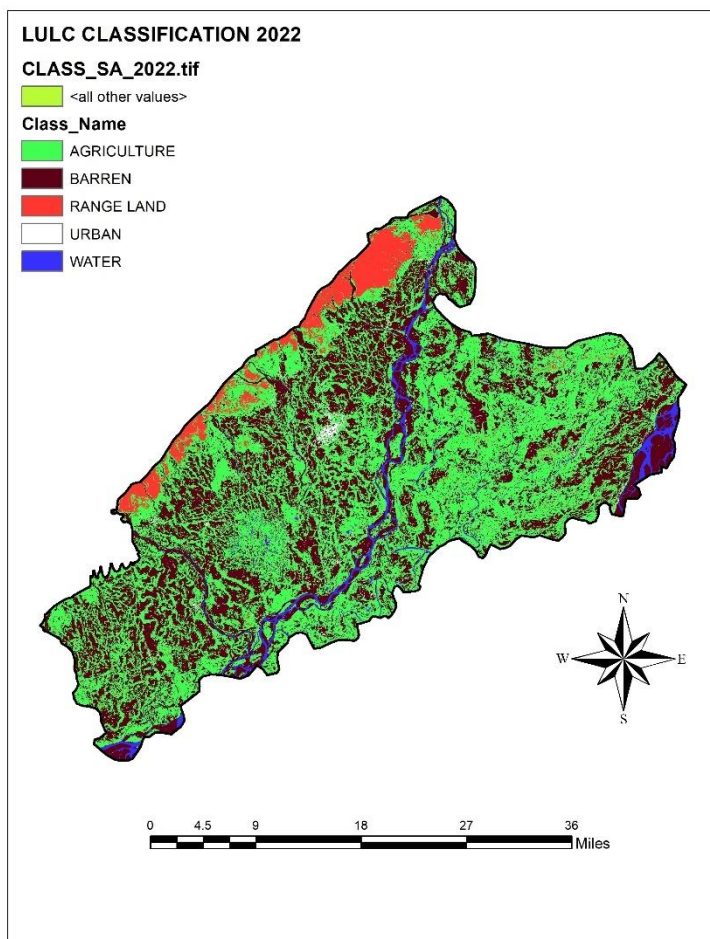


Fig: - 4.62 LU/LC MAP OF 2022

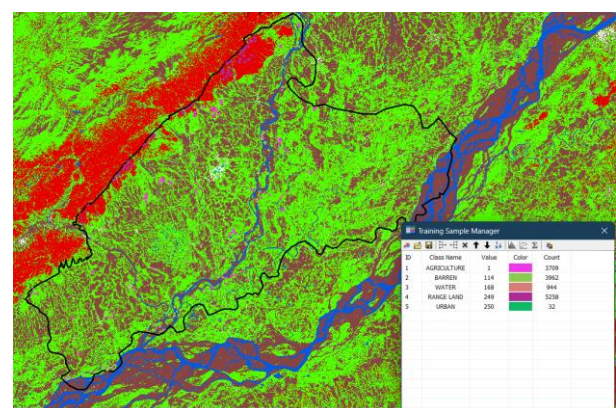
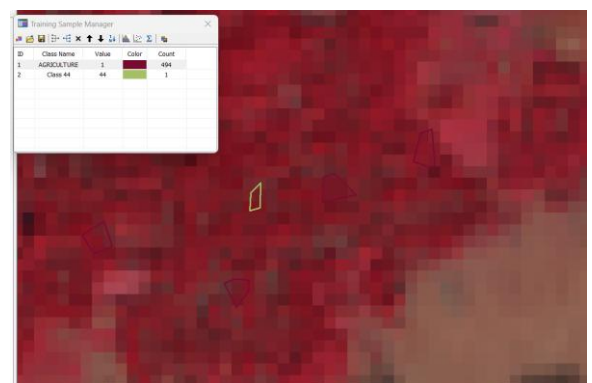


Fig: - 4.63 TRAINING SAMPLES

### 4.2.5.2.2 RECLASSIFY SLOPE AND COMBINE WITH CLASSIFICATION MAP

Here, slope is converted to percentage for evaluation of P – FACTOR. As P values varied with slope percentage which will be validate for study land use/land cover factor of the study area.

Steps for operation –

At first add Mosaic\_fill.tif files into ArcGIS window followed by layer column.

Go to Arc Toolbox > Spatial Analyst Tools > Surface > Slope

A dialog box appears add all the credentials followed by Output Measurement as Percent\_Rise with unchanged Z – factor as 1 and extract the study area followed by Extract by Mask under Extraction option in Arc Toolbox.

Now in slope percentage map, from continue dataset it converts to discrete dataset as in discrete dataset contains integer values.

So, in order to make both map discrete i.e. classification map fig [4.62] & slope percentage map combine operation is required

Go to Arc Toolbox > Spatial Analyst Tools > Reclass > Reclassify

Put slope percentage map as an input and classify the existing table with modification on table [3.7] and figure is shown Fig [4.64] & Fig [4.65] interface of the reclassify window for editing the slope value manually for accurate calculation without any error due to unavailability of filed data.

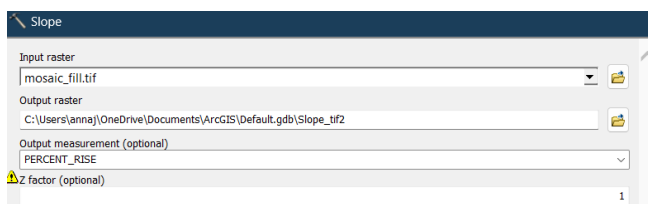


Fig: - 4.64 SLOPE PERCENTAGE INPUT DIALOG BOX

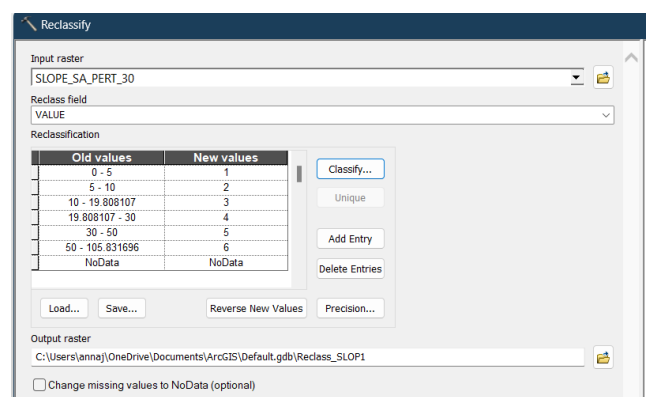
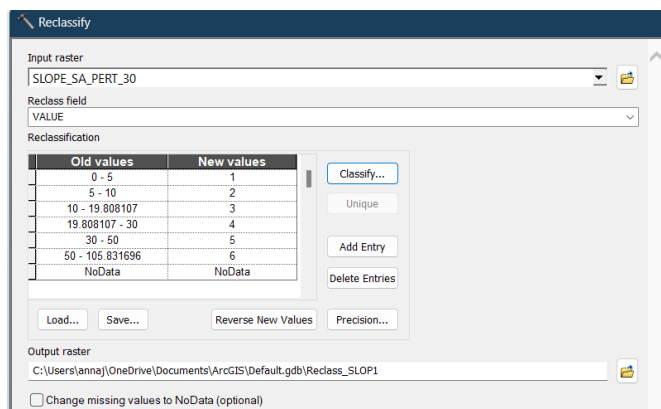


Fig: - 4.65 RECLASSIFICATION INTERFACE

After reclassification and combining the two discrete entities following map is generated for further analysis as shown in fig [4.66] & fig [4.67] respectively where 30 different classes is obtained for accurate identification.

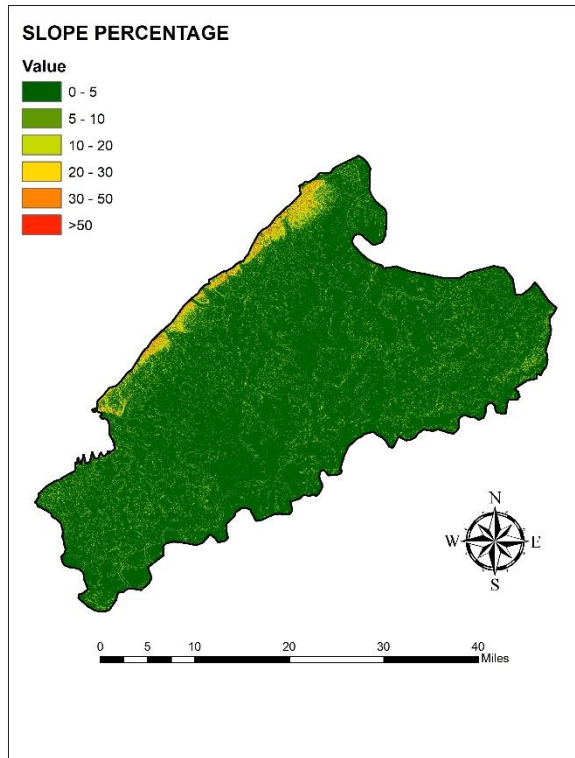


Fig: - 4.66 P\_FACTOR VALUE MAP 2022

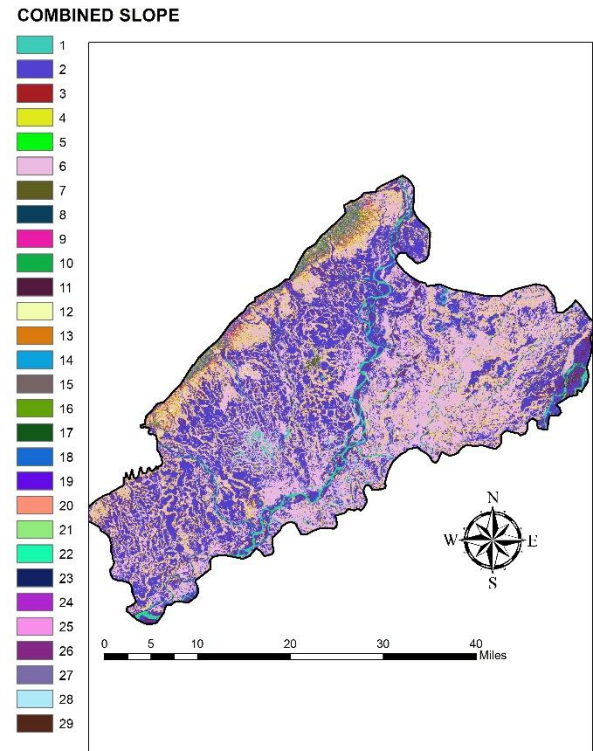


Fig: - 4.67 P\_FACTOR UTM MAP 2022

#### 4.2.5.2.3 ASSIGNING P – FACTOR VALUES FOR CLASSES IN ATTRIBUTE TABLE

Here, combined map that have generated earlier is technically a P – factor map without any assigned P – values.

So, assigning P -values is mandatory for classification of the P – FACTOR map.

Hence, assigning is done by the following steps –

Right Click on combined\_map at Layers column > click on Attribute Table

A table will pop up > Click Add field from toolbar > Name the field as P\_Factor; Type changed to Float

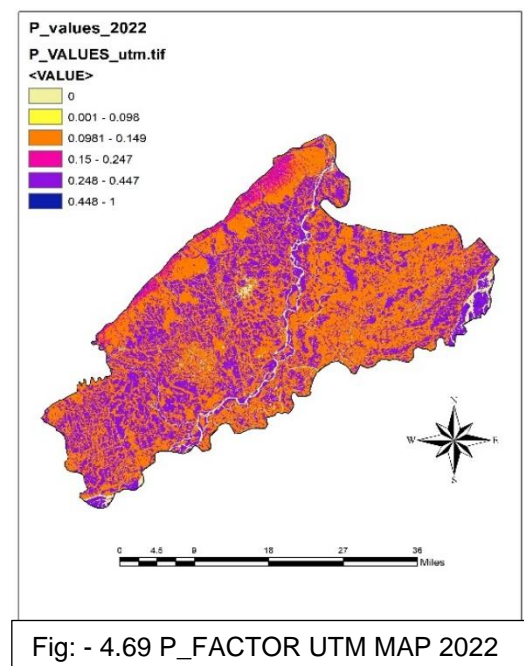
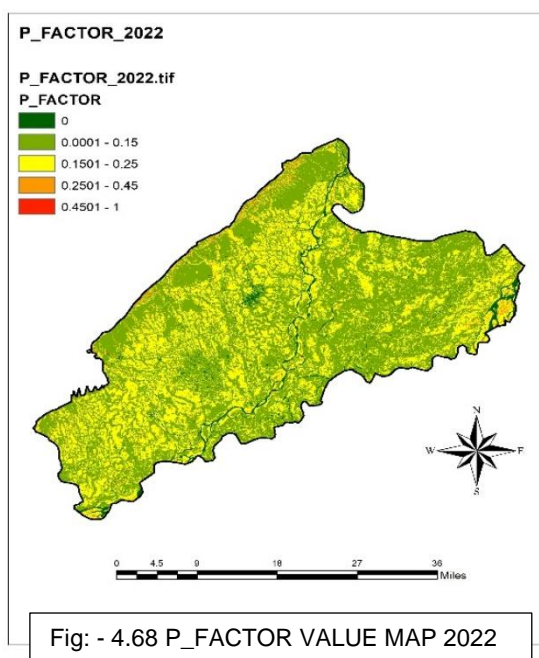
Now, assigned the value according to its class number by taking reference from table [3.7] for accurate outcome and assigned table of 2014 P -factor is table [4.5]

## ATTRIBUTE TABLE OF COMBINED SLOPE CLASS 2022

Value	Count	Reclass_Sl	CLASS_SA_2	P_FACTOR
1	81594	1	168	0.00
2	1161806	1	114	0.25
3	1382508	1	1	0.10
4	267239	2	1	0.12
5	37005	1	250	0.00
6	11407	2	168	0.00
7	99532	2	114	0.35
8	2491	3	168	0.00
9	42341	2	249	0.10
10	35596	3	1	0.14
11	10931	3	114	0.45
12	56684	1	249	0.13
13	5909	2	250	0.00
14	37902	3	249	0.15
15	444	3	250	0.00
16	4961	4	1	0.19
17	20703	4	249	0.20
18	572	4	114	0.55
19	13973	5	249	0.40
20	1870	6	249	0.70
21	33	4	250	0.00
22	2529	5	1	0.25
23	153	5	114	0.75
24	187	6	1	0.70
25	93	4	168	0.00
26	11	5	250	0.00
27	4	5	168	0.00
28	11	6	114	1.00

Table: - 4.5 Attribute table of period 2022

After assigning the value Go to Layer properties and changed Fields Value as P\_factor and classes to 5. Here, fig [4.68] is assigned P\_factor map and fig [4.69] P factor map in UTM format.



### 4.2.5.3 P – FACTOR WORKING FOR STUDY AREA 2023

#### 4.2.5.3.1 SUPERVISED CLASSIFICATION FOR THE YEAR 2023

Initially, add the composite band tif file in the ArcGIS under layers bar for classification.

Extract the study area from composite band tif file by using extract by mask in Arc Toolbox followed by Spatial Analyst tools > Extraction

Before classification, changed the colour Red to band 5 as NIR for convenient identification of vegetation while training samples.

Now, from classification bar select polygon option and start collecting samples from the study area as shown in fig [4.70] (*collecting agricultural samples*) and value will be recorded on Training sample manager.

In this way samples are selected of different types for supervised classification where final land cover image is generated.

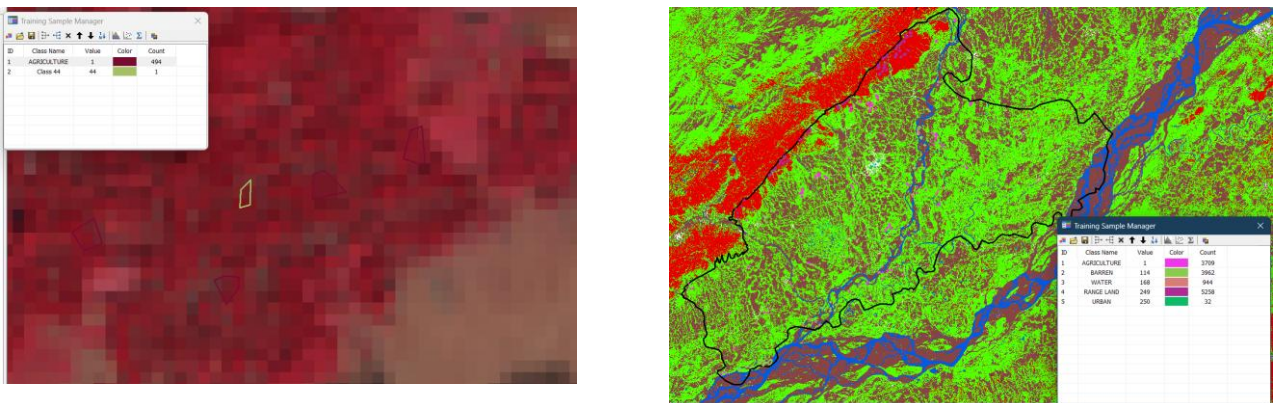


Fig: - 4.70 TRAINING SAMPLES

### 4.2.5.3.2 RECLASSIFY SLOPE AND COMBINE WITH CLASSIFICATION MAP

Here, slope is converted to percentage for evaluation of P – FACTOR. As P values varied with slope percentage which will be validate for study land use/land cover factor of the study area.

Steps for operation –

At first add Mosaic\_fill.tif files into ArcGIS window followed by layer column.

Go to Arc Toolbox > Spatial Analyst Tools > Surface > Slope

A dialog box appears add all the credentials followed by Output Measurement as Percent\_Rise with unchanged Z – factor as 1 and extract the study area followed by Extract by Mask under Extraction option in Arc Toolbox.

Now in slope percentage map, from continue dataset it converts to discrete dataset as in discrete dataset contains integer values.

So, in order to make both map discrete i.e., classification map & slope percentage map combine operation is required

Go to Arc Toolbox > Spatial Analyst Tools > Reclass > Reclassify

Put slope percentage map as an input and classify the existing table with modification on table [3.7] figure is shown Fig [4.71] & Fig [4.72] interface of the reclassify window for editing the slope value manually for accurate calculation without any error due to unavailability of filed data.



Fig: - 4.71 SLOPE PERCENTAGE INPUT DIALOG BOX

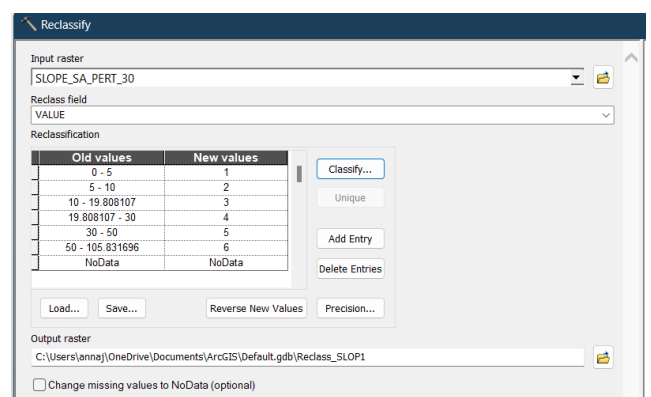
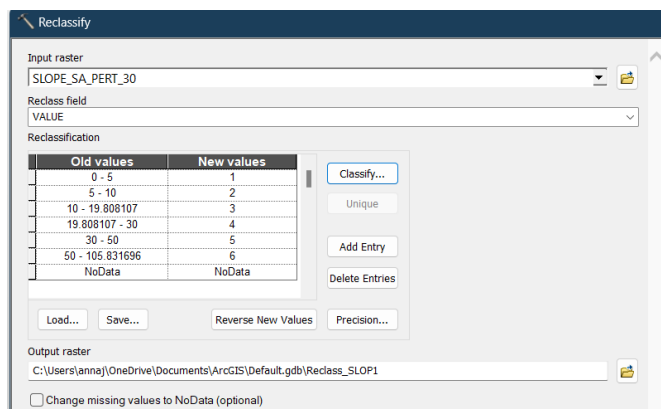


Fig: - 4.72 RECLASSIFICATION INTERFACE

After reclassification and combining the two discrete entities following map is generated for further analysis as shown in fig [4.73] & fig [4.74] respectively where 30 different classes is obtained for accurate identification.

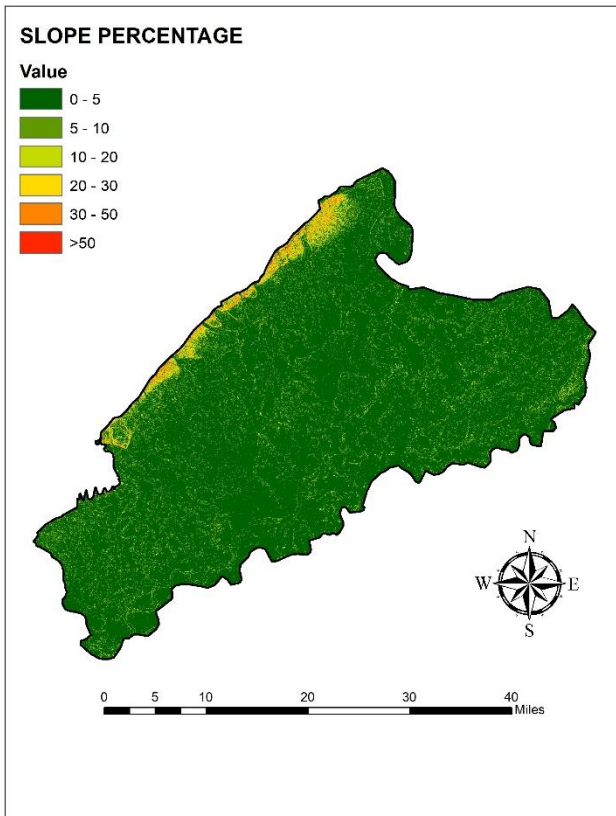


Fig: - 4.73 P\_FACTOR VALUE MAP 2023

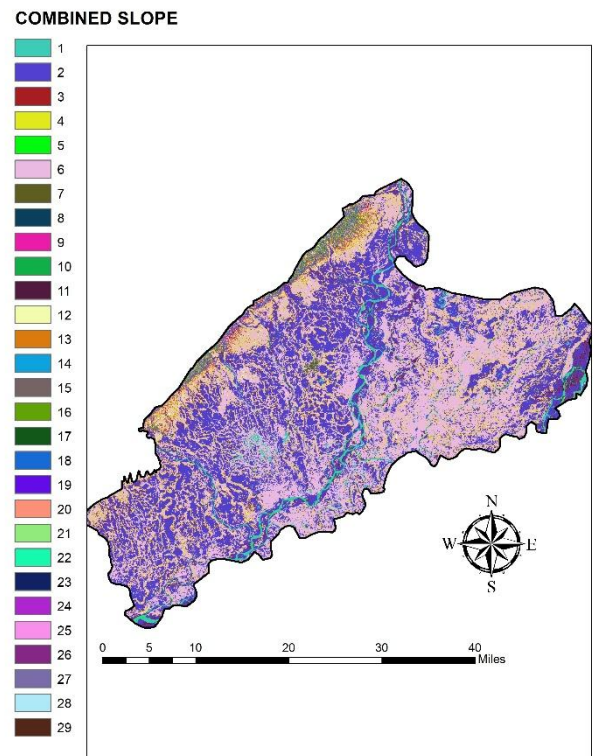


Fig: - 4.74 P\_FACTOR UTM MAP 2023

### 4.2.5.3.3 ASSIGNING P – FACTOR VALUES FOR CLASSES IN ATTRIBUTE TABLE

Here, combined map that have generated earlier is technically a P – factor map without any assigned P – values.

So, assigning P -values is mandatory for classification of the P – FACTOR map.

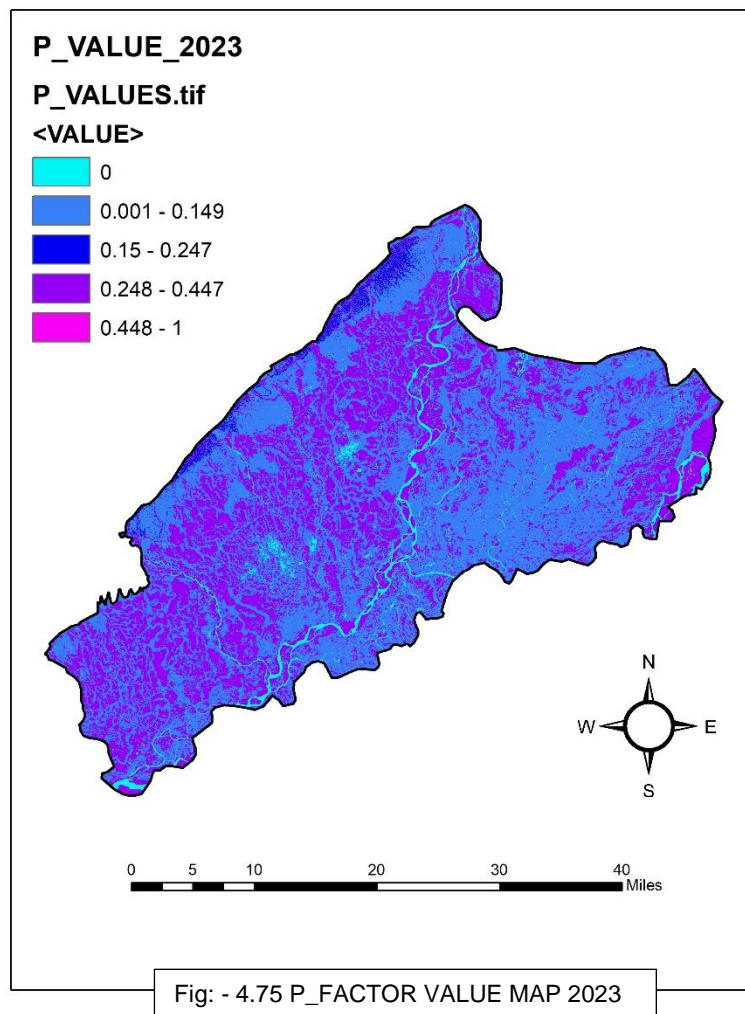
Hence, assigning is done by the following steps –

Right Click on combined\_map at Layers column > click on Attribute Table

A table will pop up > Click Add field from toolbar > Name the field as P\_Factor; Type changed to Float

Now, assigned the value according to its class number by taking reference from table []

Here, mentioned figure [4.75] is P\_factor map of 2023



## CHAPTER 5

### RESULTS AND DISCUSSION

#### 5.1 RAINFALL EROSIVITY (R) FACTOR

##### 5.1.1 ANNUAL PRECIPITATION OF STUDY AREA FOR THE YEAR 2014, 2022 & 2023

The precipitation map indicates a variation in annual rainfall across the years 2014, 2022, and 2023, with the range of rainfall being (2137.55–1666.78) mm in 2014, (2638.93–2103.29) mm in 2022, and (2138.68–1699.47) mm in 2023. Notably, 2022 recorded the highest rainfall compared to the other two years. When comparing the annual rainfall, there was an increase of approximately **23.48%** from 2014 to 2022. However, from 2022 to 2023, the rainfall decreased by about **18.96%**, reflecting a significant drop. Over the entire period from 2014 to 2023, there was a slight increase of **0.05%**, showing a nearly stable trend in long-term rainfall. These variations highlight the significant impact of climatic and regional factors influencing annual precipitation patterns as shown in table [5.1] and variation in fig [5.1]

Year	Min Rainfall (mm)	Max Rainfall (mm)	Average Rainfall (mm)
2014	1666.78	2137.55	1889.101
2022	2103.29	2638.93	2393.44
2023	1699.47	2138.68	1885

Table: - 5.1 Annual precipitation data

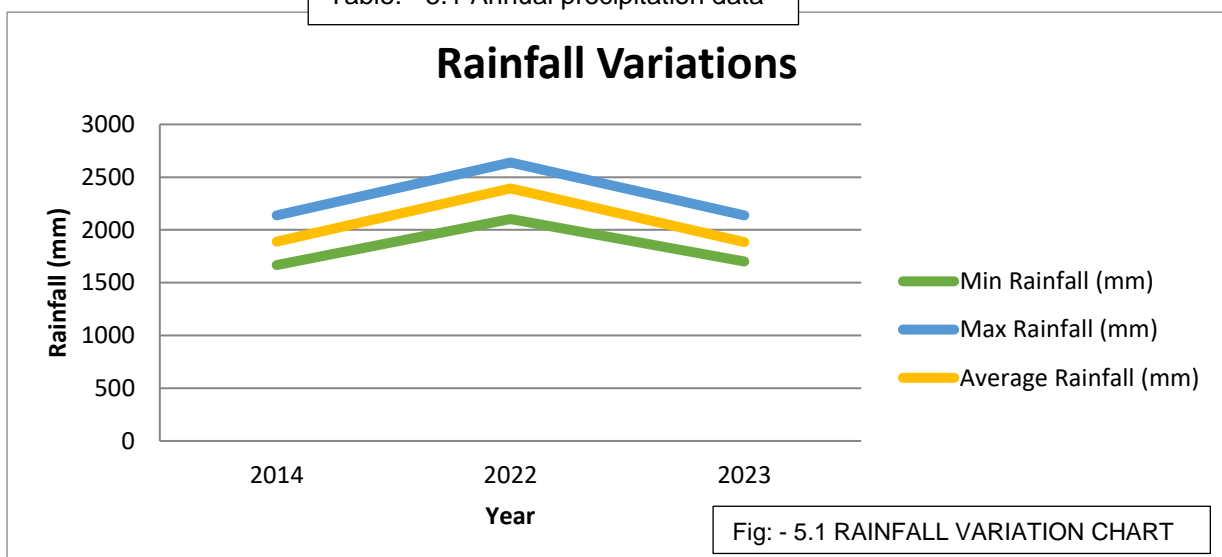
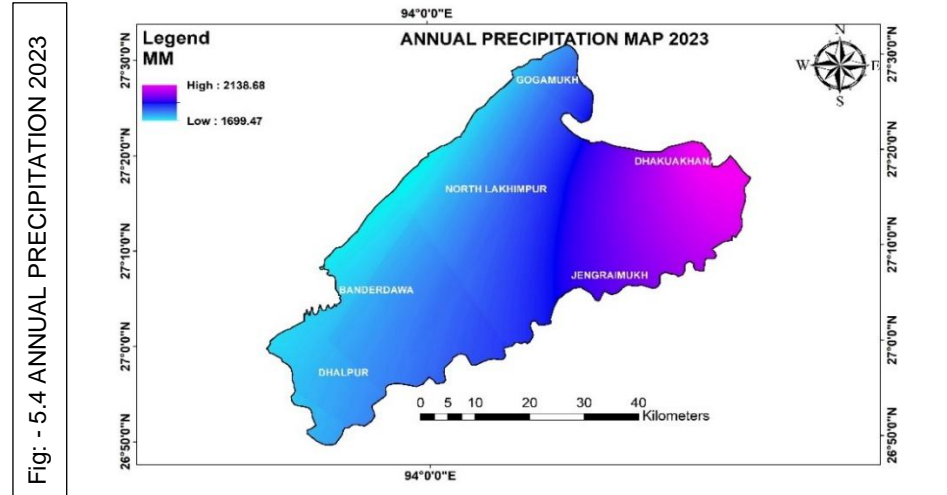
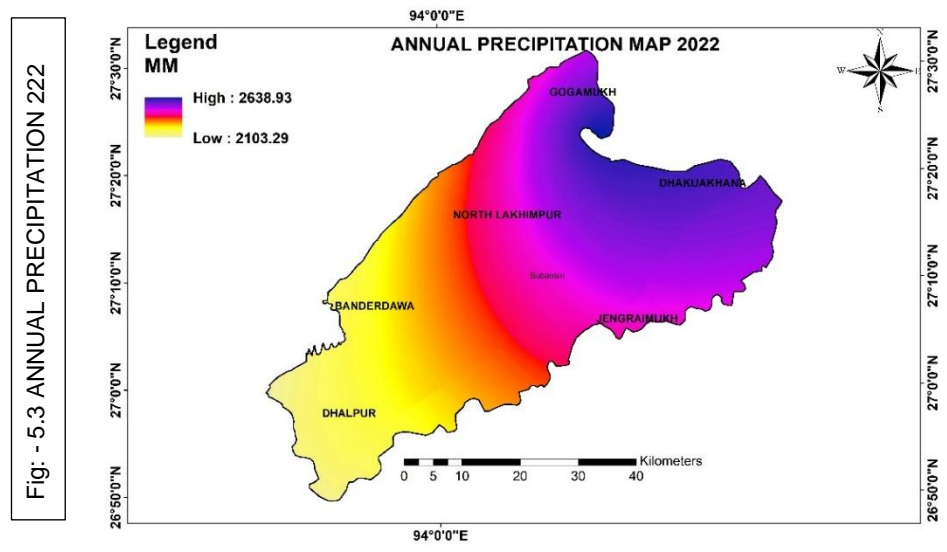
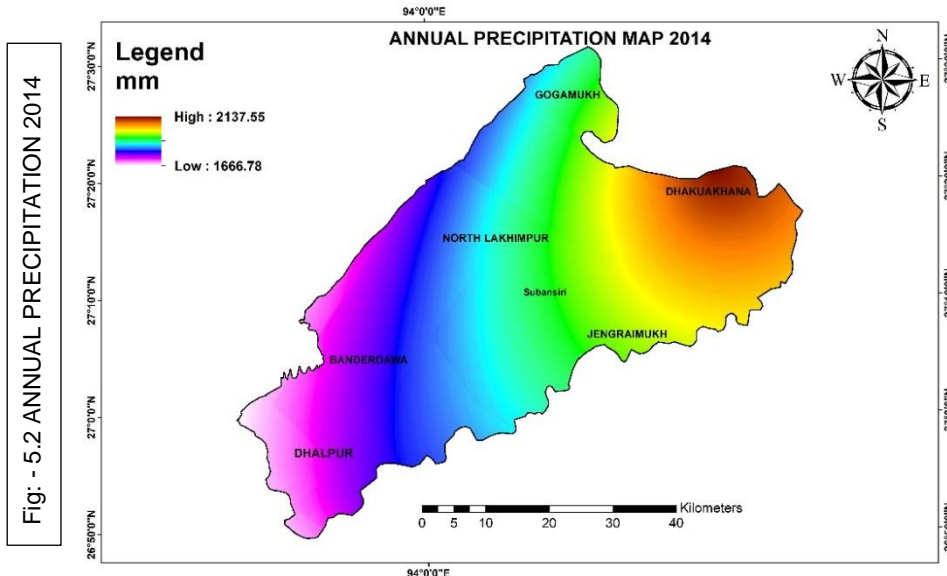


Fig: - 5.1 RAINFALL VARIATION CHART

Here, variation of precipitation of different periods i.e., 2014, 2022, 2023 annually is displayed in fig [5.2], [5.3] & [5.4] along with different locations falls in the selected area of Subansiri basin.



Average precipitation across different locations is being tabulated in table no [5.2] with variation in rainfall (mm) value in bar graph for better understanding in fig [5.5]

<b>Annual Rainfall Data Across Locations (2014–2023)</b>			
<b>Location</b>	<b>2014 Rainfall (mm)</b>	<b>2022 Rainfall (mm)</b>	<b>2023 Rainfall (mm)</b>
<b>Dhakuakhana</b>	<b>21218.73</b>	<b>2598.164</b>	<b>2097.32</b>
<b>Gogamukh</b>	<b>1908.32</b>	<b>2541.48</b>	<b>1817.6</b>
<b>North Lakhimpur</b>	<b>1835.096</b>	<b>2449.93</b>	<b>1814.78</b>
<b>Banderdawa</b>	<b>1735</b>	<b>2203.906</b>	<b>1739.797</b>
<b>Dhalpur</b>	<b>1731.97</b>	<b>2180.976</b>	<b>1963.38</b>
<b>Jengraimukh</b>	<b>1972.93</b>	<b>2442.505</b>	<b>1768.97</b>

Table: - 5.2 Precipitation data as per locations

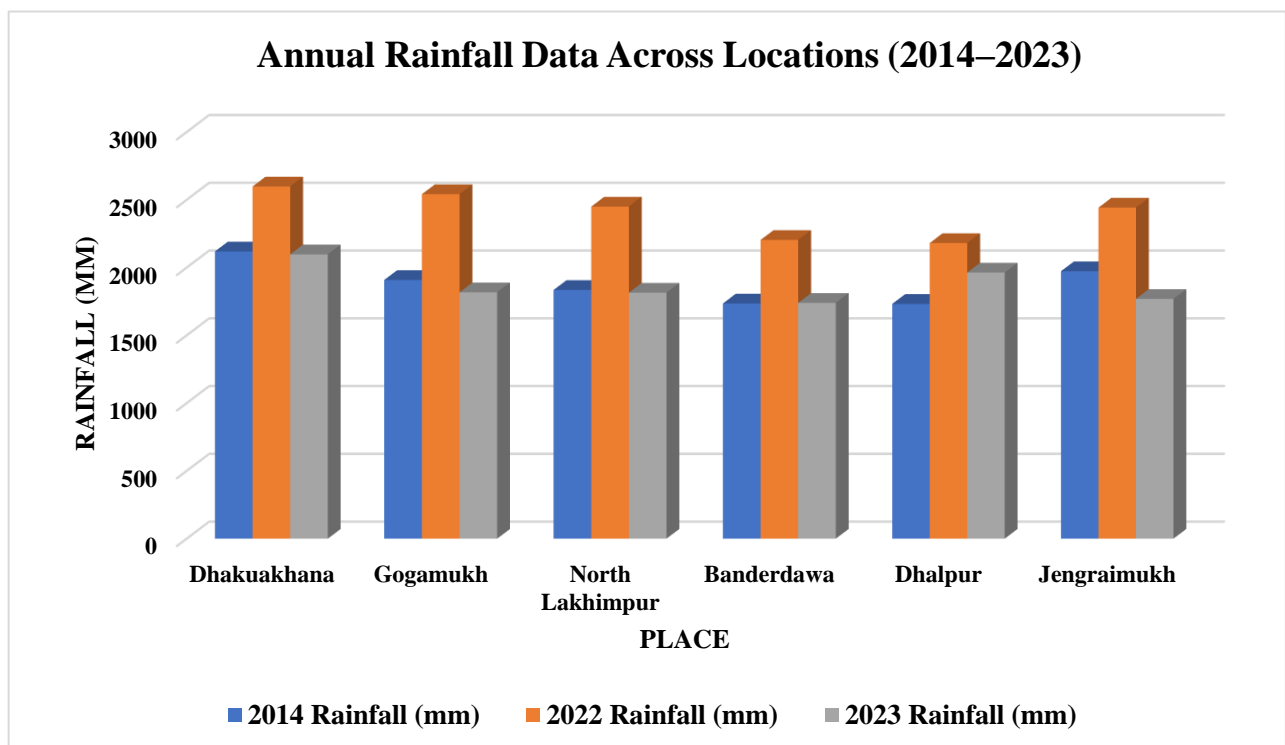


Fig: - 5.5 ANNUAL PRECIPITATION AS PER LOCATIONS

### 5.1.2 RAINFALL EROSIVITY (R) OF STUDY AREA FOR THE YEAR 2014, 2022 & 2023

Rainfall erosivity, quantified by the R factor, exhibits noticeable fluctuations across the years 2014, 2022, and 2023, reflecting the potential of rainfall to cause soil erosion. In 2014, the R factor ranged from **4930.68 to 3292.13 MJ mm/ha/h/year**, with an average value of **4047.50 MJ mm/ha/h/year**, setting a baseline for comparison. By 2022, the R factor increased significantly, ranging from **5647.75 to 3503.95 MJ mm/ha/h/year**, with an average value of **4755.97 MJ mm/ha/h/year**, representing a **17.53% rise** in mean erosivity compared to 2014. This increase highlights a period of intensified rainfall erosivity, indicating greater potential for soil erosion during this time. However, by 2023, the R factor saw a steep decline, dropping to a range of **3002.72 to 2132.15 MJ mm/ha/h/year**, with an average value of **2528.61 MJ mm/ha/h/year**. This marked a **46.84% decrease** in mean erosivity from 2022 and a **37.55% reduction** compared to 2014, signifying a substantial reduction in rainfall's erosive capacity. These variations underscore the dynamic nature of rainfall intensity and its erosive potential, driven by changing climatic factors. The peak erosivity in 2022 demonstrates the rainfall's highest capacity to erode soil during this period, followed by a pronounced decline in 2023, reflecting a shift towards less intense rainfall conditions.

Here, Variation of R – FACTOR value is arranged in a tabulated form in table [5.3] with variation graph for better understanding with change in its percentage.

Year	R Factor Range (MJ mm/ha/h/year)	Mean R Factor (MJ mm/ha/h/year)	Percentage Change
2014	4930.68 to 3292.13	4047.5	-
2022	5647.75 to 3503.95	4755.97	+17.53% (vs 2014)
2023	3002.72 to 2132.15	2528.61	-46.84% (vs 2022), -37.55% (vs 2014)

Table: - 5.3 R – factor data with different period

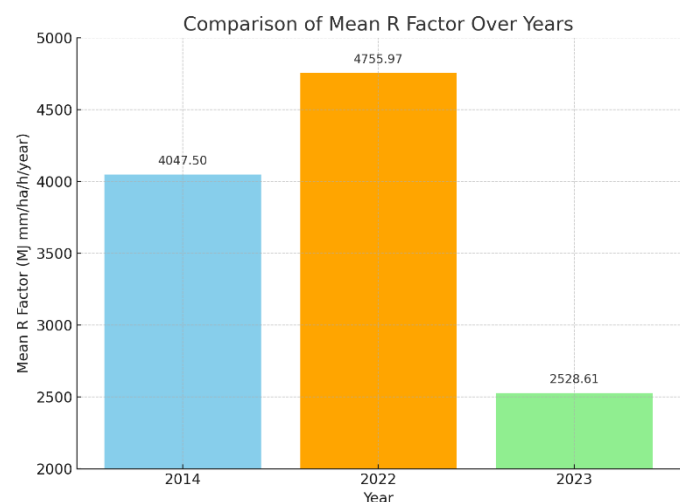
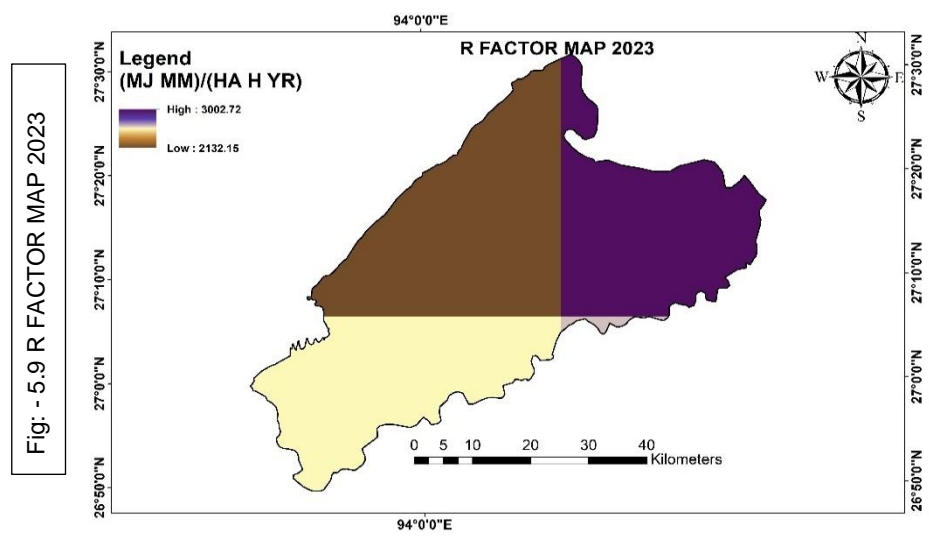
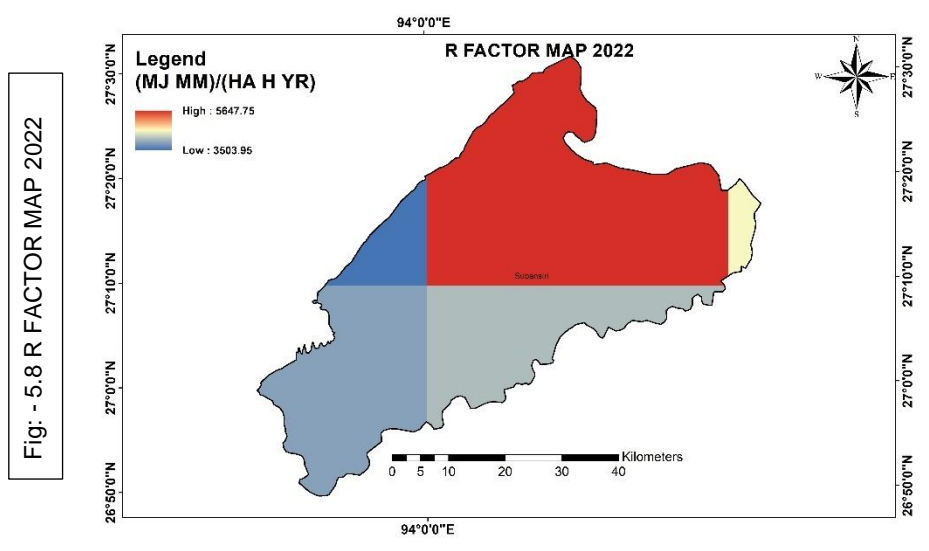
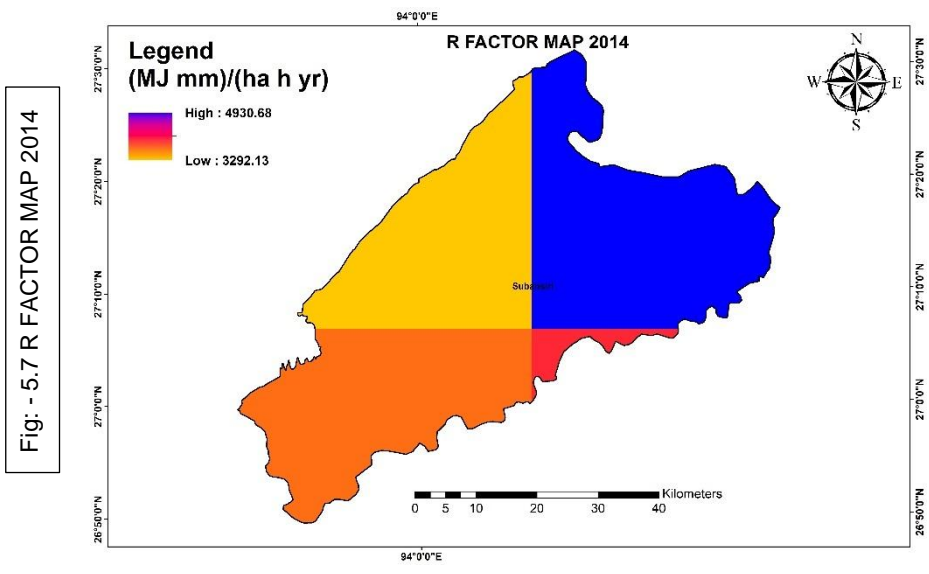


Fig: - 5.6 COMPARISON OF MEAN R FACTOR

Here, variation of R-factor of different periods i.e., 2014, 2022, 2023 is displayed in fig [5.7], [5.8] & [5.9] as generated from ArcGIS software by Kringing Interpolation method.



## 5.2 SOIL ERODIBILITY (K) – FACTOR

The soil erodibility factor (K factor) is a key measure of how prone soils are to erosion. In the study area, two primary soil types were identified: **Ao79-a** and **Be82-a**.

The **Ao79-a soil type**, which occupies the largest portion of the area at **14972 sq. km (66%)**, has a **K factor of 0.109214 (tons·yr)/(MJ·mm)**. This low value indicates that it is less susceptible to erosion. Its sandy clay loam texture contributes to this stability, as the cohesive nature of this soil type makes it more resistant to erosive forces.

In comparison, the **Be82-a soil type** spans a total area of **7855 sq. km (24% + 10%)** and exhibits a **K factor of 0.15482 (tons·yr)/(MJ·mm)**, suggesting a higher tendency for erosion. Classified as loam, this soil has a lower cohesion than sandy clay loam, making it easier to erode and transport under rainfall or runoff.

Additionally, the **USLE\_K1** values provide further insight into the erodibility of these soils. The **Ao79-a soil** has a value of **0.2727 (tons·yr)/(MJ·mm)**, whereas the **Be82-a soil** records a slightly higher value of **0.2886 (tons·yr)/(MJ·mm)**, confirming its greater vulnerability to erosion.

To summarize, the **Ao79-a soil**, which dominates the landscape, is **more stable and less erodible** due to its texture and **lower K factor**. Conversely, the **Be82-a soil**, with its higher erodibility, requires more focused soil conservation efforts to prevent erosion and maintain soil health, especially in the areas it occupies.

Moreover, the observed soil types, **Ao79-a** and **Be82-a**, align seamlessly with classifications presented in the **Indian Texture Soil Map**, fig [5.10] further validating their accuracy and relevance. This concurrence reinforces the reliability of the findings and underscores the consistency of soil characteristics within the regional context.

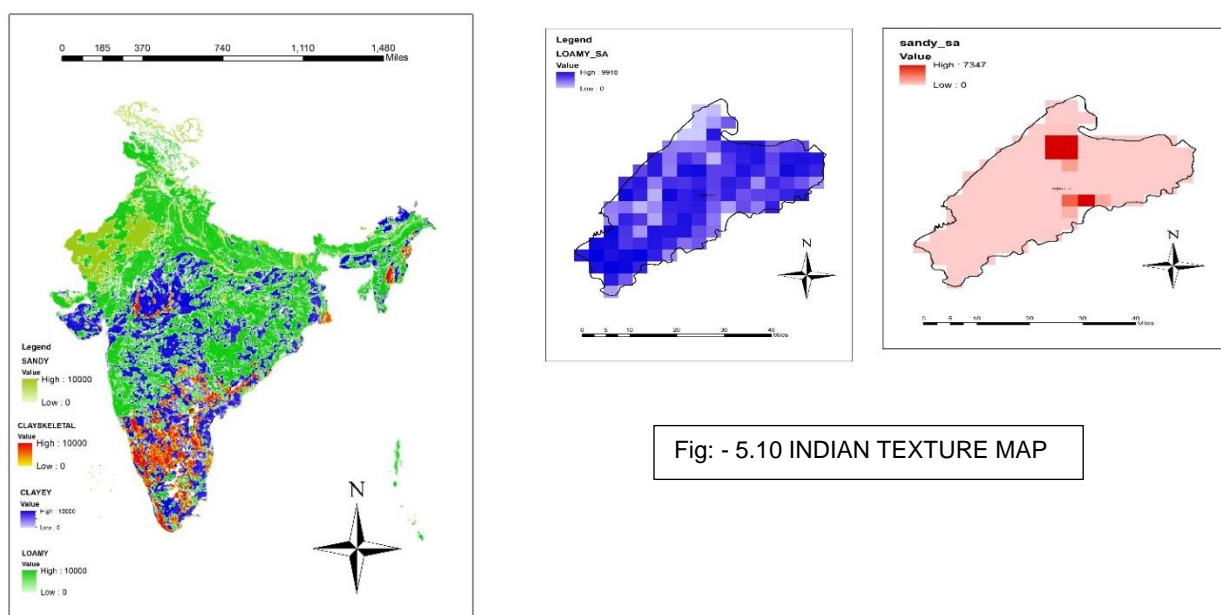
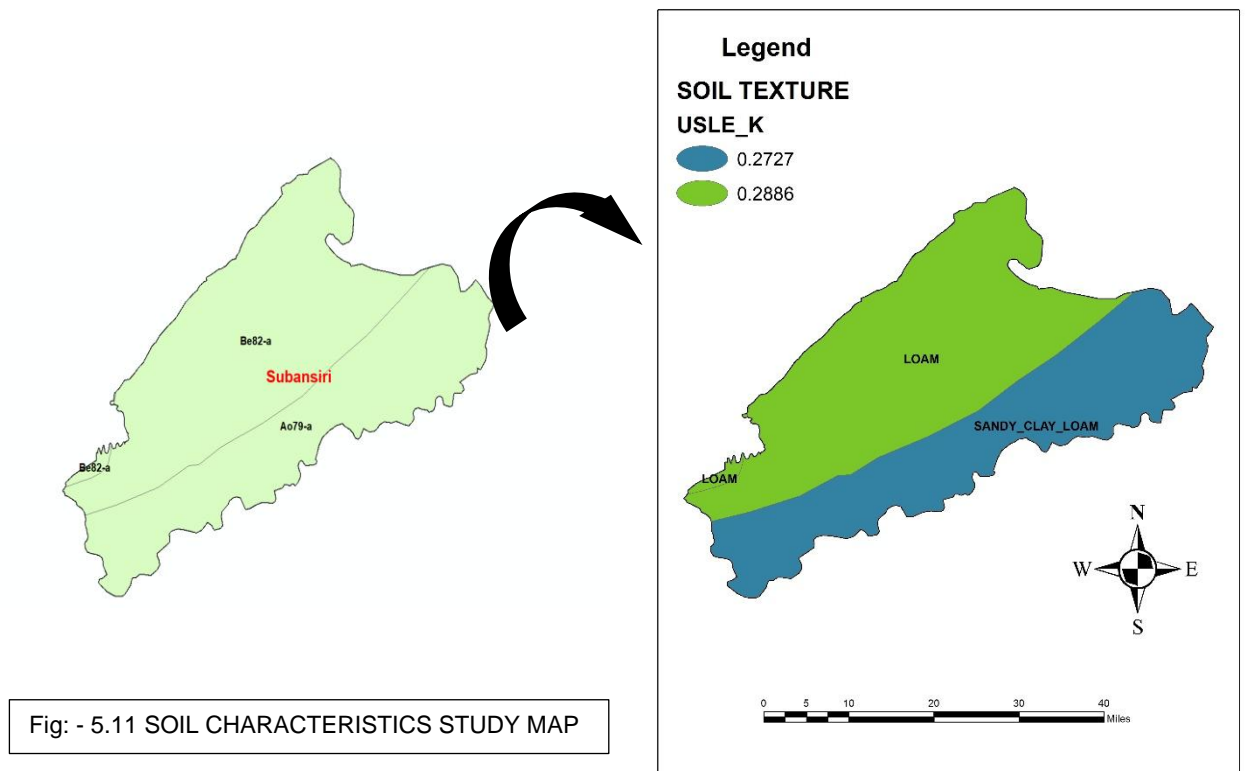


Fig: - 5.10 INDIAN TEXTURE MAP

Here, soil characteristics map generated in ArcGIS for FAO soil data is shown in fig [5.11]



Here, records of study area with different texture obtained from attribute table and variation of area coverage of different texture in the study area is displayed in bar graph and K value ( $\text{tons}\cdot\text{yr}/(\text{MJ}\cdot\text{mm})$ ) which is calculated manually by using *Williams.et.al* proposed formula as shown in fig [5.12] and table [5.4]

#### ATTRIBUTE TABLE OF SOIL MAP STUDY AREA

FI D	SNU M	FAOSOI L	DOMSOI L	CNT_NAM E	SQK M	PERCEN T COVER	COUNTR Y
0	3650	Ao79-a	Ao	IN	14972	66%	INDIA
1	3683	Be82-a	Be	IN	5587	24%	INDIA
2	3683	Be82-a	Be	IN	2268	10%	INDIA

Table: - 5.4 Attribute table of soil map of study area

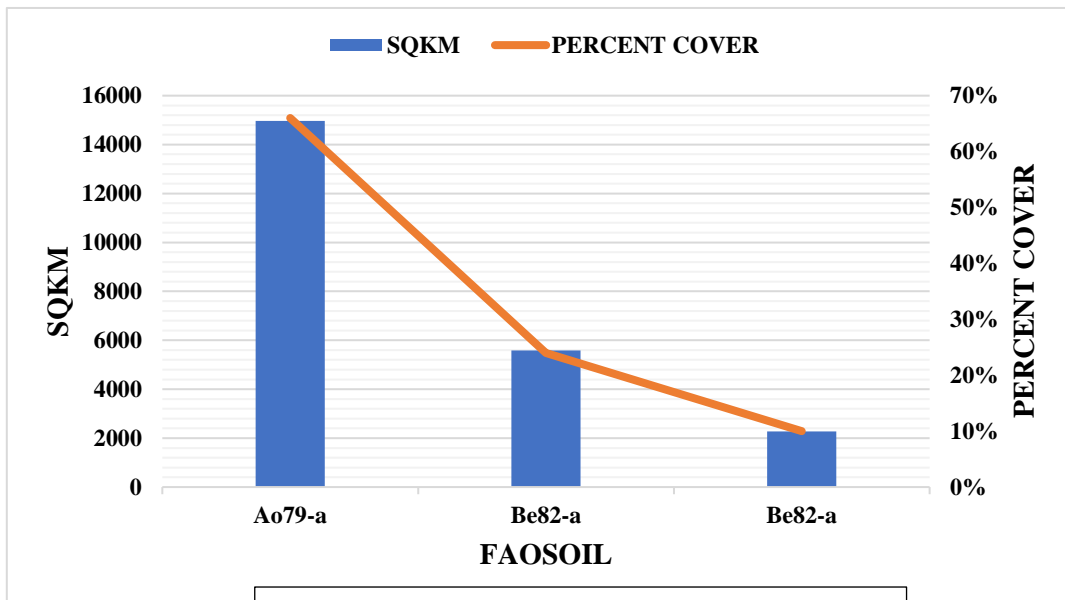


Fig: - 5.12 DOMINANT SOIL COVERAGE AREA CHART

K factor value is calculated by considering predefined data from soil texture database from FAO soil data as shown in table [] (look at literature review) and soil erodibility value (tons·yr)/(MJ·mm) is evaluated by *Williams.et.al* formula as shown in table [5.5]

Soil unit symbol	sand % tops oil	silt % tops oil	clay % tops oil	OC % tops oil	Fcsand	Fcl-silt	Forg	Fhisand	K factor
Ao	53.6	15.8	30.6	2.25	0.20000288	0.723838588	0.75586665	0.99805584	0.109214
Be	36.4	37.2	26.4	1.07	0.200862282	0.851384516	0.90537038	0.99994797	0.15482

Table: - 5.5 Soil erodibility data

Now, soil erodibility map of the study area is shown in figure [5.11] with area coverage of calculated K value (**tons·yr**)/(**MJ·mm**) shown in figure [5.13] with table [5.6] and its texture type in table [5.7];

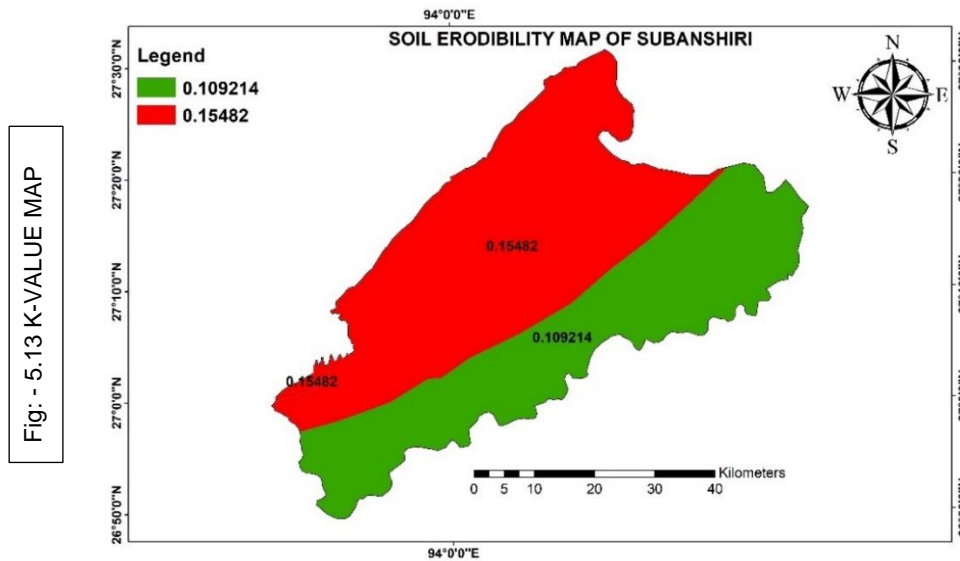


Fig: - 5.13 K-VALUE MAP

Table: - 5.6 Coverage K – factor data

FID	SNUM	FAOSOIL	DOMSOIL	SQKM	PERCENT COVER	K factor
0	3650	Ao79-a	Ao	14972	66%	0.109214
1	3683	Be82-a	Be	5587	24%	0.15482
2	3683	Be82-a	Be	2268	10%	0.15482

SNUM	FAOSOIL	SQKM	Type	Texture	USLE_K1
3650	Ao79-a	14972	Ao79-a-3650	SANDY_CLAY_LOAM	0.2727
3683	Be82-a	5587	Be82-a-3683	LOAM	0.2886
3683	Be82-a	2268	Be82-a-3683	LOAM	0.2886

Table: - 5.7 Soil texture data

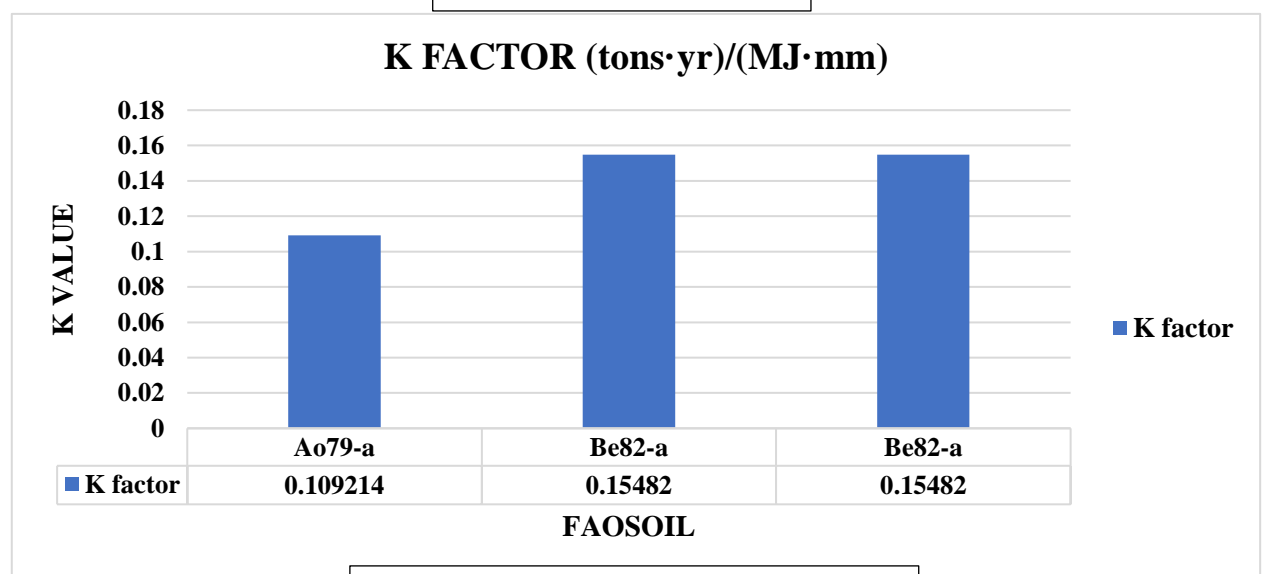


Fig: - 5.14 STUDY AREA K-FACTOR CHART

### 5.3 SLOPE LENGTH (LS) – FACTOR VALUE FOR THE YEAR 2014, 2022 AND 2023

According to various research papers it found that slope length value cannot exceed 100. So, due to unavailability of field data SAGA GIS where (0 – 74.4633) is the most appropriate software for evaluation of LS – factor value as shown in figure [] at –

**CHAPTER 4: METHODOLOGY >LS-STUDY PART**

Here, figure [5.15] of 30m resolution & fig [5.16] of 100m resolution is shown where generated by ArcGIS which is may not be considered but a prediction can be done for variation of slope length in different location of the study area.

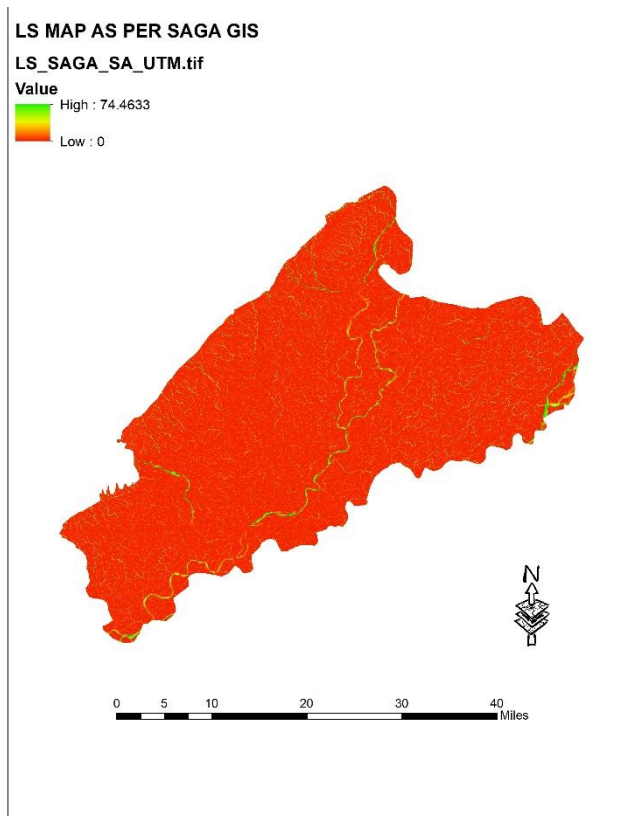


Fig: - 5.15 LS (SLOPE LENGTH) MAP

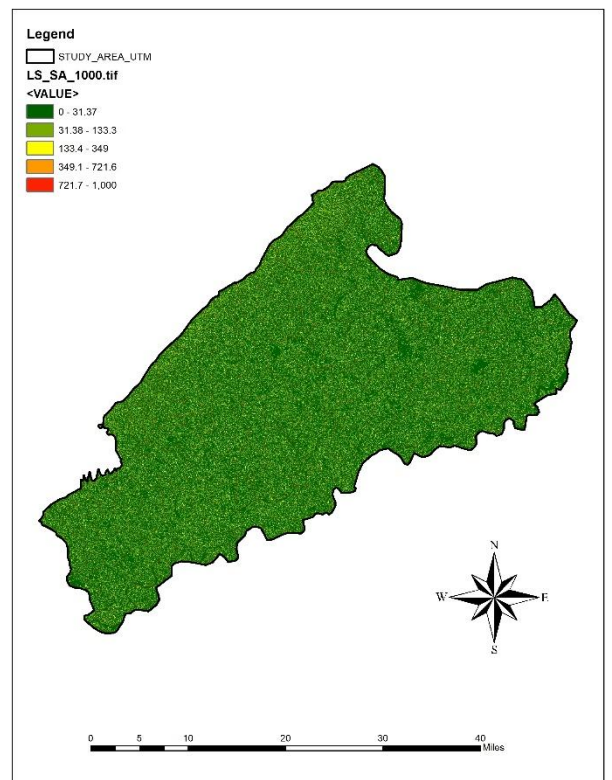


Fig: - 5.16 LS (SLOPE LENGTH) MAP UTM

## 5.4 C – FACTOR (LAND USE AND LAND COVER)

### 5.4.1 C- FACTOR STUDY FOR PERIOD 2014, 2022 AND 2023

The **C factor** in the RUSLE model, representing the cover management factor, is a crucial parameter for assessing soil erosion risk under different land cover conditions. It is defined as the ratio of soil loss from land under specific conditions to the soil loss from bare soil, where **C = 1** indicates bare soil with no protective cover, resulting in maximum erosion, and values **less than 1** reflect varying levels of erosion protection due to vegetation or soil management practices. A **C value close to 0** signifies nearly complete protection from soil erosion, typically observed in areas with dense vegetation cover, such as forests, grasslands, or well-maintained croplands. In this study, the **C factor values** were calculated using the formula proposed by **Durgion et al.**, as the formula by **Vatandaslar et al.** was deemed inappropriate for the study area. The resulting C factor values for the years **2014, 2022, and 2023** ranged from **0.233–0.584, 0.23–0.6225, and 0.2219–0.6189**, respectively.

The **NDVI (Normalized Difference Vegetation Index)**, which plays a significant role in determining the C factor, reflects the density and health of vegetation cover. Higher NDVI values indicate increased vegetation cover, which correlates with lower C factor values, providing better protection against soil erosion. The NDVI values for **2014, 2022, and 2023** were **0.534, 0.5398, and 0.556**, respectively. These results indicate a gradual increase in vegetation cover over the years, leading to reduced erosion susceptibility. Specifically, the higher NDVI in **2023** signifies improved vegetative conditions compared to previous years, resulting in a lower C factor and enhanced protection against soil erosion. The relationship between NDVI and the C factor highlights the importance of vegetation cover in controlling soil erosion, as areas with higher NDVI values are more effective in mitigating soil loss.

#### C-Factor and NDVI for Different Years

Year	C-Factor Range	NDVI Value
2014	0.233 – 0.584	0.534
2022	0.23 – 0.6225	0.5398
2023	0.2219 – 0.6189	0.556

Table: - 5.8 C -factor and NDVI data of different years

The above table [5.8] clearly demonstrates the gradual increase in NDVI values over the years, which correlates with slightly reduced C factor values. This trend highlights the positive impact of increasing vegetation cover on soil erosion control, where higher NDVI values signify healthier and denser vegetation, leading to improved erosion protection and C factor map is shown in figure [5.17], [5.18] & [5.19]

Fig: - 5.17 SOIL ERODIBILITY MAP 2014

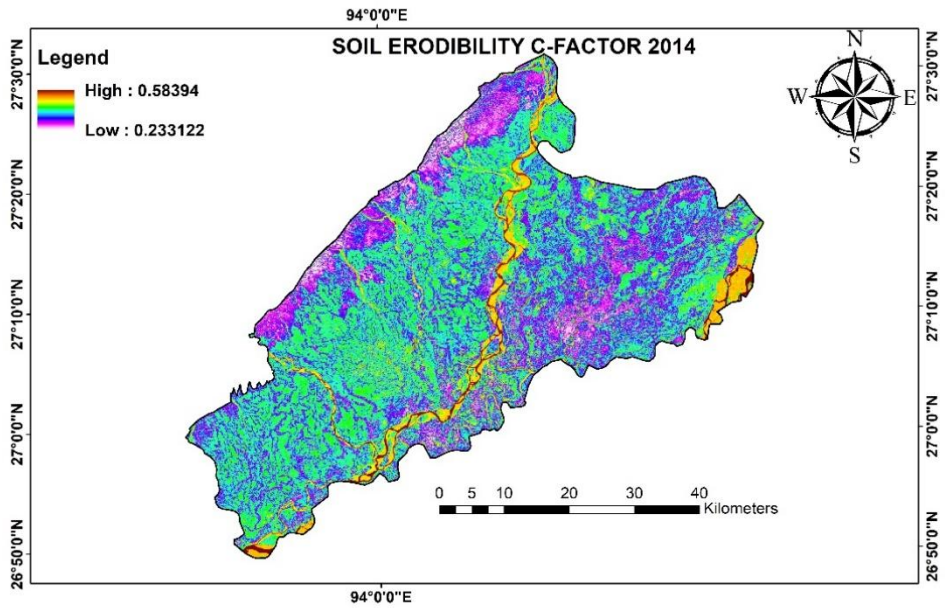


Fig: - 5.18 SOIL ERODIBILITY MAP 2022

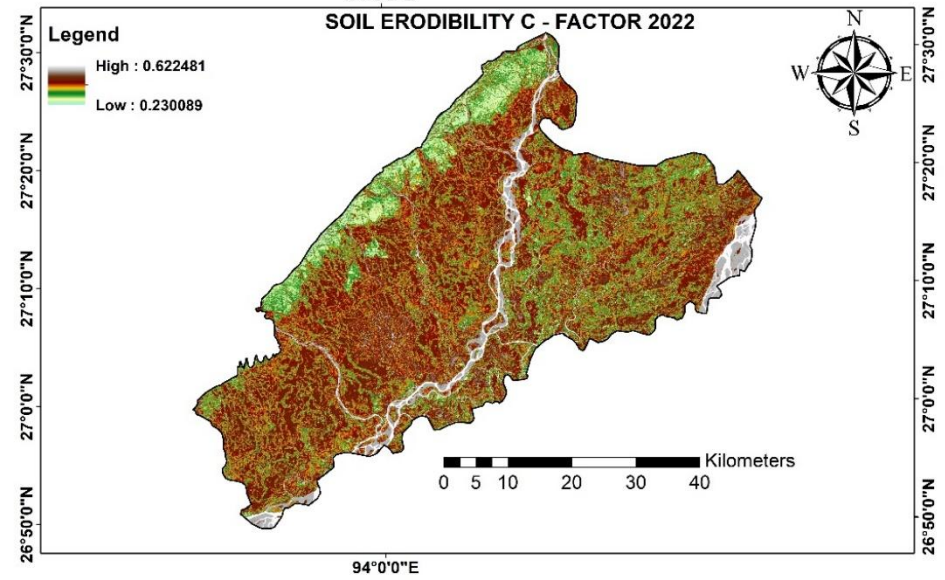
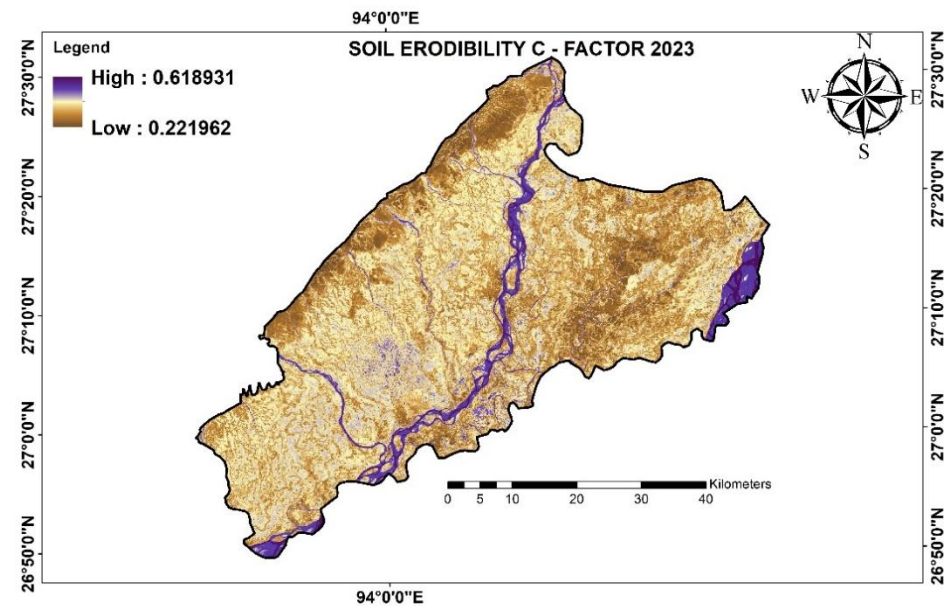


Fig: - 5.19 SOIL ERODIBILITY MAP 2023



## 5.5 P – FACTOR (CONSERVATION PRACTICE FACTOR)

### 5.5.1 P- FACTOR STUDY FOR PERIOD 2014, 2022 AND 2023

The support practice factor P express the effects of surface practices that are applied to reduced soil loss through erosion processes.

These practices include among others terracing strip cropping and contour ploughing

The P factor value ranges between 0 and 1, where 0 shows the highest effectiveness of the conservation practice and 1 indicates that there are no support practices or measures implemented.

Here, fig [5.20], [5.21] & [5.22] is the conservation practice factor map for given period for preventing soil erosion.

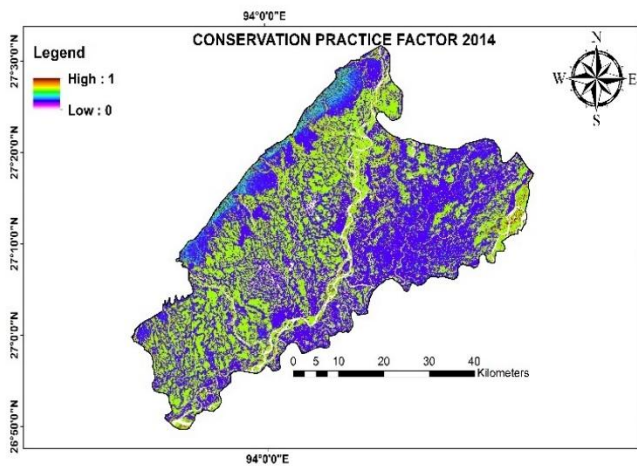


Fig: - 5.20 CONSERVATION PRACTICE MAP 2014

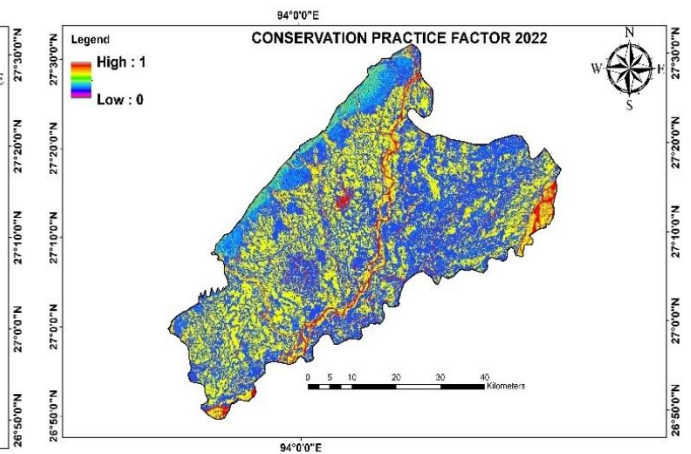


Fig: - 5.21 CONSERVATION PRACTICE MAP 2022

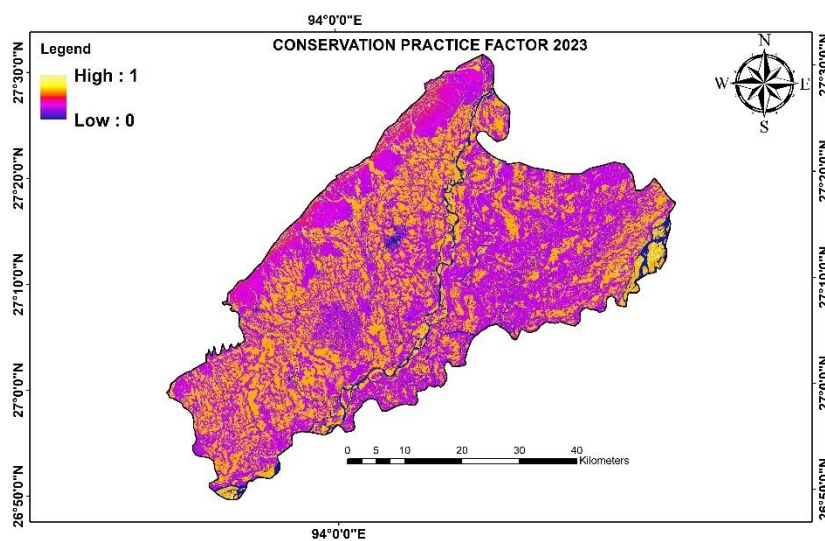


Fig: - 5.22 CONSERVATION PRACTICE MAP 2023

## 5.6 R.U.S.L.E. WORKS

### 5.6.1 R.U.S.L.E. A-FACTOR STUDY FOR PERIOD 2014, 2022 AND 2023

The **RUSLE (Revised Universal Soil Loss Equation)** model was applied to analyze the annual soil erosion intensity of the study area for the years **2014, 2022, and 2023**, using key parameters such as **rainfall erosivity (R factor)**, **soil erodibility (K factor)**, **slope length and steepness (LS factor)**, **land use land cover (C factor)**, and the **conservation practice factor (P factor)**. The A value, which represents annual soil erosion, was calculated for each year by integrating these parameters.

For **2014**, the average **rainfall erosivity** was **4047.4994 MJ mm ha<sup>-1</sup> h<sup>-1</sup> y<sup>-1</sup>**, the **land use land cover factor (C)** was **0.393**, and the **conservation practice factor (P)** was **0.162**. The resulting annual soil erosion (A factor) had a **mean value of 12 t ha<sup>-1</sup> y<sup>-1</sup>** with a **standard deviation of 84 t ha<sup>-1</sup> y<sup>-1</sup>**.

For **2022**, the rainfall erosivity increased to **4755.97 MJ mm ha<sup>-1</sup> h<sup>-1</sup> y<sup>-1</sup>**, while the land use land cover factor slightly decreased to **0.3863**, and the conservation practice factor improved to **0.1613**. Despite the improvements in land cover and conservation practices, the higher rainfall erosivity led to an increase in the annual soil erosion mean value, reaching **24.2 t ha<sup>-1</sup> y<sup>-1</sup>** with a **standard deviation of 123 t ha<sup>-1</sup> y<sup>-1</sup>**.

For **2023**, the average rainfall erosivity dropped significantly to **2528.61 MJ mm ha<sup>-1</sup> h<sup>-1</sup> y<sup>-1</sup>**, while the land use land cover factor further improved to **0.3823**, and the conservation practice factor reduced slightly to **0.1605**. These changes resulted in a substantial decline in the annual soil erosion, with a mean value of **10.78 t ha<sup>-1</sup> y<sup>-1</sup>** and a **standard deviation of 64.57 t ha<sup>-1</sup> y<sup>-1</sup>**.

The results demonstrate the dynamic nature of soil erosion, primarily influenced by changes in rainfall erosivity and moderated by land cover and conservation practices. While **2022** experienced higher erosion rates due to intense rainfall, improvements in land management and conservation practices over time contributed to lower erosion values in **2023**, highlighting the importance of sustainable practices in controlling soil loss as shown in table [5.9] and annual soil erosion A- value (**t ha<sup>-1</sup> y<sup>-1</sup>**) trend figure [].

Table: - 5.9 Annual soil erosion data

Year	Mean Annual Soil Erosion (t ha <sup>-1</sup> y <sup>-1</sup> )	Standard Deviation (t ha <sup>-1</sup> y <sup>-1</sup> )
2014	12	84
2022	24.2	123
2023	10.78	64.57

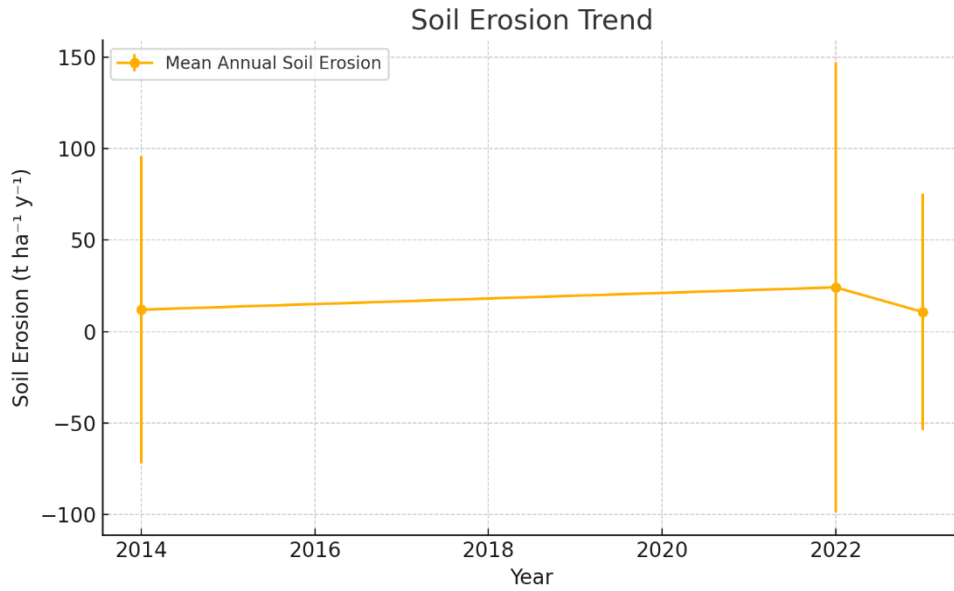


Fig: - 5.23 SOIL EROSION TREND

The RUSLE map is symbolized into 7 different classes where the entities in the map is classified as follows table [] –

Soil Loss Rate (t ha <sup>-1</sup> y <sup>-1</sup> )	Soil erosion Remarks
< 5	Very slight
5 – 10	Very severe
10 – 15	Slight
15 – 20	Severe
20 – 40	Moderate severe
40 – 80	Moderate
> 80	Extremely severe

Table: - 5.10 Soil erosion description chart

Here, annual soil erosion graph is generated with corresponding A – value by considering all required parameters in figure [5.24(a)], [5.25(b)] of 2014, fig [5.26(a)], [5.27(b)] of 2022 & fig [5.28(a)], [5.29(b)] of 2023.

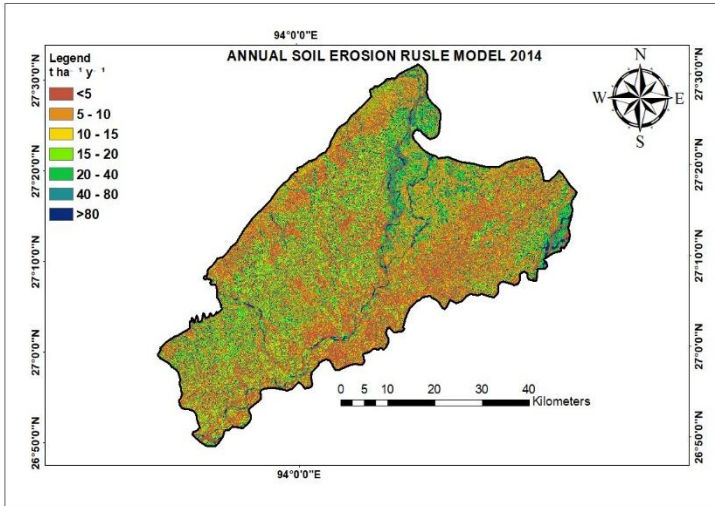


Fig: - 5.24 (a) ANNUAL EROSION MAP 2014

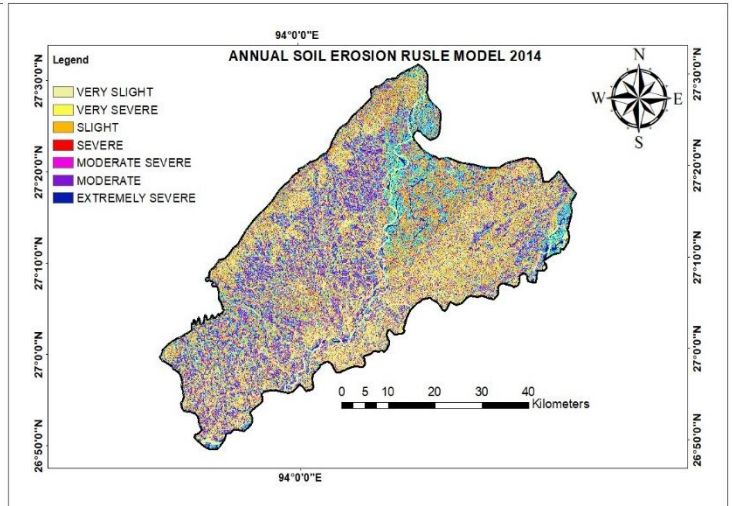


Fig: - 5.25 (b) ANNUAL EROSION MAP 2014

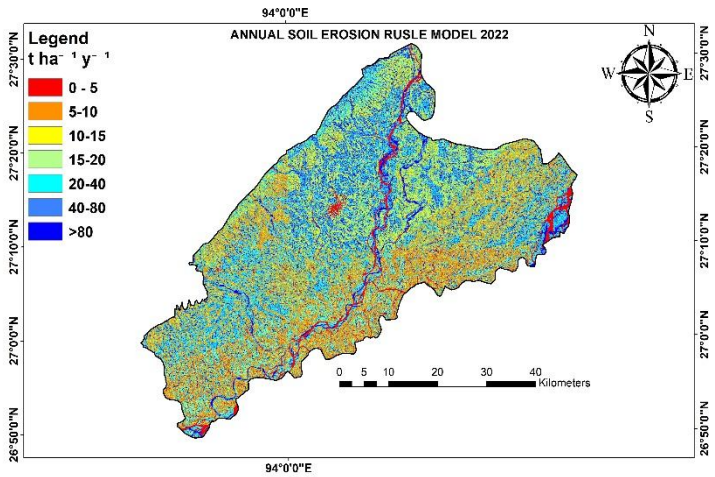


Fig: - 5.26 (a) ANNUAL EROSION MAP 2022

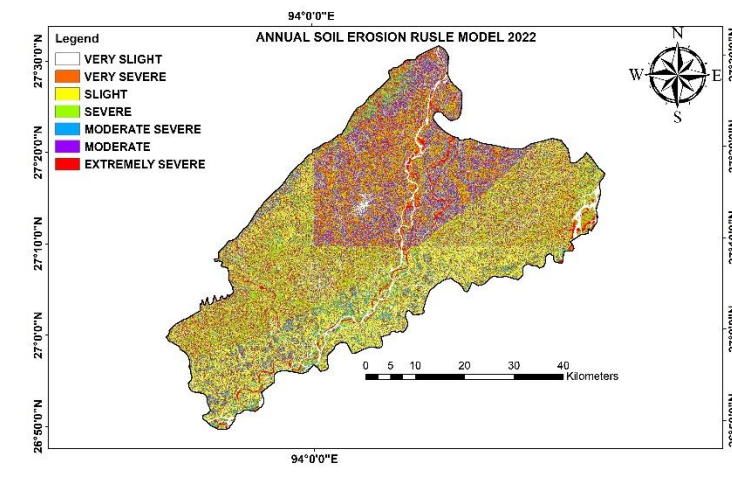


Fig: - 5.27 (b) ANNUAL EROSION MAP 2022

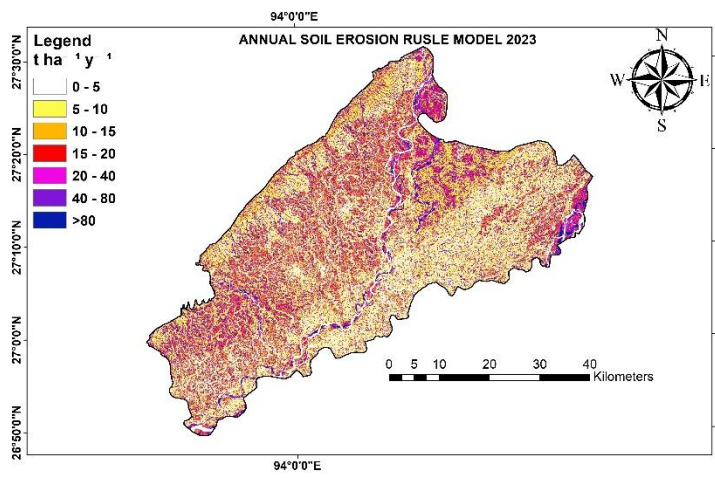


Fig: - 5.28 (a) ANNUAL EROSION MAP 2023

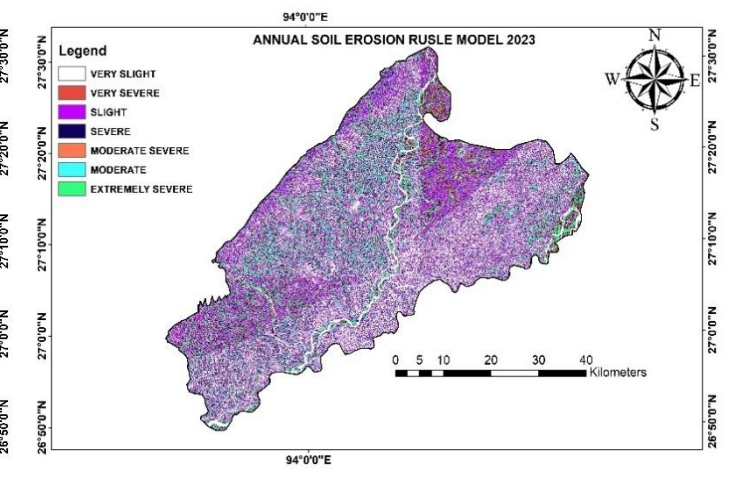


Fig: - 5.29 (b) ANNUAL EROSION MAP 2023

## **5.7 VALIDATION OF SOIL EROSION BY RUSLE KEY PARAMETERS AND SOIL EROSION & DEPOSITION DATA FOR DIFFERENT PERIODS**

### **5.7.1 Rainfall Erosivity (R-Factor)**

The R-factor measures the erosive power of rainfall, which strongly influences soil erosion rates. The analysis shows considerable variation across the studied years:

2014: The mean R-factor was **4047.5 MJ mm/ha/h/year**.

2022: The R-factor rose to **4755.97 MJ mm/ha/h/year**, indicating a **17.53%** increase compared to 2014. This rise reflects more intense and erosive rainfall, contributing to higher erosion rates.

2023: A significant reduction in rainfall intensity led to a lower R-factor of **2528.61 MJ mm/ha/h/year**, representing a **46.84%** decrease relative to 2022 and **37.55%** lower than 2014. The peak R-factor in 2022 directly correlates with increased soil erosion, while the decline in 2023 marks a period of reduced rainfall-driven erosion.

### **5.7.2. Soil Erodibility (K-Factor)**

The K-factor identifies soil's vulnerability to erosion based on its physical and chemical properties. The study area includes two dominant soil types:

**Ao79-a (Ao):** Covers **66%** of the area with a relatively low K-factor of **0.109214**.

**Be82-a (Be):** Occupies **34% of the area** (split into 24% and 10%) and has a higher K-factor of 0.15482.

The **Be82-a soil**, being more erodible, likely **experienced greater soil loss**, particularly during **2022**, when rainfall erosivity was highest. The combination of high **R-factor and K-factor** in 2022 exacerbated erosion.

### 5.7.3. Vegetation Cover (C-Factor) and NDVI

Vegetation cover reduces soil erosion by intercepting rainfall, slowing surface runoff, and stabilizing the soil. The C-factor and NDVI (Normalized Difference Vegetation Index) values highlight changes in vegetation cover:

**2014:** C-factor ranged from **0.233 to 0.584**, with an NDVI value of **0.534**.

**2022:** C-factor increased slightly, ranging between **0.23 and 0.6225**, while NDVI improved to **0.5398**.

**2023:** The C-factor dropped to a range of **0.2219 to 0.6189**, and NDVI increased to **0.556**.

The gradual improvement in NDVI values from **2014 to 2023** reflects enhanced vegetation cover, particularly in 2023. This improvement contributed to reduced soil erosion by providing better ground protection.

### 5.7.4. Soil Erosion Rates

The mean annual soil erosion rates ( $\text{t ha}^{-1} \text{y}^{-1}$ ) and standard deviations provide insight into erosion severity:

**2014:** Soil erosion averaged **12 t ha<sup>-1</sup> y<sup>-1</sup>** with a standard deviation of **84**.

**2022:** Erosion increased dramatically to **24.2 t ha<sup>-1</sup> y<sup>-1</sup>**, with a higher standard deviation of **123**.

**2023:** Erosion rates fell to **10.78 t ha<sup>-1</sup> y<sup>-1</sup>**, and the standard deviation reduced to **64.57**.

The data confirms that **2022 experienced the highest erosion rates**, driven by intense rainfall and soil susceptibility. In contrast, the **reduced erosion in 2023** corresponds to lower rainfall erosivity and improved vegetation cover.

### 5.7.5 Erosion and Deposition Analysis

Erosion and deposition dynamics further validate the soil loss trends observed between the years:

**2014 to 2022:** Soil erosion areas increased to **9331 m<sup>2</sup>**, while deposition areas covered **7453 m<sup>2</sup>**. The spike in erosion highlights the combined effect of high rainfall erosivity and erodible soils.

**2022 to 2023:** Erosion areas dropped significantly to **2462 m<sup>2</sup>**, while deposition areas expanded to **9048 m<sup>2</sup>**. This shift indicates reduced erosive forces and improved soil stability, likely due to enhanced vegetation cover and lower rainfall erosivity.

Here, river meandering and changing of course where erosion and deposition of Subansiri river affected for severe soil erosion is mentioned with trend table [5.11] and unchanged course area table [5.12] and graphical representation fig [5.31] & for better clarity with the figures [5.30] with some affected area.

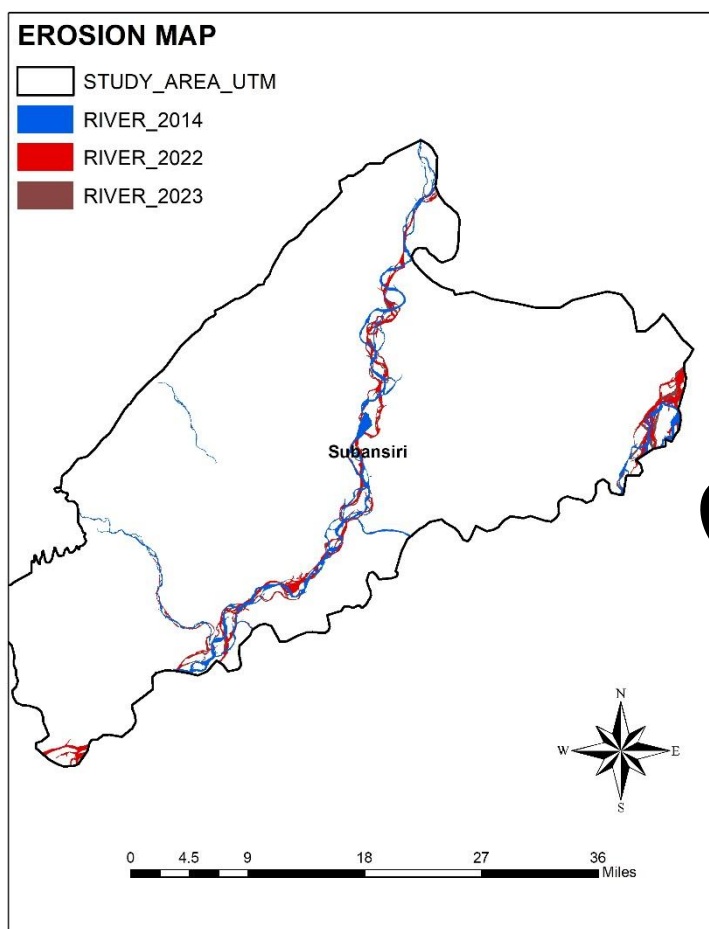


Fig - 5.30 PERIODIC RIVERCOURSE MIGRATION

Source: Google

In this figure [5.30], erosion and deposition caused by changes in the river course are observed during the periods **2014, 2022, and 2023**.

Table: - 5.11 Soil erosion and deposition trend

YEAR	PREVIOUS 8 YEARS	NEXT 8 YEARS	UNCHANGED	EROSION	DEPOSITION
2014-2022	10710	8833	1379	9331	7453
2014-2023	10710	8344	1260	9450	7083
2022-2023	5204	11789	2742	2462	9048

	AREA_2014	AREA_2023	AREA_UNCHA	EROSION	DEPOSITION
	179	3518	24	155	3494
	4828	3518	974	3854	2544
	4828	72	60	4768	13
	875	1235	203	672	1032
<b>TOTAL</b>	<b>10710</b>	<b>8344</b>	<b>1260</b>	<b>9450</b>	<b>7083</b>
	AREA_2014	AREA_2022	AREA_UNCHA	EROSION	DEPOSITION
	179	3629	27	152	3602
	4828	201	35	4793	166
	4828	3629	999	3829	2630
	875	1374	319	556	1055
<b>TOTAL</b>	<b>10710</b>	<b>8833</b>	<b>1379</b>	<b>9331</b>	<b>7453</b>
	AREA_2022	AREA_2023	AREA_UNCHA	EROSION	DEPOSITION
	0	3518	0	0	3518
	201	3518	33	168	3485
	3629	3518	2119	1510	1399
	1374	1235	590	784	645
<b>TOTAL</b>	<b>5204</b>	<b>11789</b>	<b>2742</b>	<b>2462</b>	<b>9048</b>

Table: - 5.12 Unchanged river-course area chart

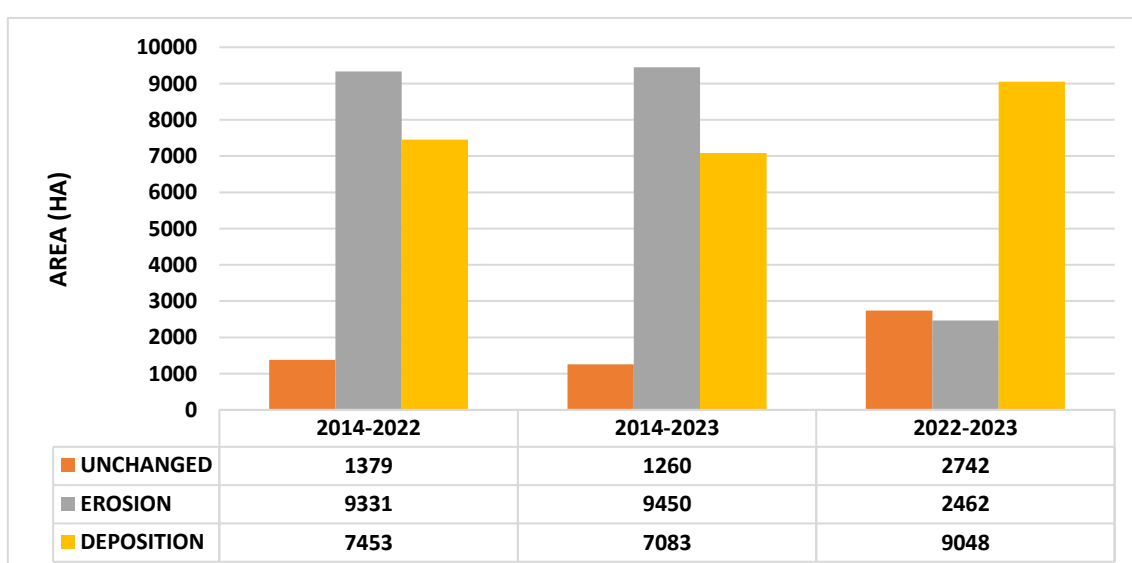


Fig: - 5.31 HISTORY RIVER EROSION – DEPOSITION STATISTICS CHART

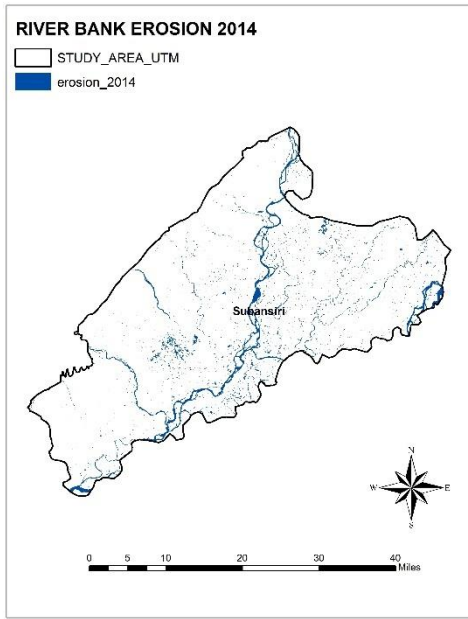


Fig: - 5.32 RIVER BANK EROSION 2014

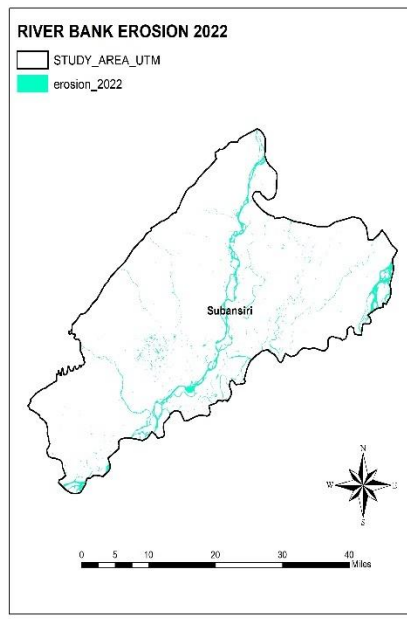


Fig: - 5.33 RIVER BANK EROSION 2022

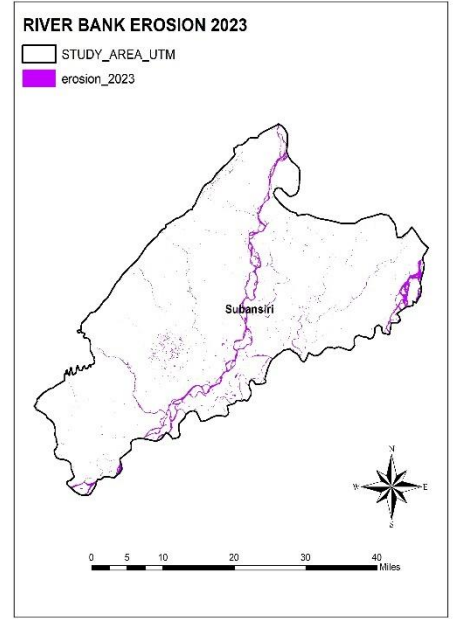


Fig: - 5.34 RIVER BANK EROSION 2023

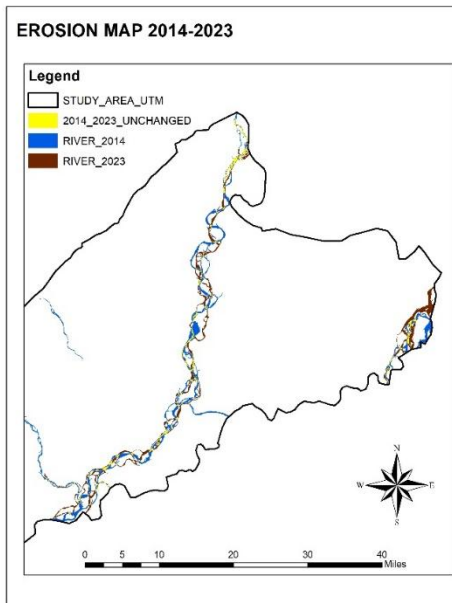


Fig: - 5.35 RIVER BANK EROSION 2014-23

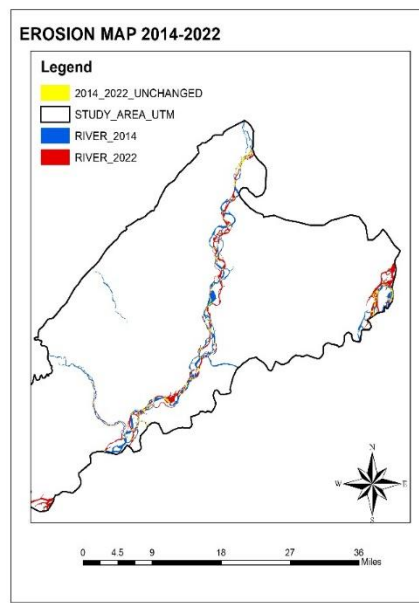


Fig: - 5.36 RIVER BANK EROSION 2014-22

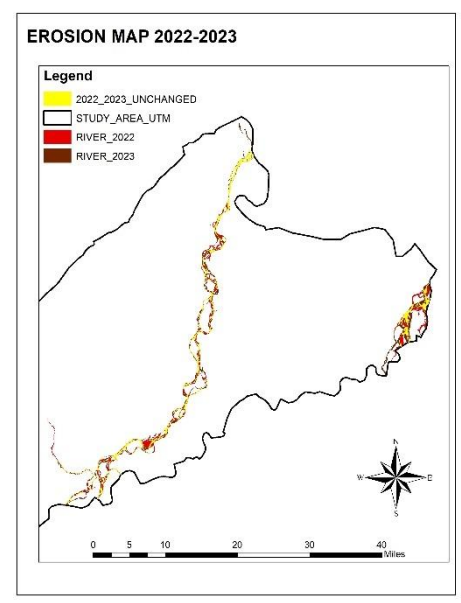


Fig: - 5.37 RIVER BANK EROSION 2022-23

## CHAPTER 6

### CONCLUSION

---

This study examined soil erosion dynamics for 2014, 2022, and 2023 using the Revised Universal Soil Loss Equation (RUSLE) model. It focused on understanding the influence of rainfall erosivity (R-factor), soil erodibility (K-factor), vegetation cover (C-factor), and associated soil erosion rates, shedding light on temporal changes in erosion and deposition patterns.

In **2022**, soil erosion reached its peak, recording an average rate of **24.2 t ha<sup>-1</sup> y<sup>-1</sup>**, nearly doubling the **12-t ha<sup>-1</sup> y<sup>-1</sup>** observed in 2014. This sharp rise correlates with a **17.53% increase** in rainfall erosivity (R-factor **4755.97 MJ mm/ha/h/year**) compared to 2014. Additionally, the significant presence of **Be82-a soil**, which accounts for **34%** of the study area, exacerbated the erosion due to its higher erodibility. Sparse vegetation cover further intensified the erosion process, expanding erosion-prone areas to **9331 m<sup>2</sup>** while deposition was limited to **7453 m<sup>2</sup>**. Conversely, **2023** demonstrated a notable improvement, with average soil erosion rates dropping to **10.78 t ha<sup>-1</sup> y<sup>-1</sup>**, marking a **55.4% reduction** compared to 2022. This positive trend resulted from a substantial decline in rainfall erosivity (R-factor **2528.61 MJ mm/ha/h/year**) and improved vegetation cover, as reflected by an NDVI value of **0.556**. Consequently, erosion-prone areas decreased to **2462 m<sup>2</sup>**, and deposition areas increased to **9048 m<sup>2</sup>**, indicating enhanced soil stability and reduced runoff impact.

The results underscore the dominant role of rainfall intensity and vegetation cover in driving soil erosion trends. The extreme erosion witnessed in **2022** highlights the vulnerability of highly erodible soils under intense rainfall conditions. In contrast, the improvements in **2023** demonstrate the effectiveness of increased vegetation cover and reduced rainfall erosivity in mitigating soil loss. This research highlights the importance of proactive soil management strategies, including the promotion of vegetation cover and stabilization of erodible soils, to reduce erosion risks. Continued monitoring and the adoption of sustainable land management practices are essential for protecting soil resources and mitigating erosion in the face of climate variability.

## CHAPTER 7

### REFERENCES

---

**Borrelli, P.,** Robinson, D. A., Panagos, P., Lugato, E., & Montanarella, L. (2017). An Assessment of the Global Impact of 21st Century Land Use Change on Soil Erosion. *Nature Communications*, 8(1), 2013. <https://doi.org/10.1038/s41467-017-02142-7>

**Das, P. J.,** & Baruah, S. (2018). Rainfall-Runoff and Soil Erosion Trends in the Subansiri River Basin of Northeast India. *Journal of Environmental Hydrology*, 26(3), 56-67.

**FAO** (2021). Soil Erosion Assessment Using RUSLE for Land Degradation Neutrality. *FAO Soils Bulletin Series*.

**Hazarika, M. K.,** & Honda, K. (2001). Estimation of Soil Erosion Using Remote Sensing and GIS: A Case Study at the Subansiri Watershed. *International Journal of Applied Earth Observation and Geoinformation*, 3(1), 20-26.

**Jaiswal, R. K.,** Tiwari, H. L., & Verma, N. (2014). Soil Erosion Modeling Using RUSLE and GIS in a Sub-Humid Region of India: A Case Study of Subansiri Basin. *International Journal of Geomatics and Geosciences*, 4(3), 485-498.

**Lal, R.** (2001). Soil Degradation by Erosion and Its Impact on Crop Productivity. *Land Degradation & Development*, 12(6), 519-539. <https://doi.org/10.1002/ldr.472>

**Mishra, A.,** Kar, S., & Singh, V. P. (2007). Soil Erosion Assessment Using GIS and RUSLE Model in a Himalayan Region. *Water Resources Management*, 21(10), 1783-1798.

**Morgan, R. P. C.** (2005). *Soil Erosion and Conservation* (3rd Edition). Blackwell Publishing.

**NDVI Data Source:** NASA MODIS Vegetation Indices. Retrieved from: <https://modis.gsfc.nasa.gov/data/dataproduct/mod13.php>

**Panagos, P.,** Borrelli, P., & Poesen, J. (2019). Soil Erosion and Vegetation Dynamics—An Interplay between Climate and Land Use Change. *Science of the Total Environment*, 658, 312-326. <https://doi.org/10.1016/j.scitotenv.2018.12.001>

**Prasannakumar, V.,** Vijith, H., & Abinod, S. (2012). Estimation of Soil Erosion Risk within a GIS Framework: A Case Study of the Western Ghats, India. *Natural Hazards*, 59(2), 791-802. <https://doi.org/10.1007/s11069-011-9798-6>

**Renard, K. G.,** Foster, G. R., Weesies, G. A., McCool, D. K., & Yoder, D. C. (1997). *Predicting Soil Erosion by Water: A Guide to Conservation Planning with the Revised Universal Soil Loss Equation (RUSLE)*. United States Department of Agriculture, Agriculture Handbook No. 703.

**Renschler, C. S.,** & Harbor, J. (2002). Soil Erosion Assessment Tools from Point to Regional Scales—The Role of Geomorphologists in Land Management Research and Implementation. *Geomorphology*, 47(2-4), 189-209. [https://doi.org/10.1016/S0169-555X\(02\)00082-X](https://doi.org/10.1016/S0169-555X(02)00082-X)

**Sarma, A. K.,** & Das, S. K. (2007). Flood and Erosion in the Subansiri River Basin: An Environmental Perspective. *Environmental Monitoring and Assessment*, 134(1-3), 327-336. <https://doi.org/10.1007/s10661-007-9614-2>

**Sharma, J. K.,** & Tripathi, N. (2020). Hydrological and Soil Erosion Assessment of Subansiri River Basin Using SWAT and RUSLE Models. *Journal of Hydrology*, 6(4), 132-145.

**Subansiri River Basin Data Source:** India-WRIS (Water Resources Information System). Retrieved from: <https://indiawris.gov.in>

**Vrieling, A.,** Sterk, G., & Beaulieu, N. (2008). Erosion Estimates Derived from NDVI: A Case Study in Kenya. *Geomorphology*, 97(3-4), 491-503. <https://doi.org/10.1016/j.geomorph.2007.08.006>

**Wischmeier, W. H.,** & Smith, D. D. (1978). *Predicting Rainfall Erosion Losses: A Guide to Conservation Planning*. United States Department of Agriculture, Agriculture Handbook No. 537.